Analysis of Deformation in Disordered Materials: Connecting Atomistic Simulations and Rheological Measurements to Continuum Theory

by

Adam Ross Hinkle

A dissertation submitted to The Johns Hopkins University in conformity with the requirements for the degree of Doctor of Philosophy.

Baltimore, Maryland

December, 2016

Abstract

Central to the description of plasticity in disordered solids is the development of constitutive laws capable of encoding the necessary atomistic processes responsible for deformation within continuum-level field theories. Recently considerations of non-equilibrium thermodynamics have shown that an effective temperature may be essential in describing the degree of disorder of the evolving amorphous structure under an imposed shear. This thesis presents theoretical and computational analyses of the deformation of two distinct glassy materials. In the case of a simple yield stress fluid undergoing Couette shear, an effective-temperature model for transient shear-band formation is presented and quantitatively compared with the results of rheological experiments. Then molecular dynamics simulations of a metallic glass are used to propose a methodology for coarse-graining discrete, atomic energies into an effective-temperature field. A strain criterion is established and used to distinguish the coarse-grained degrees-of-freedom inside the emerging shear band from those of the surrounding material. The statistics of the potential energy are used to define a signal-to-noise ratio as a metric to assess the influence of the coarse-graining

ABSTRACT

lengthscale on shear-band identification. We investigate the effect of different coarse-graining lengthscales on the initial condition to a two-dimensional, numerical implementation of the shear transformation zone (STZ) theory. Direct comparisons of the evolving amorphous structure and the macroscopic response of the atomistic data and the continuum model are made.

Primary Reader: Michael L. Falk

Secondary Reader: Michael D. Shields

Acknowledgments

My deepest appreciation and gratitude is owed to my advisor, Michael. His encouragement and high expectations have always come to me with kindness and understanding. In particular, I now am a bit more persistent when doing my work, and far more critical of my own conclusions than I ever was before writing this dissertation.

My time as a graduate student at Johns Hopkins has been a very rich and fulfilling one. Through Michael's collaborations, colleagues, and friendships, I found an energetic research environment that extends far beyond Baltimore. Often lengthy departures from the U.S. landed me in England, Germany, France, and Italy, and I returned each time having learned more about my own research, as well as a great deal about related fields. For six months I was a visiting student at Düsseldorf Universität in the group of Jürgen Horbach, while Michael was on sabbatical in Paris. During that time in Europe, I met Thibaut Divoux and Sébastien Manneville who graciously shared the details of their experiments and their encouragement. Many of the wonderful discussions at Ecole Normale Supérieure de Lyon led to a substantial part of my research while a graduate student.

ACKNOWLEDGMENTS

A great amount of thanks is owed to many people who have directly or indirectly helped me with the content of this thesis. At Johns Hopkins this has included Mark Robbins, Pengfei Guan, Sylvain Patinet, Peng Yi, Jun Ding, and fellow graduate students Thomas O'Connor and Tristan Sharp in the physics department, as well as Tonghu, Yuchong, Darius, Dihui, and Anindya in the Falk group. I am tremendously thankful for the collaboration with Michael Shields and Chris Rycroft whose expertise and mentoring has guided some of this work in substantially new and exciting directions. A number of other researchers at various places have extended me a platform to discuss my work at department seminars and colloquia, especially Emanuela Del Gado, Paulo Arratia, Martin Müser, and Lars Pastewka. I have also benefited from workshop discussions with Suzanne Fielding about rheology. Much of the basics about effective temperature and amorphous plasticity I learned from Lisa Manning's wonderfully written early papers, and from the theory of non-equilibrium thermodynamics of Eran Bouchbinder and James S. Langer.

I also must thank my remaining committee members for their time and consideration of my thesis: Howard Katz, Vicky Nguyen, and Oleg Tchernyshyov. And lastly, a very special thanks indeed goes to Bob Cammarata, who was a member of the committee for my thesis proposal, but who's untimely passing while I was a graduate student saddens me still. From him I learned a great deal about the basics of materials science, as well as the value and reward of helping others.

At Johns Hopkins I have benefited from the National Science Foundation's IGERT

fellowship program which has funded 3 years of my graduate studies.

Contents

List of Tables

List of Figures

Kein Material überwindet so sehr die Materie wie das Glas.
Das Glas ist ein völlig neues, reines Material,
in welchem die Material ein- und umgeschmolzen ist.
Von allen Stoffen, die wir haben wirkt es am elementarsten.
Es spiegelt den Himmel und die Sonne,
es ist wie lichtes Wasser,
und es hat einen Reichtum der Möglichkeiten
an Farbe, Form, Charakter,
der wirklich nicht zu erschöpfen ist,
und der keinen Menschen gleichgültig lassen kann.
Alle anderen Stoffe wirken neben dem Glase abgeleitet
und wie Reste, wirklich wie Menschenprodukte.
Das Glas wirkt außermenschlich, als mehr denn menschlich.

- Adolf Behne, von *der Wiederkehr der Kunst*

Chapter 1

Introduction

The microscopic basis of amorphous plasticity is still somewhat unsettled. Unlike the theory of dislocations in crystalline solids, no such simple or consensus description even presently exists.[1] A leading candidate for a theory of amorphous plasticity is based on the notion that the analog to dislocation formation and movement is the local transitional rearrangements of small zones of about 10 atoms or molecules.[2] Continuum-level field theories, on the other hand, provide a means of characterizing mechanical deformation in a material through a *constitutive law* or *constitutive relation*, an equation or set of equations encoding the underlying microscopic physics through the evolution of one or more continuous fields with the goal of accurate, quantitative predictions. In the case of plastic deformation, the complex and inherently irreversible changes occurring in the microstructure of the deforming material pose a significant challenge for the constitutive modeling of solids. Non-crystalline

or "amorphous" materials in particular, such as metallic glasses, silicates, foams, colloids, gels, and granular media posses additional and unique complications: They lack periodicity and long-range order in their atomic network, and are thermodynamically out of equilibrium. As such the development of continuum models for amorphous materials which are both computationally efficient and predictively accurate remains a long sought-after goal.

Continuum mechanics is essentially a theory that describes a body undergoing "a motion", which can be rigid, where the positions between all material points within the continuum remain at a fix relative distance, or deformable where these relative distances change.[3] In the latter case, the need for a constitutive law, in addition to Newton's Laws, is required to determine how these distances between material points change. The constitutive law is a grand synthesis of the underlying atomistic mechanisms responsible for these changes, and the proper formulation of such a law must provide a means of reducing the vast number of degrees of freedom $\sim 10^{23}$ to a single differential equation (or set of a few equations) capable of capturing the changes of the system to within an acceptable level of accuracy. Because mechanical deformation is an inherently non-equilibrium process, the difficulty of extending the familiar equilibrium statistical mechanics to a system far from equilibrium, is necessary to achieve such an acceptable continuum description. All attempts so far have been necessarily phenomenological, with the introduction of various order-parameters in an attempt to overcome the limitations presented by the extraordinarily complex config-

urational phase-space of a glass which largely prohibits the direct calculations of the glassy state from any purely fundamental physics. Within the last ten years however, a thermodynamics of non-equilibrium solids has been developed with the particular goal in mind of connecting the disordered structure of a glassy to its macroscopic mechanical response when it is driven further out-of-equilibrium through a deformation mode like applied shear. This link between the atomic structure and a set of dynamics that accounts for the irreversible changes taking place in the glass is made through the temperature of the system.[4–6] Temperature in amorphous materials is a far more subtle quantity than is usually ever considered in the study of equilibrium systems.

Motivation for the work contained in this thesis comes from both fundamental and applied considerations. Amorphous solids have many desirable properties that make them attractive for potential engineering applications and designs, but suffer from a complex and poorly understood evolving microstructure when deforming. For example, the advantage of the high strengths of metallic glasses is countered by the catastrophic brittle fracture that precipitates their failure. Similarly yield stress fluids are ubiquitous materials used in household and cosmetic products and are essential to the pharmaceutical market, however they exhibit a range of complex behavior impacting industrial advances. Predictive and accurate constitutive equations for these materials would undoubtedly lead to new engineering feats and expand industrial possibilities. From the perspective of the fundamental physics of materials, a well-

formulated constitutive law would necessarily come from an understanding of the connection between the atomistic and micromechanical mechanisms of plasticity, as well as from comparisons with experimental measurements.

In Chapter 2 of this thesis the effective temperature formalism for disordered materials in the context of the shear transformation zone (STZ) theory is reviewed. Chapter 3 adapts this effective-temperature theory to the phenomenon of transient shear banding in a yield stress fluid, and quantitative comparisons with the measurements of corresponding rheological experiments are made. Then in Chapter 4 the phenomenon of shear banding in metallic glass is studied through atomistic simulations and a two-dimensional numerical implementation of the effective-temperature description. Chapter 5 concludes with a discussion about possible future research directions.

Chapter 2

Foundations of amorphous plasticity and the role of an effective temperature

As discussed in Chapter 1 amorphous materials include a wide variety of seemingly distinct materials including metallic glasses, where the constituent elements interact through metallic bonds and the structure is like a random packing of spheres, and polymeric gels where the arrangement of the molecules can form intricate honeycomb regions that are several microns in size. The unifying theme of all of these systems however is that the organization of the atoms or molecules in their structures is distinctly different from what is found in crystalline materials.[1] In a crystalline solid, atoms (or groups of atoms or molecules) are arranged on a lattice so that a single unit

cell is all that is needed to describe the structure. A crystal structure possesses a high degree of symmetry that is well defined, as the unit cell simply repeats itself in every direction in a periodic fashion. Most metals and covalently bonded solids have this type of so-called "long-range order." Non-crystalline solids, like the gels and metallic glasses mentioned above, lack this long-range order and are said to be "amorphous" (literally,'without form'). However, if we restrict ourselves to very small scales, e.g. a few atomic diameters, even a liquid will exhibit some degree of order reminiscent of a crystal, and amorphous materials have been found to have a great deal of short-range—even medium-range order. even though they can have important short-range order that is quite well defined. Still, the absence of long-range order implies that there is no precise unit cell up which a physical theory can be constructed to predict how the structure might change in the presence of some external agent for instance.[7]

While amorphous materials have long since presented a great scientific challenge due to the nature of their disordered structure, a great deal of progress has been made with regard to a theoretical foundation. More recently an increased interest in these materials has arisen because of their unique properties which make them particularly suitable for specific applications. The lack of grain structure in metallic systems, for instance, has made them ideal for microelectromechanical systems[8] and protective coatings.[9] On the other hand investigations into the complex rheology of gels and colloids have been essential to the availability of products and processing methods of the pharmaceutical and cosmetic industries.[10] Despite this, there is still a lack of an

agreed upon approach for characterizing their mechanical behavior, including their modes of deformation and failure mechanisms. In one sense this seems strange because amorphous materials find themselves pinned between two extremes, crystalline plasticity and the Navier-Stokes theory of fluids, both of which provide complete (or relatively so) descriptions within their respective domains. At the molecular level, amorphous solids are structurally very similar to fluids in that they share a random placement of atoms over large lengthscales. But they also exhibit properties that define solidified media such as rigidity, through elastic moduli, and perhaps most importantly, a well-defined yield (flow) stress.[11,12]

A subset of amorphous materials is characterized by an important additional thermodynamic distinction in addition to the non-crystalline structure; materials in this subset are known as glasses. Perhaps the clearest definition of a glass comes from how a glass is created from a liquid that is in thermodynamic equilibrium at some high temperature T. When this liquid is cooled from T, it may either crystallize when the melting temperature T_m is reached, or instead become supercooled. Figure 2.1 shows the temperature dependence of the specific volume, entropy or enthalpy, and other properties under constant pressure as such a liquid is cooled during this process. The particles (atoms, molecules or ions) forming crystalline materials are arranged in orderly repeating patterns, with elementary building blocks (unit cells) extending to all three spatial dimensions. The structures of crystalline solids depend (predictably) on the chemistry of the material and the conditions of solidification (starting tempera-

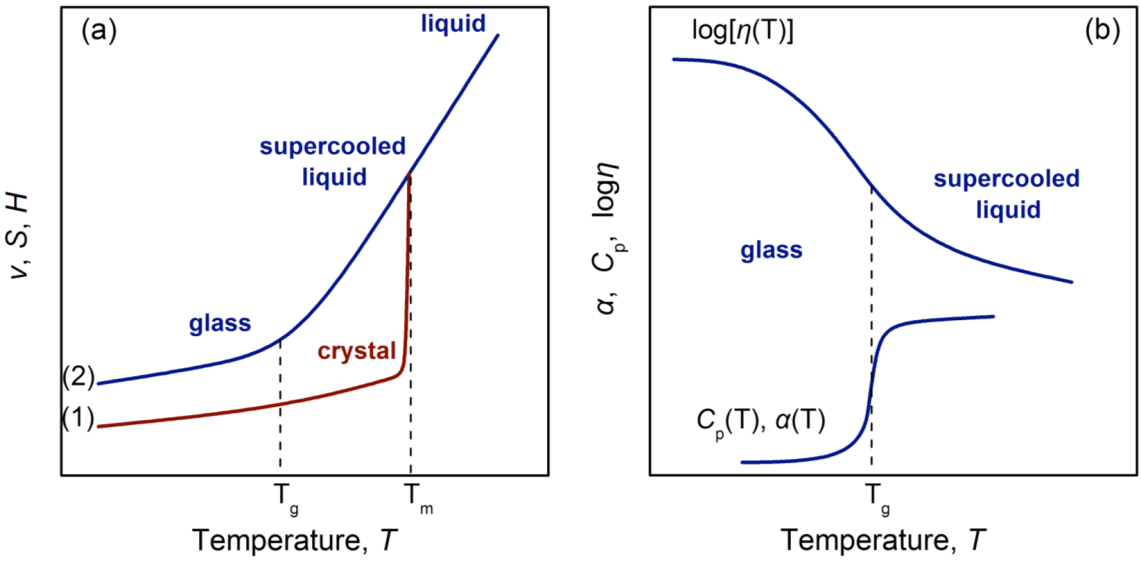

Figure 2.1: The temperature dependence of the specific volume (v), entropy (S), or enthalpy (H) of glasses and crystals. (b) The temperature dependence of the coefficient of thermal expansion α, heat capacity C_p and viscosity (η) near the glass transition temperature T_g.[13]

ture and cooling rate, ambient pressure, etc.), and can be described easily in detail by combining crystallographic notions with diffraction/scattering data.[12,13] Supercooled liquids, on the other hand, demonstrate a rather intriguing behavior. Upon further cooling below T_m, their particles progressively lose translational mobility, so that around the glass transition temperature T_g rearrangements to regular lattice sites are no longer possible. As the liquid is cooled through T_g, its viscosity increases by as much as 17 orders of magnitude. This phenomenon is distinctive of the formation of a glass, and is referred to as the "glass transition".

The exact nature of the glass transition remains controversial, and is considered one of the significant, long-standing problems in classical physics. There is not a

clear agreement as to whether the glass transition is indeed a genuine phase transition or rather it is a dynamical arrest. When a transition takes place between two distinct phases, the change of heat capacity and other thermodynamic quantities is consistently understood in a theory of phase transitions.[14] The glass transition essentially describes a disordered system, a liquid, forming a similarly disordered solid, a glass, without a transition into a distinctly different phase, and yet the heat capacity changes with a characteristic jump at T_g, as seen in Fig. 2.1b. The jump is considered a hallmark of the glass transition, and defines glass transition temperature T_g. The heat capacity jump immediately presents a problem that is at the heart of glass transition: how can the jump be understood if there is no distinct second phase? Alternatively the glass transition is a kinetically controlled phenomenon in the sense that it exhibits a range of T_g depending on the cooling rate with a maximum T_g at the highest rates of cooling.[15–17]

A glass exhibits a long-range structure close to that observed in the supercooled fluid phase, while displaying solid-like mechanical properties on the timescale of practical observation. Both in a glass and in a crystal it is only the vibrational motions of the atoms or molecules and some rotational motions that remain active whereas translational motion is essentially arrested. However, a characterization of amorphous solids based solely on the movement and arrangement of the microscopic ingredients is insufficient, in that it overlooks an import distinction: not all amorphous materials are glass formers. Glasses are thermodynamically distinct from the overarching

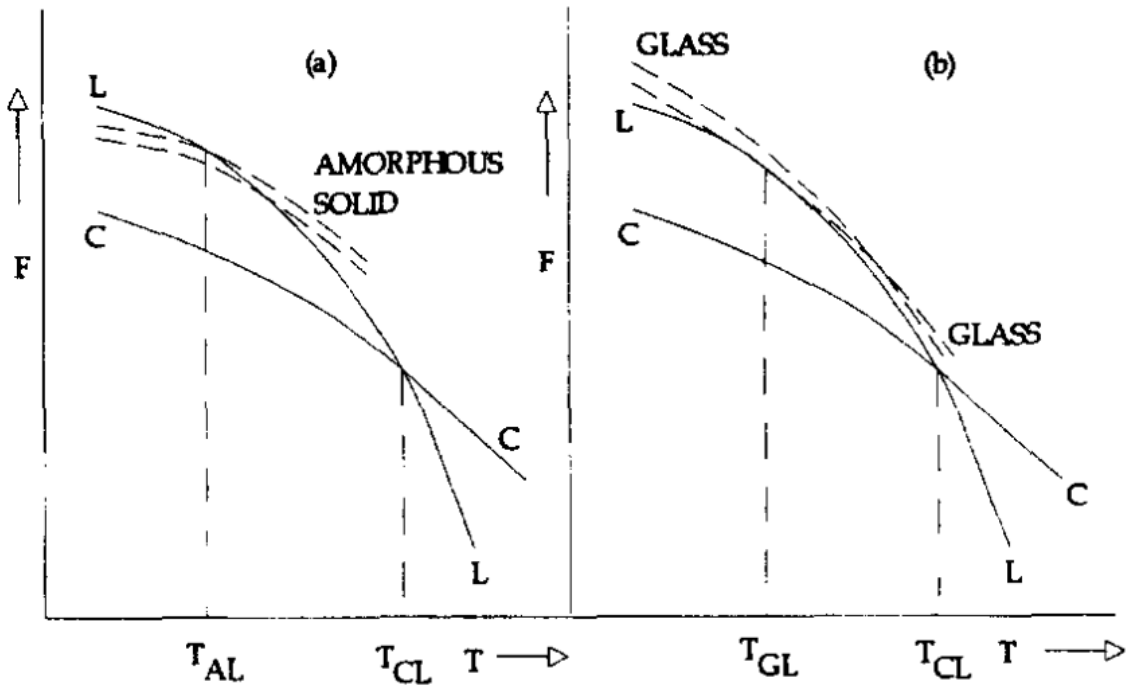

Figure 2.2: Schematic variations with respect to temperature, T, of molar Gibbs free energy F of crystal (C), liquid (L), amorphous solid (a) and glass (b). T_{CL} and T_{AL} are the melting temperatures of the crystal and amorphous solid, respectively. T_{GL} is the glass transition temperature. Two dashed curves are shown for a-solid and for glass to indicate that the free energy of these non-equilibrium materials is history-dependent.[18]

category of amorphous solids. Figure 2.2, illustrates the thermodynamic difference between a genuine glass and a material with an amorphous structure, but has not gone through a glass transition. The most important difference between an amorphous solid and a glass is that the free energy of an amorphous solid is less than that of the liquid phase below the melting temperature of the amorphous solid, while for a glass this energy is higher than that of the liquid. More generally the free-energy surface of a glass is tangential to the free energy surface of the liquid at the glass

transition temperature and pressure, and at any other temperature and pressure, the free energy of the glass is greater than that of the liquid. Consequently there is no discontinuity in the derivatives (entropy or volume), but there are discontinuities in the second derivatives of the free energy (heat capacity, coefficient of expansion, and compressibility) at the liquid-to-glass transition which makes the glass transition similar to a second-order phase transition. Free energy curves, like those shown in Fig 2.2 for amorphous solids have been calculated for amorphous Si[19] and for amorphous Ge[20] from their respective heat capacity data. The multiple free-energy curves for the amorphous solid and the glass in Fig. 2.2 indicate a feature that distinguishes them from the liquid and crystal phases. While free energy curves are unique for the crystal and liquid states, the free energy curves for amorphous solids and glasses are not; they are history dependent, and a different curve exists for each method of formation.

In general glasses are most frequently produced by a melt that is cooled below its glass-transition temperature sufficiently fast to avoid formation of crystalline phases. Metallic glasses, in particular, need to be cooled quickly to avoid crystallization. Some specific experimental methods of glass formation include:

- quenching from melt[21]
- vapor decomposition[22]
- solid-state reactions (thermochemical and mechanical methods)[23,24]

- liquid-state reactions (sol-gel method)[25,26]
- irradiation of crystalline solids (radiation amorphization).[27,28]

The most quintessential of these glass-forming methods is the rapid cooling of a molten material leading to an apparent solidification while preserving the structural disorder, mentioned above. Glasses formed in this way are often referred to as molecular glasses. A molecular glass is consequently arrested in a high-free energy state and falls out of thermodynamic equilibrium. However, in the case of some materials like colloids, gels, and foams, often referred to as "soft glassy materials", the concentration of the constituents leads to a similar kind of arrest. A rapid increase in the concentration of constituents causes structural arrest in colloidal systems while preserving the disorder associated with the liquid state. More specifically, the glass transition in colloidal suspensions can be achieved by increasing the volume fraction ϕ.[29–31] This is in contrast to supercooled liquids which can be driven towards their glass transition by rapidly quenching their temperatures. The resultant soft, solid-like substance is typically represented as a "colloidal glass" when compared with a molecular glass. Molecular glasses, like metallic glasses, are generally more easily formed when the composition of the material is more complex with many different species of elements. However, the rapid temperature decrease during the quenching process is more likely to be the dominant factor for the formation of such glasses, since it has been shown that simple, single-element metals can also form a stable glass.[32]

These two different ways to form a glass illustrate the natural desire to extend the

notion of a "glass transition" from a transformation characterized by the change in properties at a temperature T_g to a more general concept involving parameters that are not necessarily thermodynamic. As already discussed, a liquid with low viscosity solidifies into a glass when the temperature is lowered. But a flowing foam can becomes rigid when the applied stress is lowered, and a colloidal suspension loses the ability to flow when the density is increased. In each of these cases, a different control parameter is varied to bring the system into the rigid phase, yet the structure does not change appreciably at the transition. Both phases are amorphous, and it is difficult to specify an unambiguous order parameter to tell the two apart. Just as there are similarities between how different fluids nucleate into a crystal, there are similarities in the way different systems lose the ability to flow while still remaining amorphous. A relatively new framework known as "jamming" has been developed to reveal the connections between these seemingly disparate phenomena, where the temperature, inverse-density, and applied stress together determine when a material is jammed and when it flows.[33] In the context of jamming, the traditional glass-transition is a special case where one only considers the relationship between temperature and inverse-density.

A unifying feature of glassy materials is their non-ergodic nature. In statistical mechanics, the term "ergodic" refers to an equivalence of the time and ensemble averages of the properties of a system. Ergodicity is an essential assumption in equilibrium statistical mechanics. In the case of glasses however, the ensemble average

of certain thermodynamic properties can be different from the corresponding time average. For example, an ensemble average includes frozen-in fluctuations that may not be present in a time average of the same property.[34–36] For any experiment, the question of ergodicity is really a question of timescale. Specifically, there are two relevant timescales of interest: an internal relaxation timescale τ_{int} on which the system loses memory of its preceding states, and an external observation timescale τ_{ext} on which properties are measured. The ratio of these two timescales is known as the "Deborah number"[37]

$$D = \frac{\tau_{int}}{\tau_{ext}} \tag{2.1}$$

in honor of the prophetess, Deborah, who sings "...the mountains flowed before the Lord..."(Judges 5:5). Mountains, like glasses, have analogous timescales to human observers. Figure 2.3a summarizes D at different stages during the formation of a glass by quenching a liquid. A $D > 1$ implies a non-ergodic system, since there is insufficient time for the system to equilibrate during the time of measurement. On the other hand, $D < 1$ indicates that the system has sufficient time to relax to equilibrium during the observation time window, implying that the condition of ergodicity can be satisfied. The fundamental difference between a liquid and its corresponding glass is that the liquid is ergodic with $D < 1$, while the glass is inherently non-ergodic with $D > 1$. The glass transition occurs at $D = 1$ and constitutes a change from an ergodic liquid phase to a non-ergodic glassy state.[36]

The formation of a glass involves freezing the kinetic processes that enable ther-

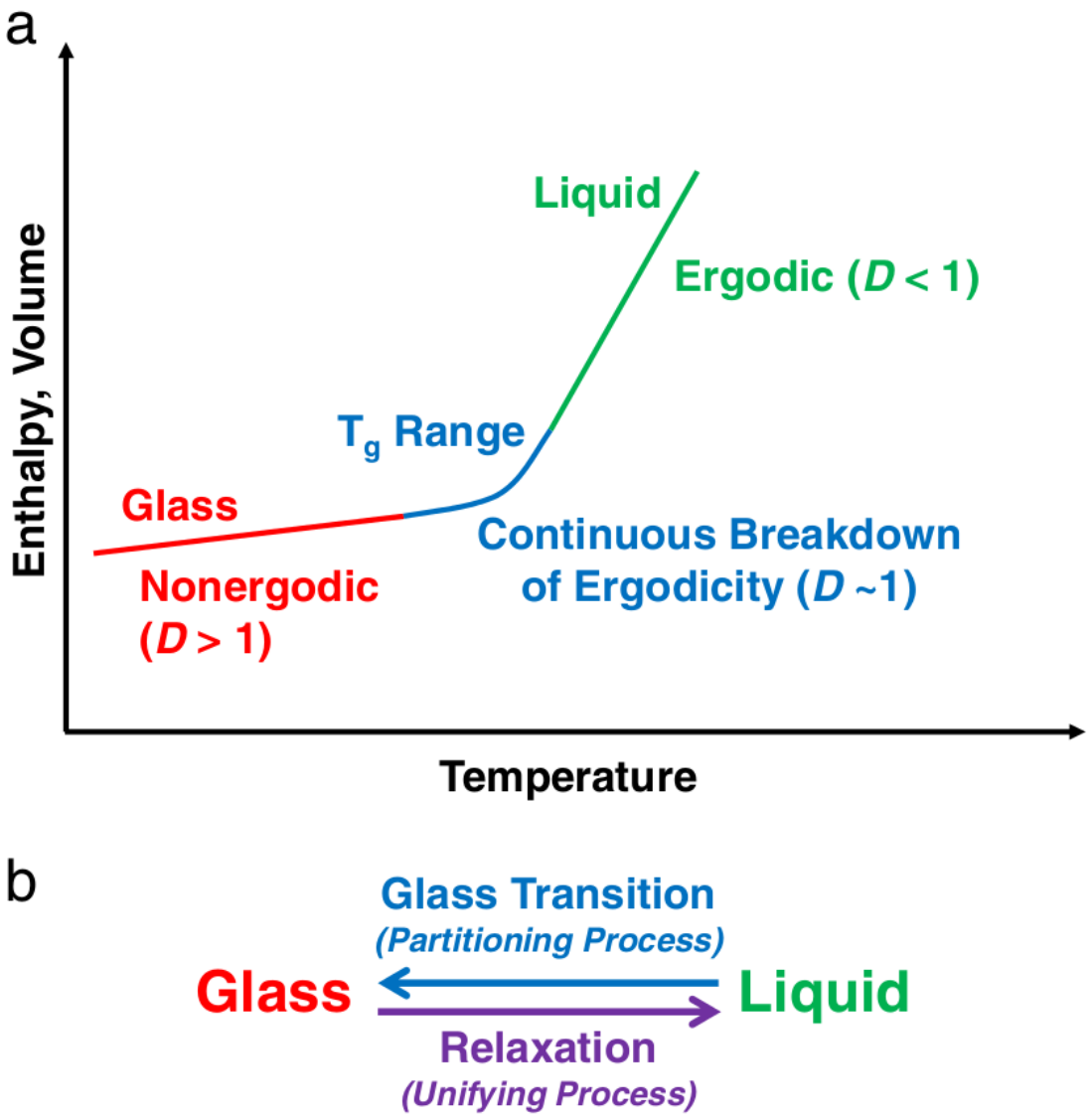

Figure 2.3: The glass transition involves a continuous breakdown of ergodicity as the ergodic liquid at high temperature becomes trapped in a subset of configurational phase space in the nonergodic glassy state at low temperatures. (b) The glass transition is termed a partitioning process since configurational degrees of freedom are lost as the system becomes kinetically trapped in the non-ergodic glassy state. The opposite process, structural relaxation, involves the spontaneous lifting of this kinetic constraint, allowing the system to explore additional configurational degrees of freedom. This is termed a unifying process. Figure directly reproduced from.[36]

modynamic equilibrium and ergodicity of the statistical mechanical phase space. A very interesting feature of glasses, however, is that their properties change with time, through a process called "aging" or relaxation. As Fig. 2.3b illustrates the relationship between glass formation and glass relaxation is an inverse, where relaxation is an attempt by the structure to evolve towards the equilibrium liquid phase and thereby lowering it's free energy. Aging is generally only possible if the constituents have sufficient mobility for the necessary molecular rearrangements. The rate of aging gradually slows down with time.[10,38] Temperature is known to have a significant effect upon aging, and the process of aging is usually faster at higher temperatures due to enhanced thermal energy leading to higher mobilities.[10] Moreover, the process of aging itself can be reversed. For glassy materials in which aging is present, a deformation field can reverse aging by destroying the structures evolved during the aging and inducing mobility among the constituting entities. This process is known as rejuvenation.[39] Aging in the presence of deformation is generally very slow compared to conditions where the aging is the only relevant timescale. Nonetheless the effects of aging, rejuvenation, and stress relaxation are important aspects of the rheology of glassy materials.[40,41]

A complete description of deformation in amorphous solids is still a work in progress, although significant strides have been made in terms of both a microscopic and continuum-level understanding. The disordered structure of glasses and other amorphous materials is a rich and complex realm, and many of the ideas, both re-

viewed and presented by this thesis, have emerged through a development of important new physics for glassy phenomena. While amorphous solids are essentially indistinguishable from fluids in their microscopic view, they are unlike fluids in that they exhibit a yield stress below which they respond elastically to external forces, while fluids flow under any external strain. Once an amorphous solid is subjected to a stress that exceeds the yield stress, it can flow plastically in a manner that depends on the temperature, the shear-rate, and the density.[42] Some of the first investigations of amorphous deformation were bubble raft experiments that were used as an analog for the atomic-scale structure of metallic glass. These experiments lead to the realization that localized clusters of molecules undergo irreversible rearrangements in response to applied shear stresses; these clusters were originally named "shear transformations".[43–45] In a very rough sense, these rearrangements in amorphous materials are believed to play the role of dislocations in crystals by being the agents of plastic deformation.[2] Early theoretical developments largely centered around a theory of "free volume" which provided a means of characterizing the liquid and glass phases, and posited that an increase in free volume is associated with the glass-to-liquid transition.[46,47] These ideas were extend to provide detailed dynamics for the change in free volume and how it connected to "flow defects" in the context of metallic glasses,[48] and the constitutive models for amorphous polymers.[49,50] All of these theories have a number of features in common, perhaps most importantly they begin with a stress-assisted thermal activation Eyring formalism[51] as the basis for the

molecular rearrangements occurring during plastic deformation.

The advent of modern computational capabilities has been perhaps the most important tool used to propel investigators towards a theory of amorphous plasticity. Large-scale atomistic simulations, e.g. Molecular Dynamics (MD), have revealed many details about the deformation mechanisms in amorphous materials particularly in terms of local, short-range structure and orientational correlations.[52–60] Other more recent simulations have suggested that the plastic events in the amorphous material are composed of localized rearrangements which organize into lines of slip[61] with particular scaling properties, and related avalanche models based on bursts of spatially localized plastic activity.[62–64] Mesoscopic approaches have been proposed based on the time-dependent Ginzburg-Landau theory,[65] as well as others that have used Markovian stochastic processes and the dynamic Monte Carlo method to simulate the effect of local molecular rearrangements of atoms.[66] Many of these ideas have proliferated in recent years and have been extended across the spectrum of the many different types of amorphous systems in an effort to help unify the field. For example an elasto-plastic model for yield stress fluids that is also based on collective plastic events as well as a microscopic yield stress has been used to study the resulting spatiotemporal deformation during flow.[67] Further removed from these defect-centered approaches are fundamentally different models which begin with a fluid-based description such as mode-coupling theory,[68,69] which starts from a liquid-like, many-body description and predicts the onset of solid-like behavior at high densities and low

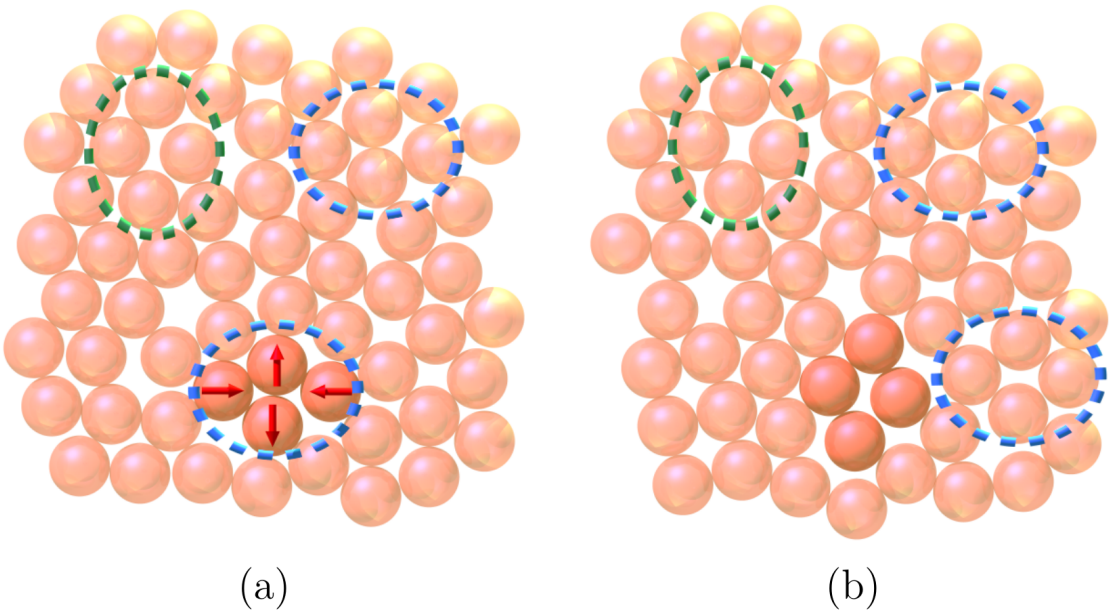

Figure 2.4: Shear transformation zones in an amorphous material under shear. (a) The green and blue ellipses represent STZs of four atoms. Under a shear stress the STZs depicted by the blue ellipse can change their collective orientation to the new configuration shown by the green ellipse. The red arrows show the direction of movement of the atoms during this transform from one orientational state to another. (b) At some later time, one of the STZs that was observed at an earlier time is no longer present in the same location, but new STZs have been created nearby.[70]

temperatures.

One theory in particular has been able to account for many aspects of the phenomenology of sheared metallic glasses such as strain hardening, the Bauschinger effect, and the emergence of a yield stress. In this new picture[59] the original notions of "shear transformations" and "flow defects have been extended to provide a specific set of dynamics for the populations of these transforming regions referred to as "shear transformation zones" (STZs), illustrated in Fig. 2.4. The STZs are hypothesized to consist of 5-10 atoms or molecules and possess a set of specific properties:[71]

- STZs are orientational in nature: they transform preferentially under a particular applied stress.
- STZs are two-state systems: after transforming once they can reverse their transformation, but they cannot continuously undergo repeated transformations in the same direction.
- STZ transformations may be thermally activated or mechanically driven.

The STZs are, in effect, the transition states that enable these rearrangements. When an STZ appears, if it is properly oriented with respect to the stress, it rapidly undergoes a shear transformation. Otherwise, it rapidly disappears, and no irreversible deformation takes place. The so-called STZ theory[2,4–6,59,72–79] has been developed greatly since it was first proposed[59] and is a general framework for characterizing plasticity in amorphous materials. The theory is a phenomenological continuum-level mean-field approximation for flow based on an assumption of local rearrangements of a material's structure via the activation of the STZs . Here, STZs are orientational point defects that mediate plastic flow by accommodating rearrangement. A distinguishing feature of the STZ theory is that it is based on a specific model of molecular rearrangements, which have been observed directly in numerical simulations and analog experiments.[2,80,81] The STZs themselves have been postulated to have internal degrees-of-freedom.[2] The STZs not only transform from one orientation to another; they are created and annihilated during configurational fluctuations at a rate that

has been shown to be proportional to the rate of energy-dissipation per STZ.[72]

One critical way the STZ theory differs from its predecessors (and indeed other theories) is through the introduction of an "effective temperature" that quantifies the structural changes, i.e. the disordering of amorphous materials when they deform, in the form of a scalar field. The historical foundation of the concept of effective temperature can be found in the early theories of glasses,[82–89] especially the theories of free volume v_{free} which described the intrinsically disordered state of non-crystalline materials. Those investigators recognized that the relevant definition of free volume is not an extensive excess volume measured from some densely packed state, but as an intensive quantity, namely *the inverse of the derivative of a configurational entropy taken with respect to the volume.* This is the dimensionless entropy associated with the mechanically stable molecular positions, without kinetic or vibrational contributions. This thermodynamic consideration was connected to the picture of local defects, e.g. the STZs, by postulating that the defects might be proportional to a Boltzmann-like factor

$$\exp\left(\frac{-A}{v_{free}}\right) \tag{2.2}$$

where A is a constant with dimensions of volume, and not simply to v_{free} itself.[2] This idea v_{free} was further developed and later applied to the statistical mechanics of athermal materials like powders,[90] and other dense, sheared amorphous systems.[91,92]

The origin of an effective temperature as it specifically relates to the configurational entropy and energy lies in the complex and unusual energy landscape of glassy

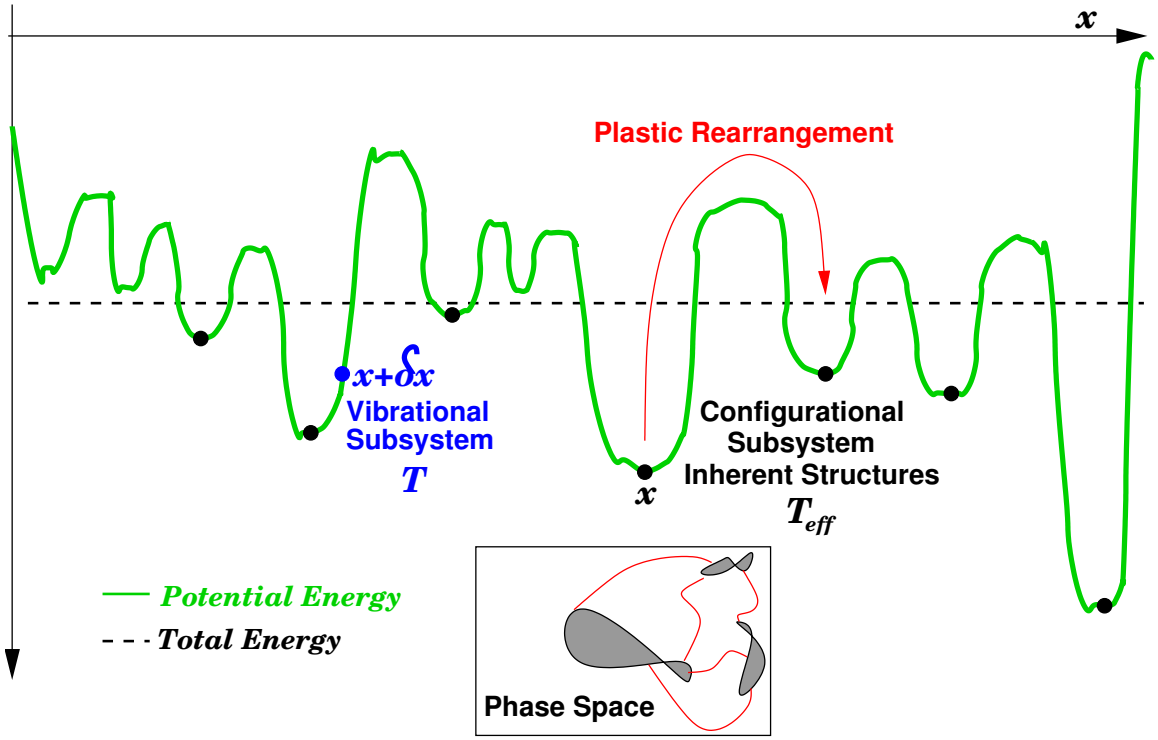

Figure 2.5: A one-dimensional sketch of the potential-energy landscape of the glass (green) with surface of constant total energy (dashed line). A denumerable set of low-lying minima at x defines a configurational subsystem described by an effective temperature, in contrast to the kinetic-vibrational subsystem defined by small displacements δx from the minima and characterized by the familiar thermalized temperature. The corresponding non-ergodic phase-space contains many separate regions connected by a relatively few narrow filaments corresponding to the improbable molecular events like the kind occurring during plastic deformation where transitions from one energy minimum to another take place.

materials. In particular, for shear-driven amorphous materials below the glass transition temperature, it has been proposed that the degrees-of-freedom can be separated into two parts: a set of configurational coordinates describing the mechanically stable positions of the atoms or molecules in their inherent structures,[5,87–89] and a separate set pertaining to the remaining kinetic and vibrational variables. These two sets of degrees-of-freedom are thought of as two weakly coupled subsystems (the configura-

tional subsystem and the vibrational subsystem) of the system as a whole, in analogy to the usual thermodynamic analysis in which two neighboring subsystems of a larger system are brought into weak contact.[4–6] Figure 2.5 shows a sketch of the potential-energy landscape of a glass with N atoms, and the corresponding Nd dimensional phase-space of configurations. The intersection of the system's surface of constant energy and the potential-energy landscape defines a subset of local energy minima referred to as inherent structures, corresponding to particular molecular arrangements of the N atoms. The configurational subsystem is defined by the denumerable set of these inherent structures, while the kinetic-vibrational subsystem is defined only by small displacements from the potential-energy minima. A molecular rearrangement of the kind that occurs during plastic deformation corresponds to the motion of a system point from the near neighborhood of one inherent state to that of another. The few paths in the phase-space which connect the inherent structures are narrow filaments corresponding to improbable, collective events effecting the transition from one potential-energy minima to another. Similarly the filaments correspond to saddle points in the potential-energy landscape.

Perhaps the most important distinction between these two subsystems is the timescale of each. The kinetic-vibrational degrees-of-freedom are fast and move at molecular speeds. The configurational degrees of freedom are slow and change on timescales no shorter than those associated with the molecular rearrangements in glassy materials. If these two timescales are comparable to one another, then the

system is in the liquid state and the concept of an effective temperature for the configurational subsystem is irrelevant.[5] For a material clearly in the glassy state, it is the effective temperature that characterizes the structural changes relevant to plasticity. The effective temperature as a continuum field is the coarse-grained continuum description of the effect of the changing population density and spatial distribution of the STZs. The effective temperature T_{eff} can be formally defined as defined as

$$T_{\text{eff}} = \frac{\partial U_c}{\partial S_c} \ , \tag{2.3}$$

where U_{c} and S_{c} are the material's potential energy and entropy respectively of only the configurational degrees-of-freedom, i.e. those degrees-of-freedom associated with the structure of the material. This is to be distinguished from the usual thermalized temperature T which accounts for the degrees-of-freedom which relax on timescales short compared to the observation time. The typical definition of T is applicable to the fast, i.e. vibrational degrees-of-freedom, but the configurational degrees-of-freedom are typically out of equilibrium. Above the glass transition, T_{eff} equilibrates with the ambient temperature T, but as the system falls out of equilibrium at low T below the glass transition or when molecular disorder is generated by mechanical deformation, T_{eff} is a descriptor of the configurational subsystem. In analogy to the free-volume

formula, the steady-state density of STZs is proportional to the Boltzmann factor

$$\exp\left(\frac{-E_z}{k_B T_{eff}}\right) \tag{2.4}$$

where E_z is a characteristic STZ formation energy and k_B is the Boltzmann constant.

Some limited attempts to experimentally measure an effective temperature for disordered materials have been made,[93] as well as other direct, quantitative comparisons with experiments of bulk metallic glasses.[81] Atomistic simulations of two-dimensional glasses have already suggested that T_{eff} is linearly related to the local potential energy per atom,[94] and earlier many arguments were made for the existence of the notion of an effective temperature, related to the entropy, that characterizes the number of phase-space paths available to the system.[76,92,95] Current proposals also exist to use sophisticated computational tools such as nested sampling to identify and count the configurational degrees-of-freedom of a glass and compute T_{eff} directly.

Chapter 3

A Small-gap Effective-Temperature Model of Transient Shear Band Formation During Flow

3.1 Introduction

Yield stress fluids (YSFs) are ubiquitous in everyday life, and their special properties have merited intense research.[96–104] Examples include gels, clay suspensions, foams, concentrated emulsions, and colloids. These seemingly distinct substances exhibit a similar mechanical response when subjected to shear deformation: Below a critical (yield) stress these materials remain elastic, behaving as solids, but above this critical stress they are able to deform and flow as viscous liquids. This char-

acteristic ability makes them extremely sought-after for many applications.[105] YSFs are often categorized by the degree of thixotropy they present. Thixotropic YSFs have memory and aging effects that lead to a history dependence, marked e.g. by flow curves that are significantly different when the applied shear rate is ramped up compared to the ramp down. In contrast, nonthixotropic or "simple" YSFs have no apparent history dependence over the timescales of observation. More important is the fact that thixotropic YSFs, regardless of the particular material, easily form shear bands, regions of highly localized strain, while experiments of simple YSFs report conflicting accounts of the formation of shear bands: In some instances shear bands are observed and yet in others the system (sometimes the same system) remains completely homogeneous under shear.[106–114] These contradictory findings have prompted investigations of simple YSFs with greater attention to the specific material and composition, the shear procedure, and the influence of the geometry of the apparatuses.

Carbopol gel is widely regarded as a quintessential simple YSF and as such has generally been believed to transition from the solid to the liquid state uniformly as a homogeneous system.[97,98] Recent Couette-cell experiments of shear in a carbopol gel have instead revealed the conspicuous formation of transient shear bands before the gel reaches a uniform steady state characterized by a linear velocity profile and Herschel-Bulkley rheology.[111] More importantly because of the small width of the particular Couette cell, the shear stress measured in these experiments was observed

to be nearly uniform across the gap, and the stress gradient was reported to not play a significant role in the formation of the transient shear band.

The onset of plastic flow in YSFs and other similar materials has been investigated by other theoretical approaches, but direct, quantitative comparison has been lacking with regard to shear banding and the process of fluidization. Among these theoretical frameworks are soft glassy rheology (SGR).[115] The SGR model in particular has been successful in qualitatively describing the general steady-state power-law behaviors seen in experiments, and criteria have been proposed to characterize the onset of shear banding.[116] It has also been able to capture aging. One drawback of SGR is that it assumes the existence of a "noise temperature" that controls activation rates of plastic processes. The physical basis for this noise temperature is however not clear, and its dynamics have not been derived from fundamental or mesoscale principles.

A minimal theoretical model of a Newtonian fluid using the Krieger-Dougherty constitutive relation[117] has been used to qualitatively model transient shear banding in a Couette-cell geometry. The shortcomings of this approach are that it does not describe a yield stress or solid-state elastic response, nor does it quantitatively capture key experimental observations of shear banding in YSFs, i.e. the correct spatial and temporal evolution of the shear band and fluidization times of the system. More importantly, this model attributes transient shear banding to the nature of the Couette-cell apparatus itself. Specifically it suggests that the gradient in the stress field, which exists simply due to a cylindrical geometry, leads to a higher shear rate

and unjamming of material near the inner cylinder of the Couette cell.

Motivated by the possibility that heterogeneities in the microstructure of the gel may be the dominant driver of the observed shear band, we propose an alternative description of the phenomenon of transient shear banding during plastic flow based on fluctuations in the structure of the gel. We adapt the effective-temperature hypothesis of the shear transformation zone (STZ) theory as a rheological model for shear localization in a simple YSF. In this description, structural changes described by an effective temperature[6] account for the observed plastic flow. The formation of a transient shear band is the primary mode of deformation of the carbopol gel. This occurs simultaneously alongside a distinct, uniform fluidization. We then make quantitative comparisons of stress-time behavior and velocity profiles with recent small-gap Couette-cell experiments of a carbopol gel.

The STZ theory is a general framework for characterizing plasticity in amorphous materials, and provides a continuum-level mean-field approximation for flow based on an assumption of local rearrangements of a material's structure via the activation of STZs.[2,4–6,59,72–79] STZs are orientational point defects that mediate plastic flow by accommodating rearrangement. In this paper we use data from the aforementioned experiments in[111] to determine the physical parameters of the theory and make precise experimental connections. A distinguishing feature of the STZ theory is that it is based on a specific model of molecular rearrangements, which have been observed directly in numerical simulations and analog experiments.[2,80,81] The present formu-

lation of the STZ theory has been extended from the original work of Argon[43,44] and his proposal of "shear transformations" to explain plastic deformation in metallic glasses, as well as from the free-volume and flow-defect theories of Turnbull, Cohen, Spaepen, and others.[46,48] The STZs themselves have been postulated to have internal degrees-of-freedom.[2] The STZs not only transform from one orientation to another; they are created and annihilated during configurational fluctuations at a rate that is proportional to the rate of energy-dissipation per STZ.[72] A coarse-grained continuum description of the effect of the changing population density and spatial distribution of the STZs is defined by an effective-temperature field. In this paper we present equations of motion for the effective temperature and plastic-strain where the steady state is set by a Herschel-Bulkley rheology, and no explicit dependence of the STZ internal variables, local strain rate, or flow history appears.

A flow rule for the plastic component of the rate-of-deformation tensor $\mathbf{D}^{\mathrm{pl}}$, which we will subsequently call the plastic-strain rate as a matter of convention follows from the STZ dynamics. For a monotonically loaded, athermal system where there are no rate-dependent processes such as aging, which compete with the STZ-transition rates, and where we assume there to be a low STZ density, the flow rule can take the form,

$$\mathbf{D}^{\mathrm{pl}} = \mathbf{F}\, e^{-1/\chi} \ , \tag{3.1}$$

where $\mathbf{F} = \mathbf{F}(\mathbf{S})$ is a monotonic tensor-function of the deviatoric Cauchy stress $\mathbf{S}$. One

critical way the STZ theory differs from its predecessors (and indeed other theories) is through the introduction of the quantity χ and its relationship to the effective temperature T_{eff} discussed in Chapter 2. In the effective-temperature STZ formalism, the dimensionless scalar field χ is defined as $\chi = k_B T_{\text{eff}}/E_z$, where k_B is the Boltzmann factor. Although χ is a dimensionless form of T_{eff} we shall subsequently refer to it as simply "the effective temperature" for readability. Here E_z is a typical energy required to create an STZ. In the athermal limit the dynamical equation for the effective temperature χ takes the form

$$\dot{\chi} = \frac{\mathbf{S} : \mathbf{D}^{\text{pl}}}{c_{\text{eff}}} (\chi_\infty - \chi) + D_\chi \nabla^2 \chi \ . \tag{3.2}$$

The first term on the RHS in Eq. 3.2 represents a source of plastic work per unit time that does mechanical work on the structural degrees-of-freedom. The parameter c_{eff} is the volumetric effective-heat capacity with dimensions of energy per unit volume, determining the energy input per unit increment of effective temperature. In flowing regions χ converges to a limiting value χ_∞, which represents the steady-state effective temperature where the work done to shear the structure no longer causes an increase in disorder. The initial value χ_o characterizes the structure of the gel in the pre-sheared state, and ideally would come from an analysis of the microstructural information of the system's constituents. In the absence of this molecular-level information, the form of χ_o including the mean value and any seeding of fluctuations about the mean

are usually chosen in a way to best match the macroscopic behavior, e.g. the stress-strain curves of the material.[77–79,81] Although the range of values of χ_o for a particular system is significantly restricted by the nonlinear form of Eq. 3.2 and its stability.

The final term in Eq. 3.2 describes the diffusion of the effective temperature through an effective thermal diffusivity $D_\chi = k_{\text{eff}}/c_{\text{eff}}$ with dimensions length-squared per unit time, where k_{eff} is the effective thermal conductivity. Here we consider the simplified case where D_χ is a constant and diffusion occurs only in the presence of changes in the gradient of χ. The diffusivity D_χ itself sets a lengthscale for the simulation that is approximately the size of an STZ. We plan to address the general case of the possibility of a strain-rate-dependent diffusivity in a subsequent paper.

The effective-temperature theory as a rheological model is established in Sec. 3.2. Section 3.3 presents the results of the small-gap effective-temperature model, making direct and quantitative comparisons with the recent experimental results of,[111] including stress, fluidization time, and velocity data. The unique two-state fluidization that occurs during the transient is described and explained in terms of the dynamics of the effective-temperature constitutive law. The robustness of the model, as parametrized for a particular applied shear rate, is discussed in terms of the power-law behavior found by the experimenters. We conclude in Sec.3.4 with a discussion of the model and its implications for understanding transients during plastic flow in YSFs, and comment on the on-going development of this model.

3.2 Basic Theory

In this section we adapt the effective-temperature definition taken from the STZ theory for a small-gap Couette-cell system, whose geometry is described in Fig. 3.1a. The symmetry of the Couette cell allows us to treat the problem as an effectively one-dimensional system. We deliberately move to the small-gap limit where the curvilinearity vanishes as shown in Fig. 3.1b. This is consistent with experimental findings of a negligible inhomogeneity in the stress field across the gap such that the stress was reported as being uniform.[111–114] The complete absence of any stress gradient in the model allows us to test whether the transient shear banding can be accounted for purely by a microstructural heterogeneity occurring near the moving rotor. Indeed, we find that the effective-temperature theory is able to reproduce the experimental phenomenon in nearly every detail without including the stress gradient. We further assume that we are in the inertial limit, namely $\nabla \cdot \mathbf{S} = \mathbf{0}$ which is also consistent with the experimental conditions.

A key experimental observation of the rheology of simple YSFs is that the steady-state behavior of the system is described by the well-known Herschel-Bulkley (HB) relation,[111–114] and this will be used to determine a flow rule for $\mathbf{D}^{\mathrm{pl}}$.

3.2.1 Plastic-Strain Rate

The one-dimensional plastic-strain rate $\dot{\epsilon}^{\mathrm{pl}}$ from the STZ theory takes the form

$$\dot{\epsilon}^{\mathrm{pl}} = f(s)e^{-1/\chi} \ . \tag{3.3}$$

We next assume that the steady-state behavior of the gel is given by a HB form, namely $s = s_c + A\left(\dot{\epsilon}^{\mathrm{pl}}\right)^n$ for some parameters n and A which characterize a system that begins to unjam and flow plastically when the deviatoric stress s reaches s_c, the critical stress. Here the HB coefficient A has units of Pa·s^n, and sets the timescale for the fluidization of the gel. The plastic-strain rate is related to the measure of disordering by a function $f = f(s)$. We require that Eq. 3.3, a form of the constitutive law in the STZ theory, reduce to a HB relation when $\chi = \chi_\infty$. Therefore $\dot{\epsilon}^{\mathrm{pl}}$ in the steady state $\dot{\epsilon}^{\mathrm{pl}}_\infty$ must be

$$\dot{\epsilon}^{\mathrm{pl}}_\infty = \left(\frac{s - s_c}{A}\right)^{1/n} \ . \tag{3.4}$$

This allows f to be determined so that

$$\dot{\epsilon}^{\mathrm{pl}}_\infty = f(s)e^{-1/\chi_\infty} = \left(\frac{s - s_c}{A}\right)^{1/n} \tag{3.5}$$

and we find

$$f(s) = \left(\frac{s - s_c}{A}\right)^{1/n} e^{1/\chi_\infty} \ . \tag{3.6}$$

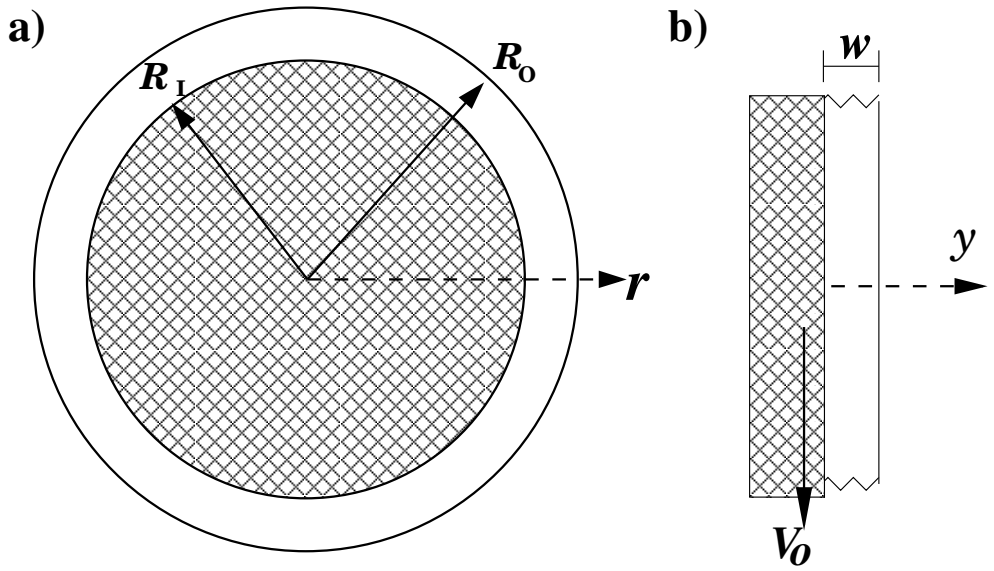

Figure 3.1: a. The edge of the inner Couette-cell cylinder ($R_{\rm I}$ = 23.9 mm) and outer cylinder edge ($R_{\rm o}$) with gel (white) where the gap width $w = R_{\rm o} - R_{\rm I} = 1.1$ mm. The inner cylinder is held at constant velocity $v_o = 0.77$ mm/s. The nucleation of a shear band begins at $R_{\rm I}$ and then broadens outward in the y-direction. b. The Couette-cell system in the small-gap limit where the curvilinearity vanishes, transforming the Couette-cell problem to a simple shear geometry. Here the system is fixed at $y = w$ and driven with speed v_o at the boundary $y = 0$.

Upon substituting the expression for f into Eq. 3.3, we arrive at the expression for the plastic-strain rate, namely

$$\dot{\epsilon}^{\rm pl} = \left(\frac{s - s_c}{A}\right)^{1/n} e^{1/\chi_\infty - 1/\chi} \ . \tag{3.7}$$

This result provides a continuum constitutive-law relating the plastic-strain rate to the deviatoric stress within the framework of an effective temperature.

3.2.2 Stress Rate

To derive the differential equation for the deviatoric-stress rate we express the strain rate as the sum of the elastic and plastic components, namely

$$\dot{\epsilon} = \dot{\epsilon}^{\rm el} + \dot{\epsilon}^{\rm pl} \ . \tag{3.8}$$

The velocity $v = v(y)$ as a function along the Couette-cell radius y in Fig. 3.1 is then given by

$$v(y) = \int \dot{\epsilon}\ dy = \int \dot{\epsilon}^{\rm el}\ dy + \int \dot{\epsilon}^{\rm pl}\ dy \tag{3.9}$$

and when integrated across the full gap-width, one finds

$$v_{\rm o} = \frac{\dot{s}w}{\mu} + \left(\frac{s - s_c}{A}\right)^{1/n} e^{1/\chi_\infty} \int_{R_{\rm o}}^{R_{\rm I}} e^{-1/\chi}\ dy \tag{3.10}$$

where μ is the shear modulus (with dimensions of stress), and $\bar{\dot{\gamma}} = v_o/w$ is the average strain-rate across the gap found by imposing a velocity v_o at the inner cylinder. The shear experiment reported in,[111] to which we are seeking to compare in detail, uses a $\bar{\dot{\gamma}} = 0.7\ \mathrm{s}^{-1}$. We use this rate in all of our simulation results, except for the stress-time profiles of Fig 3.7 where each curve corresponds to a unique $\bar{\dot{\gamma}}$. Because plastic flow is the dominant flow process for the transient shear band formation reported in,[111] we have assumed for simplicity that the elastic response is linear and that all non-linear behavior results from the plastic response. While the ramp-up of the elastic response is very brief, linear-elastic strains persist throughout the simulation and act to drive the plastic flow. The shear banding itself is an inherently plastic phenomenon and the relevant timescale for the transient dynamics comes from the plastic response. Rearranging we find that

$$\dot{s} = \mu\bar{\dot{\gamma}} - \mu\left(\frac{s - s_c}{A}\right)^{1/n} e^{1/\chi_\infty} \frac{1}{w}\int_{R_o}^{R_I} e^{-1/\chi}\, dy\ . \tag{3.11}$$

3.3 Model Simulations

The equations of motion (EOM) of the effective-temperature model that we have presented in Sec. 3.2 are

$$\dot{\epsilon}^{\mathrm{pl}} = \left(\frac{s - s_c}{A}\right)^{1/n} e^{1/\chi_\infty} e^{-1/\chi} \tag{3.12}$$

PARAMETERS	SYMBOL	UNIT	VALUE
Herschel-Bulkley exponent	n	-	0.55
Herschel-Bulkley yield stress	s_c	Pa	29.4
Herschel-Bulkley coefficient	A	Pa·s^n	1.60
Diffusivity	D_χ	mm^{2}s^{-1}	10^{-6}
Shear modulus	μ	Pa	95
Volumetric effective-heat capacity	c_{eff}	Pa	5×10^3
Steady state χ	χ_∞	-	0.064

Table 3.1: The parameters characterizing the small-gap effective-temperature model's constitutive law are presented with the values found to best match the stress-time and velocity measurements of the experiments. The "-" denotes the parameter is dimensionless. A, n, and s_c are from the Herschel-Bulkley rheology. The c_{eff}, D_χ, and χ_∞ are from the effective-temperature constitutive model.

$$\dot{s} = \mu\bar{\dot{\gamma}} - \mu\left(\frac{s - s_c}{A}\right)^{1/n} e^{1/\chi_\infty}\frac{1}{w}\int_0^w e^{-1/\chi}\, dy \tag{3.13}$$

$$\dot{\chi} = \frac{2s}{c_{\text{eff}}}\left(\frac{s - s_c}{A}\right)^{1/n} e^{1/\chi_\infty - 1/\chi}\left(\chi_\infty - \chi\right) + D_\chi\frac{\partial^2\chi}{\partial y^2}\ . \tag{3.14}$$

The three nonlinear PDEs take the form of coupled, partial integro-differential equations which we integrate in time. At time $t = 0$, $s = 0$ so that the fluid is initially unstressed in our analysis. Boundary conditions for χ must also be placed at the rotor and the outer wall of the Couette cell. We impose a no-conduction boundary condition $\partial\chi/\partial y = 0$, since χ is restricted to the gel itself.

As discussed in the Introduction the initial value of the effective temperature χ_o should ideally follow from a detailed analysis of the microstructural information about the gel. Without such detail, we are left to conjecture an appropriate χ_o. We began by following the work of Manning et al.,[77] where we assume the initial condition can

be decomposed into a background term and a fluctuation term about the background

$$\chi_o = \chi_o^{\mathrm{BG}} + \delta\chi_o \quad . \tag{3.15}$$

To simulate the disordering of the gel near the inner cylinder (rotor) we chose the simplest type of fluctuation term—a perturbation near the inner cylinder. Equation 3.15, which is shown in Fig. 3.2 was given the explicit form of a spatially uniform background $\chi_o^{\mathrm{BG}} = 0.041,\ \forall y :\ 0 \leq y \leq w$ with a perturbation $\delta\chi_o = 0.001,\ \forall y : 0 \leq y \leq 0.05$, near the inner cylinder where disordering of the structure would likely first occur, and thus nucleate a shear band.[111] We found that this value for χ_o^{BG} generated a stress-time curve that reasonably matched the range from the experiment, and the value of $\delta\chi_o$ was as small as possible without inducing purely homogeneous fluidization. The surfaces of both the inner and outer cylinders also present sites for structural heterogeneities. The slightly larger stress at the rotating inner cylinder favors localization there. Indeed, a boundary layer is known to form at the inner cylinder in the experiments, although we do not explicitly model the layer here. As discussed earlier, we ignore the stress gradient in our numerical analysis as it is assumed to be negligible for a small-gap width, other than to preference the nucleation at the inner cylinder. The ability of this fluctuation at the inner rotor to grow and lead to strain localization in the form of a shear band depends on both the size of the perturbation and the average value of χ_o, in addition to the chosen constitutive law. It

was shown in detail that small-amplitude perturbations can possibly grow during the transient regime if χ_o and its fluctuations meet an explicit criterion.[77] However, even if they grow, implying that the equation of motion for χ is unstable over some time interval, it does not guarantee that the fluctuations will form a shear band. According to,[77] the magnitude of χ_o must be below a limiting value for linear stability during the transient regime in order for strain localization to be possible. Furthermore the χ_o chosen here has a numerical localization number which is within the range corresponding to at least partial to full strain-localization. We found this χ_o field matches experimental width measurements of the shear band at early times, while also keeping the perturbation at the inner wall small enough to be a linear instability. Since larger values of the perturbation only enhance localization, we have deliberately chosen a value that would conceivably test the growth of a linear instability into a fully developed shear band. Alternatively a universal criterion for shear band formation in time-dependent fluids has been proposed by[116] whereby the shape of the stress-time curve determines when shear banding can initiate. In particular the condition that $\partial_\gamma s + \dot{\gamma}\partial_\gamma^2 s < 0$ was calculated to hold $\forall t : t \geq 3$ s. The first noticeable growth in χ (but not yet reaching χ_∞) occurs at 5 s and is shown in Fig. 3.2, exactly after the linearly elastic regime ends and flow is initiating in the form of a shear band. This criterion is therefore consistent with the onset of shear banding in the effective-temperature model.

Table 3.1 contains the values of the parameters which appear in the small-gap

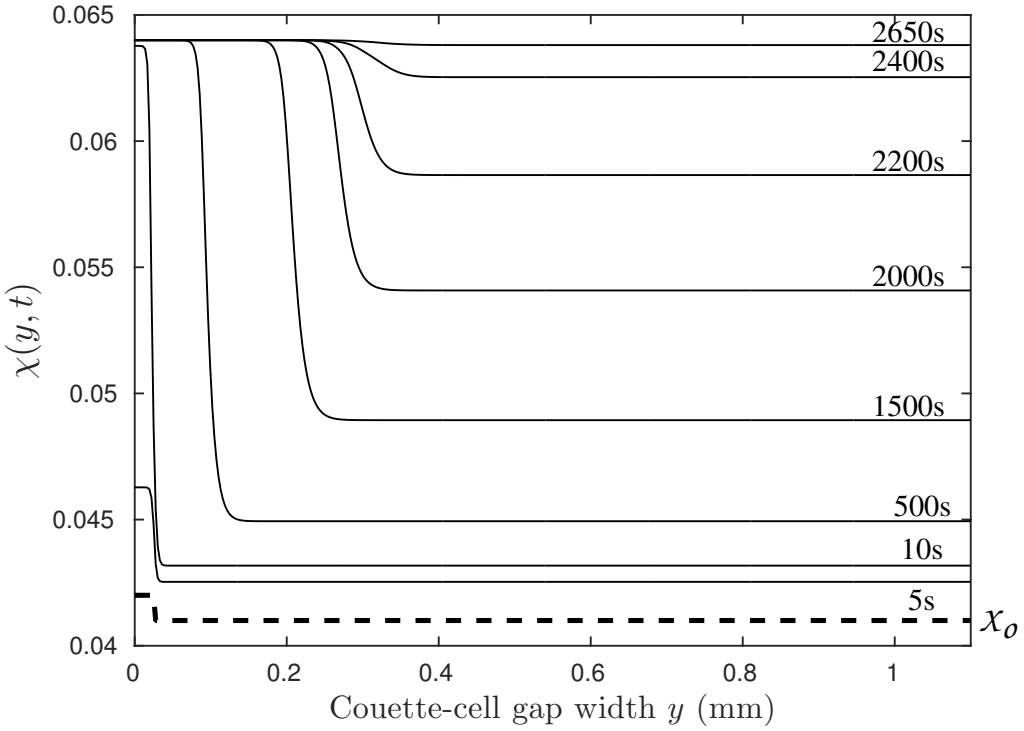

Figure 3.2: The effective temperature χ at various times during the shear-induced deformation of the small-gap model simulation. The initial field $\chi(y,0) = \chi_o$ (heavy black dashed line) containing a perturbation near the inner wall ($y = 0$) into a shear band as time evolves. The increasing value of χ shows the band broadening across the gap (y-direction) before reaching a uniform steady-state. A strain rate $\bar{\dot{\gamma}} = 0.7\ \mathrm{s}^{-1}$ is applied at the rotor.

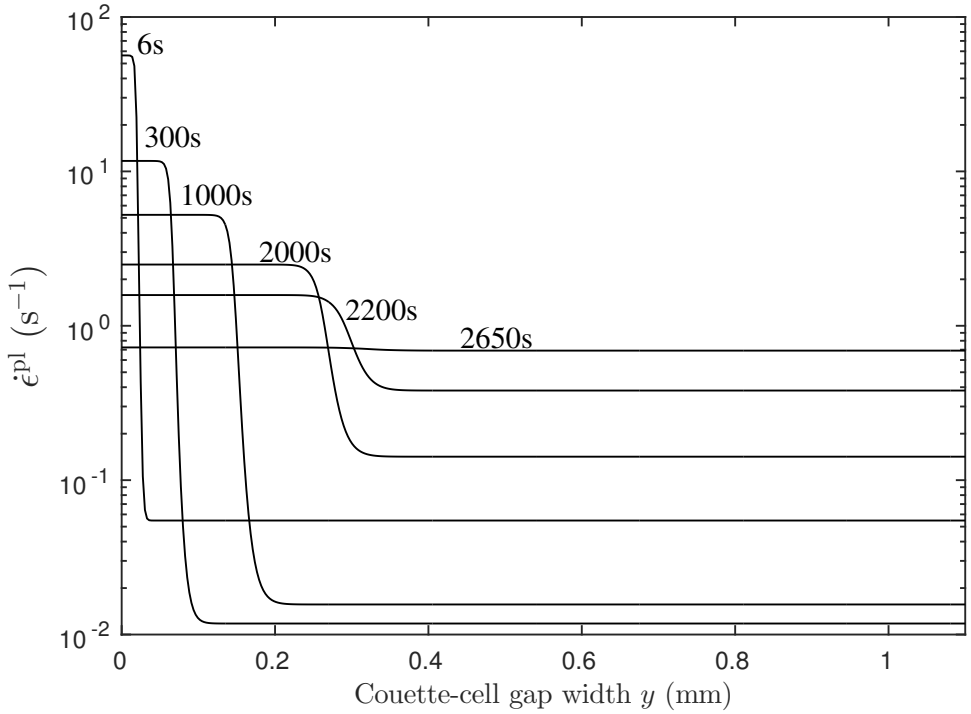

Figure 3.3: Plastic-strain rates at different times across the gap during the small-gap model simulation. As plastic strain develops in the gel, $\dot{\epsilon}^{\rm pl}$ takes on a large value near the shearing rotor ($y = 0$). As a shear band forms and traverses the gap the system fully fluidizes via a two-state process, until steady state is reached and everywhere $\dot{\epsilon}^{\rm pl} = 0.7$, the value of the applied shear-rate.

model's EOM. It includes those parameters which arise from the effective-temperature phenomenology of the model $c_{\rm eff}$ and D_χ, as well as those associated with a HB Law A, n, and $s_{\rm c}$. Once the initial effective temperature field χ_o was chosen and found to produce results which were within the range of the experimental stress-time profile, the parameters of the model were fit to the experimental velocity profiles and fluidization time, and to the precise inflection and shape of the stress-time curve. The central parameter in the effective-temperature hypothesis is the volumetric effective-

heat capacity c_{eff} which appears in the equation for $\dot{\chi}$. The quantity c_{eff} has the physical significance of being the amount of plastic work per unit volume required to cause a fractional relaxation of χ to its steady state, and its value was found to significantly determine the fluidization time and the abrupt transition of the entire system to the steady state. The shear modulus μ was set to match the experimental stress-time curve.

The experimenters also reported a flow curve in a separate set of experiments from which they extracted values for a HB steady-state rheology. The values of these experimentally reported parameters, $A = 9.8$ (Pa s^n), $n = 0.55$, and $s_{\text{c}} = 26.9$ (Pa) are inconsistent with the experimentally reported "steady-state" condition in the shear experiment that was used to produce the stress-time curve in Fig. 3.5. This is in part due to a waiting time of 100s before each stress measurement was made in the flow curve experiment, compared to the shear experiment, which we are modeling here, where the steady state does not emerge until 10,000s. The values of A and s_c are also likely dependent upon the particular sample and its preparation while the exponent n is believed to be more robust. Our constitutive law for the plastic-strain rate assumes some HB form would also hold at the long-times in the shear experiment, and hence cannot account for this discrepancy between the two types of experiments. As a starting point we initially used the HB value for A reported from the flow-curve experiments and then adjusted it to match the long-time behavior of the experiment plotted in Fig. 3.5, from which the value of s_c was extracted. We also confirm the

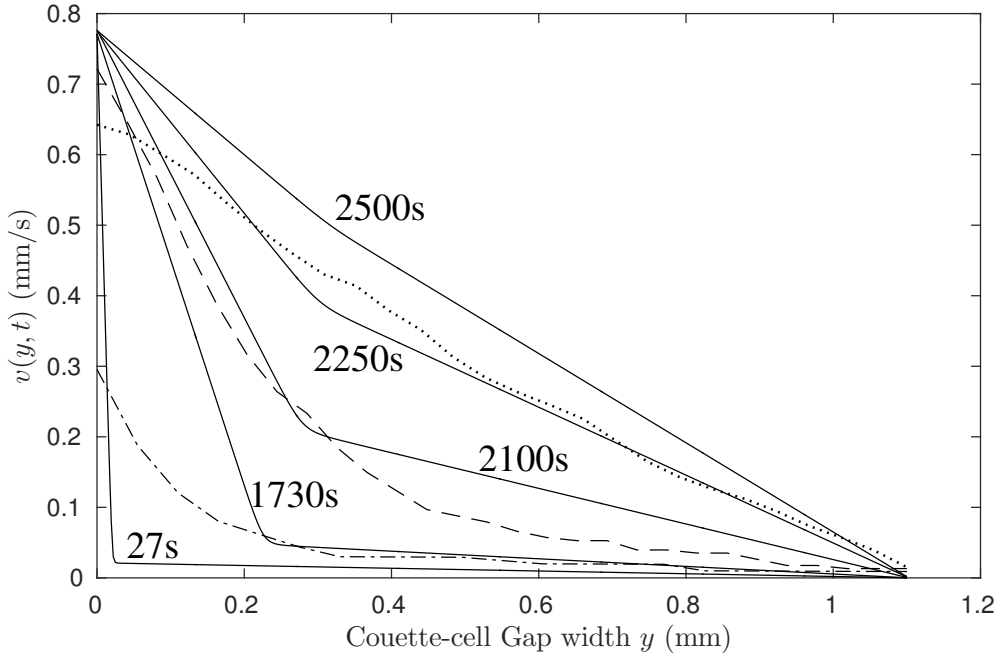

Figure 3.4: Velocity profiles at different times during the small-gap model simulation (solid curves) compared to experimental measurements at times 27 s ($-\cdot-$), 1,730 s ($--$), and 2,250 s ($\cdots$). The velocity evolves from a discontinuous profile over the gap, indicating the coexistence of a shear band with more gradual fluidization in the material outside the band. There is significant wall slip at early times in the experiments. A nearly linear profile in the steady state is observed in both the experimental measurements and the simulations.

robustness of the exponent n, as the same value of $n = 0.55$ reported experimentally also best matched the data in the model.

In the shear experiment where the rotor's velocity was held at $v = 0.77$ mm/s, the gel was initially prepared to remove memory effects using the same protocol before each experiment:[111] A pre-shear lasting 60 s at 10^3 s^{-1} was applied in the clockwise direction. Then 60 s at 10^3 s^{-1} was applied in the counterclockwise direction. The shear was then instantaneously stopped and the gel was allowed to rebuild for 120 s. The experiments then involved shearing at a constant rate for 10^4 s while the stress

was measured. A shear band was observed to nucleate near the rotating inner wall of the cell. After nucleation the band widened until the onset of fluidization, at which point the entire gel transitioned to a homogeneously flowing state, revealing a distinct process of unjamming. During the transient characterized by the broadening of the shear band, the shear rate and velocity profile of the gel outside the band were found to be non-zero.

The gel's restructuring under shear is captured by the evolution of χ during the numerical simulations. In Fig. 3.2, χ is plotted at different times during the deformation. The bottom-most, dashed black curve in Fig. 3.2 illustrates $\chi(y,0) = \chi_o$, the state before shearing begins. The time-evolution of the plastic-strain rate is described in Fig. 3.3, and reflects these changes in χ. Central to the theory is the notion that the local plastic-strain rate depends on the changing state of the amorphous structure, which is described by $\chi = \chi(y,t)$. At any time, χ quantifies the disordering of the material as it is strained or stirred. In the athermal limit, the time-evolution $\dot{\chi}$ will be nonzero only if a state of stress greater than a critical stress is present or if there are spatial variations large enough to activate diffusion through $\nabla^2\chi$. Stresses above the critical stress induce microstructural rearrangements which cause χ to evolve towards its steady-state value χ_∞.

In our effective-temperature model the steady state is determined by the two terms on the RHS of Eq. 3.2, a source term $\mathbf{S} : \mathbf{D}^{\mathrm{pl}} (\chi_\infty - \chi) / c_{\mathrm{eff}}$ and a Laplacian term $D_\chi \nabla^2 \chi$ which acts to diminish gradients in χ. As such, the steady state simply

occurs when $\chi = \chi_\infty$, since the Laplacian of χ becomes negligible in the steady state.

As was observed experimentally, the simulations reveal the formation of a shear band, which nucleates from the perturbation near the inner cylinder and begins to grow, broadening across the gap. In the simulations this is followed by an abrupt transition during which the gel reaches a fully unjammed state and completely fluidizes. We found the value of $\chi_\infty = 0.064$ to best match the sudden transition to homogeneous flow. The stress-time curve of the simulation also agrees with the experimental measurements as seen in Fig. 3.5, where in the model the gel undergoes an extremely brief, linearly elastic regime followed by plastic flow (including the transient shear banding) until the steady-state stress given by the HB relation is reached. The time needed for the shear band to grow sufficiently to accommodate the strain rate imposed across the gel results in the overshoot in the stress that is seen in Fig 3.5. This is related to the value of the initial condition for the effective temperature. For example, a stiffer, stronger, more ordered system (lower χ_o), will have a larger stress-overshoot.

The sudden fluidization of the gel after the formation of the shear band is also evident in the velocity profiles shown in Fig. 3.4. The portion of the velocity curves with the significantly steeper slope near the inner cylinder is indicative of a shear band, while the lower slope near the outer cylinder suggests that the gel outside the shear band is also gradually flowing as it fluidizes. Experimental measurements confirm the non-zero velocity for the gel in front of the shear band. Direct, quantitative comparisons of the velocity profiles of the simulations and the published experimental

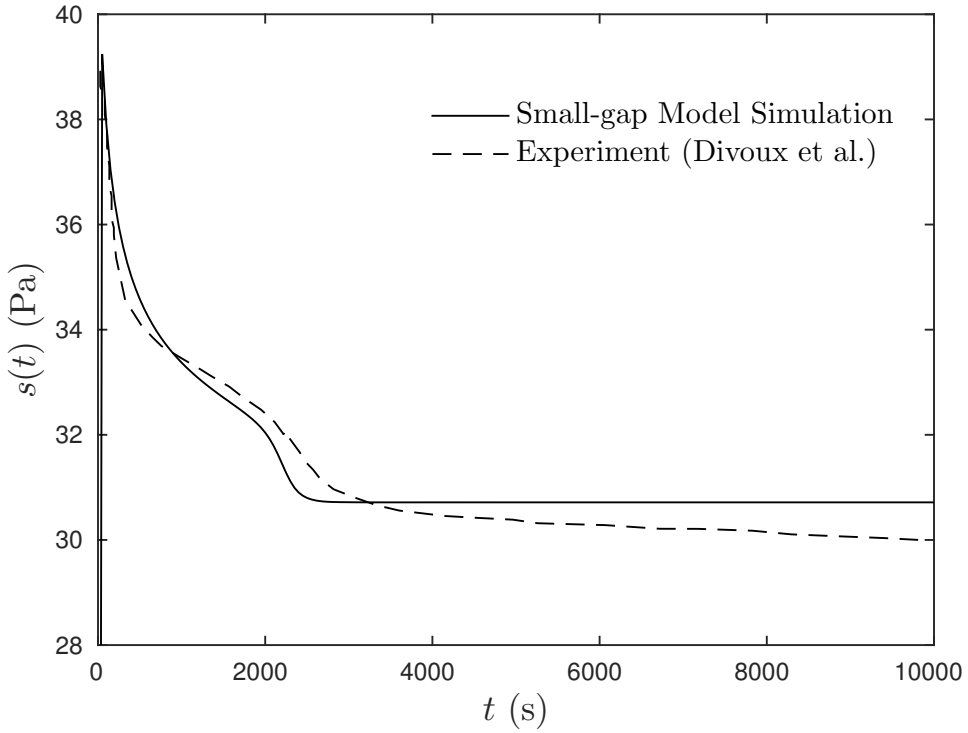

Figure 3.5: The deviatoric shear stress as a function of time for the small-gap model and the experimental stress measurements[111] under an applied strain-rate $\bar{\dot{\gamma}} = 0.7\ \mathrm{s}^{-1}$ at the rotor. Complete fluidization of the gel is experimentally observed between 2500-3000s, and is well captured by the simulation.

data are difficult because of the significant wall slip found in the experiment especially at early times, effects which are not included in the model. In Fig. 3.4 we have compared three instances from the simulations against the experimental data with reasonable agreement as the fluidization time is approached, experimentally between 2500-3000 s.

We see the presence of the two distinct fluidization processes in the model as a result of the effective-temperature dynamics and the particular form of the constitutive law from the STZ theory that we are using. The equation of motion for χ takes the form of a second-order parabolic PDE (e.g. the heat equation) with source and Laplacian terms as seen in Eq. 3.2 or 3.14. In the case of spatially homogeneous solutions, like those found in the steady state, Eq. 3.14 reduces to $\dot{\chi} = g_\chi(\chi)$, where $g_\chi(\chi) = \frac{2s}{c_{\text{eff}}} \left(\frac{s-s_c}{A}\right)^{1/n} e^{1/\chi_\infty - 1/\chi} (\chi_\infty - \chi)$ is a nonlinear, inhomogeneous term in χ. Here, the function $g_\chi(\chi)$ is similar in form (although asymptotically different) to the logistic reaction term found in the F-KPP equation that describes solidification and reaction-diffusion fronts.[118–120] In the case of the F-KPP equation, a consideration of the stability of equilibria reveals that there is one unstable fixed-point corresponding to a metastable state, and two stable fixed points into which material can be transforming as illustrated in Fig. 3.6. Similarly, g_χ also has a stable fixed-point which corresponds to the shear-banding region where χ has reached the steady-state value χ_∞. But instead of a metastable state outside the shear band, $g_\chi \to 0$ exponentially, as $\chi \to 0$. Consequently the gel outside the shear band is extremely sluggish, al-

though it remains subject to gradual fluidization in the presence of a shear stress, even far from the shear-banding region. Ultimately it is the competition between the slow fluidization of χ outside the shear band and the forward growth of the shear band that begins at the inner cylinder, that acts as the crucial element in the effective-temperature model leading to the sudden transition to homogeneous flow.

From Fig. 3.5 we see the simulation reaches the steady-state stress after approximately 2,600 s. This is also observed from the velocity profile across the gap shown in Fig. 3.4. The experimentally reported fluidization time for an applied shear-rate of $\bar{\dot{\gamma}} = 0.7$ s^{-1} was also approximately between 2500-3000 s. The experiments report a power law for the fluidization time $\tau_f \sim \dot{\gamma}^{-2.3}$ as a function of the applied shear rate $\dot{\gamma}$ over a range $0.08 \leq \dot{\gamma} \leq 10$ (s^{-1}) using several boundary conditions and sizes of gap width. The effective-temperature model is able to recover approximately the same exponent for a subset of the rates from about $0.1 \leq \bar{\dot{\gamma}} \leq 2.0$ centered on $\bar{\dot{\gamma}} = 0.7$, the specific $\bar{\dot{\gamma}}$ for which the model's parameters have been determined with $w = 1.1$mm and where a no-slip boundary condition is implicitly assumed. The faster the shear rate in the model is, the faster fluidization and homogeneous flow is reached, and consequently the transient shear band travels a shorter distance across the gap. Figure 3.7 shows the power-law fit for our simulations. Outside this subset the τ_f predicted by the model begins to deviate by about an order of magnitude. Interestingly however, the experimental fluidization times outside this subset can still be recovered if c_{eff} is adjusted (re-parametrized) to a lower value for very small shear

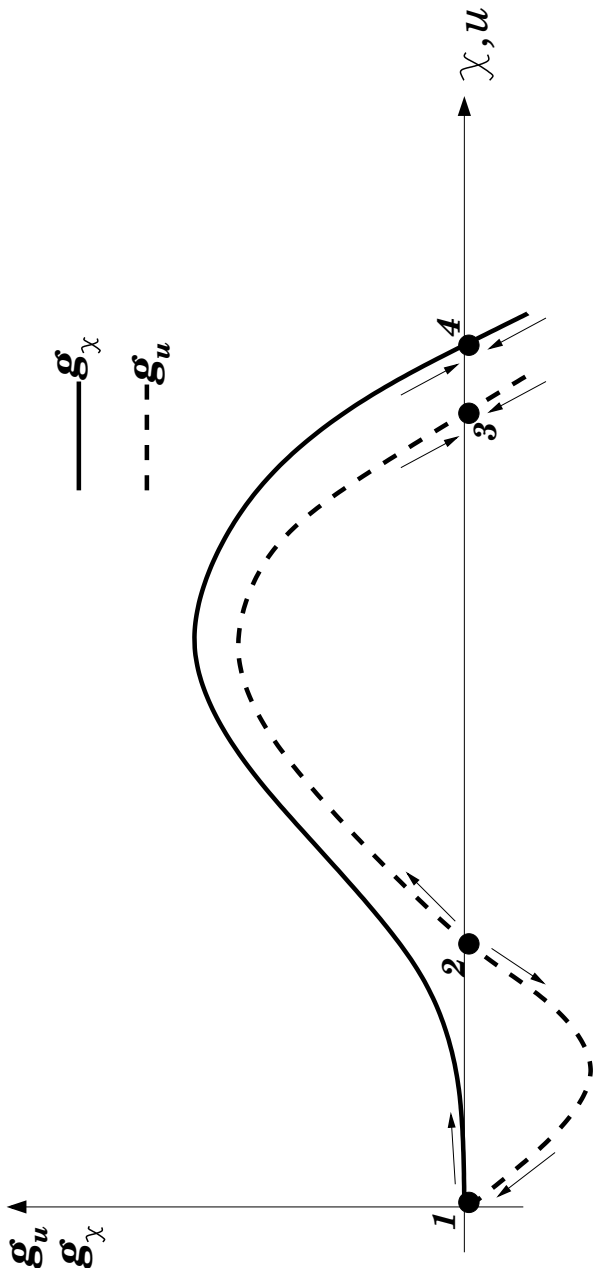

Figure 3.6: Fluidization outside the transient shear band: A comparative sketch of the form of the F-KPP equation $\partial_t u - \partial_x^2 u = g_u(u)$ (dashed curve) and $\partial_t \chi - D_\chi \partial_x^2 \chi = g_\chi(\chi)$ (solid curve) in the effective-temperature theory. Points 1 and 3 represent stable fixed-points for $g_u(u)$ which can describe distinct stable phases of a system into which material that is in a metastable state, represented by the unstable fixed-point at 2, could be transforming. In the effective-temperature model however, only one fixed point exists at 4; it is stable and corresponds to the shear band where $\chi = \chi_\infty$, the flowing steady state. For small χ near point 1, corresponding to the gel outside the shear band, $g_\chi(\chi) \to 0$ due to $e^{-1/\chi}$. However no fixed point exits at 1 for $g_\chi(\chi)$, and this feature allows the gel outside the shear band to slowly fluidize through a distinct process of its own.

rates, and increased for the largest shear rates. This would imply that the fraction of plastic work that goes into disordering the gel increases (decreases) as the strain rate increases (decreases), and the power law of the fluidization time $\tau_f \sim \dot{\gamma}^{-\alpha}$ may arise in part from this aspect of the physics. This could reflect rate effects in the gel's mechanical response which cause the gel to accommodate deformation through structural disordering at high rates that it could accommodate through independent relaxation processes at low rates. An analysis of the effect of strain-rate dependence is beyond the scope of the theme of this paper, since the model here has not explicit rate-independent. We nonetheless think this is an important direction for future work. To our knowledge no other theoretical models describing the solid-fluid transition make any quantitative predictions for the fluidization times which agree (within an order of magnitude) with these experiments over any range of rates.

3.4 Conclusions

We have presented a phenomenological effective-temperature model for the small-gap limit of Couette-cell shear experiments of a carbopol gel where transient shear banding is observed. This theoretical model is based on the STZ description, and results in two distinct fluidization processes: the shear band formation and the simultaneously competing homogeneous fluidization. We have made direct, quantitative comparisons with experiments which demonstrate reasonable agreement with the

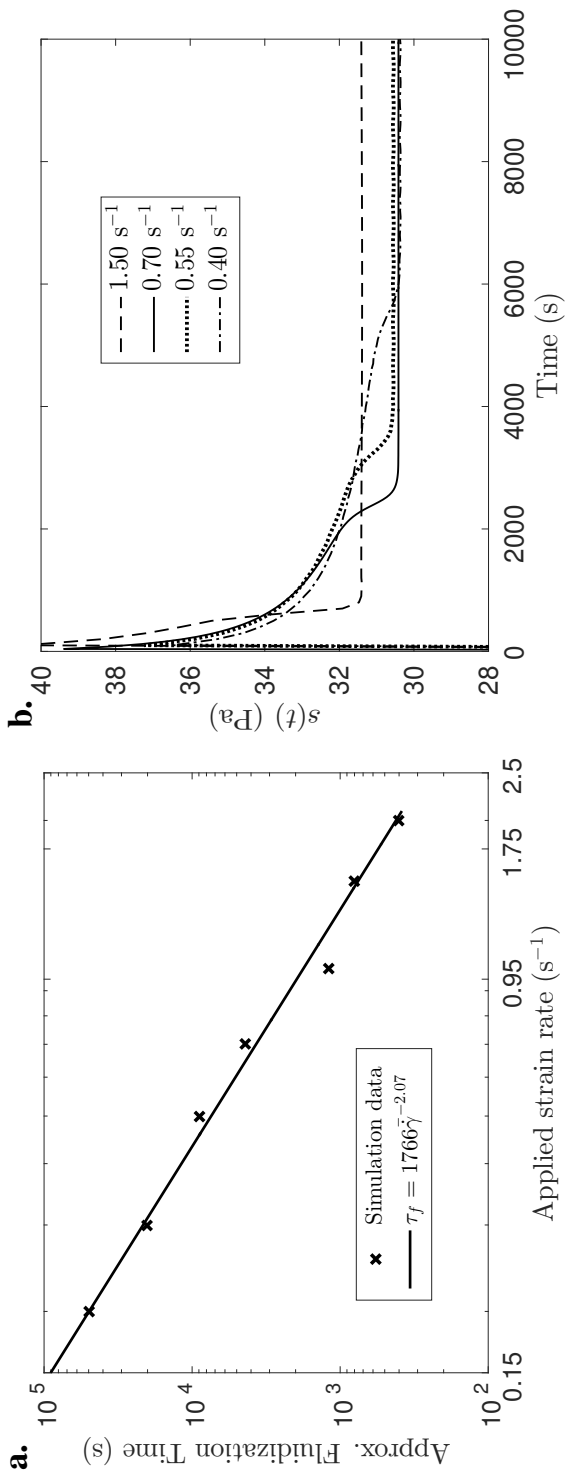

Figure 3.7: a. The simulated fluidization times τ_f of the model which was parameterized for the case $\bar{\dot{\gamma}} = 0.7\ s^{-1}$ where $w = 1.1$mm, and assuming a rough boundary condition. Experimenters have reported a universal power law $\tau_f \sim \dot{\gamma}^{-2.3}$ for a wider range of shear rates, various boundary conditions, and several different gap widths. b. The stress-time curves at different imposed strain-rates (inner cylinder velocities) from which the fluidization times (at the onset of the steady state) were extracted.

stress-time behavior and velocity profiles of the gel.

In this theory, consistent with the interpretation of,[111] stress gradients are not the primary cause of the strain localization or the fluidization. The small-gap limit of the effective-temperature model strongly suggests that the transient shear banding and sudden fluidization is primarily a result of microstructural disordering originating from structural heterogeneities at the inner cylinder of the Couette cell where the rotor applies the shear. While the gradient is at least negligibly present kinematically, our analysis suggests that it may play little role in the constitutive relation for a YSF under shear—and no role for a small-gap system. This is in contrast to other theoretical descriptions in which the strain localization is directly associated with the fluidization and comes solely from the non-linear response of the fluid coupled to the stress inhomogeneity that arises from the cylindrical geometry of the Couette-cell.[117] One possible experimental check would be to see if such transient shear banding and fluidization would take place if the experiment[111] were repeated for a different shear geometry, such as shearing the gel between two parallel plates. The absence of any normal stresses from the model's constitutive law suggests to us that such stresses are not necessary to account for the transient shear banding, as was also found by the λ-based rheological models discussed in the Introduction.

The effective-temperature theory also improves several aspects of existing visco-plastic models which lack any notion of a yield stress, a defining physical feature of YSFs. The mechanical response of the gel is quantitatively well captured by the small-

gap simulations, as evidenced by the stress-time curve. The small-gap simulations in this paper reveal the two-stage fluidization seen in experiments, and we have shown that in the model it is directly attributable to the particular form of the constitutive law postulated by the effective-temperature theory. The parameters of the theory provide a physical connection to the thermodynamics of the gel's structural state under shear. One open question is the origin of the strain-rate dependence of the fluidization time for very large and very small rates . A possible explanation is that the volumetric effective-heat capacity, describing the fraction of plastic work that disorders the gel and emerges phenomenologically in the effective-temperature dynamics, is strain-rate dependent and can no longer be approximated as uniform over a wide-enough range of rates.

The effective-temperature approach that we have proposed offers an important rheological model for both current and future experiments, and responds to a need that was identified by the experimenters for developed theoretical models of transient shear banding in simple YSFs.[111] We also believe our approach would benefit from further development, and are currently investigating an extension of this approach for finite-gap systems with non-negligible stress gradients. We are also currently attempting a version of this theory with a rate-dependent diffusivity and steady-state effective temperature. Beyond this a number of consequential phenomena exist which we have largely ignored in the present model, e.g. aging and wall slip, both of which are known to play at least some role in the recent shear experiments of carbopol.

A generalization of this model and incorporation of such additional physics is also a matter of our on-going research.

3.5 The Case of Finite-gap Width and Radially Dependent Stress

As discussed in the Introduction, the ability of the λ-based rheological model in[117] to exhibit transient shear banding depends only on the gradient of the stress field due to the cylindrical geometry of the Couette cell. In the Sec. 3.3 we presented an effective-temperature description based on the STZ theory of plastic flow in the small-gap limit where we dealt only with a uniform stress field across the gap. The changes in the structure of the gel were therefore attributable entirely to the dynamics of the effective temperature and the growth of an instability. Our small-gap model would therefore imply that a microstructural process is the likely origin of the transient shear band. However the influence of the stress-gradient in forming the transient shear band remains unclear. We now turn to the case of a Couette-cell with a finite-gap width where a gradient in the stress field contributes to the effective-temperature dynamics.

3.5.1 Equations of Motion

To investigate the effect of a radially varying stress in our model, we derive similar equations of motion for a cylindrical curvature representative of a gap of finite width. If a shear stress $s_o = s_o(t)$ is imposed by the rigid inner-cylinder at R_I in Fig. 3.1 (now with cylindrical coordinates so that $y \longrightarrow r$), the resulting stress along the radial direction $s = s(r,t)$ in the inertial limit is

$$s = \frac{R_\mathrm{I}^2 s_o}{r^2} \quad \forall r: \; R_\mathrm{I} \leq r \leq R_\mathrm{I} + w \tag{3.16}$$

The constitutive law for the plastic-strain rate and the effective temperature, analogous to Eqs. 3.12 and 3.14 are,

$$\dot{\epsilon}^\mathrm{pl} = \left(\frac{\frac{R_\mathrm{I}^2 s_o}{r^2} - s_c}{A} \right)^{1/n} e^{1/\chi_{ss}} e^{-1/\chi} \tag{3.17}$$

$$\dot{\chi} = 2\frac{R_\mathrm{I}^2 s_o}{c_\mathrm{eff} r^2} \dot{\epsilon}^\mathrm{pl} (\chi_\infty - \chi) + D_\chi \frac{\partial^2 \chi}{\partial y^2} \tag{3.18}$$

$$\tag{3.19}$$

A similar integration of Eq. 3.8 with respect to the radial position r, yields an expression for the velocity along the gap,

$$v(r) = \int_{R_\mathrm{I}}^{r} \dot{\epsilon} \; dr = \int_{R_\mathrm{I}}^{r} \dot{\epsilon}^\mathrm{el} \; dr + \int_{R_\mathrm{I}}^{r} \dot{\epsilon}^\mathrm{pl} \; dr \tag{3.20}$$

$$= \frac{R_\mathrm{I}^2}{\mu} \dot{s}_o \int_{R_\mathrm{I}}^{r} \frac{dr}{r^2} + \int_{R_\mathrm{I}}^{r} \dot{\epsilon}^\mathrm{pl} \; dr \tag{3.21}$$

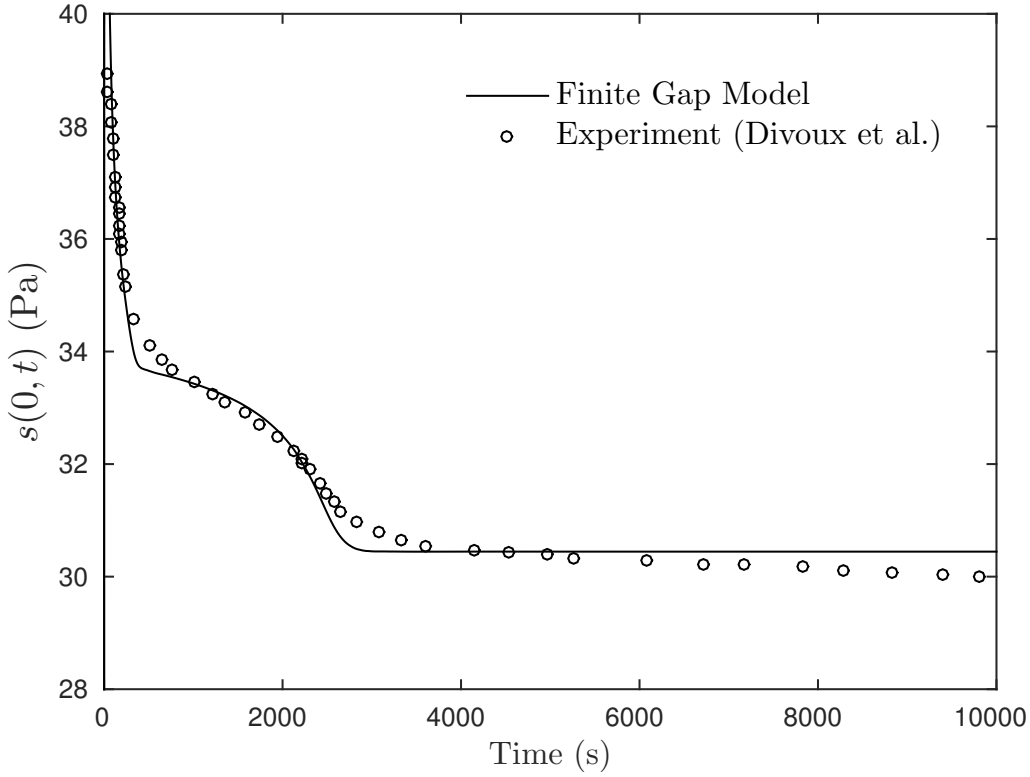

Figure 3.8: The deviatoric stress at the inner cylinder (rotor) of the Couette cell as a function of time for the finite-gap model and the experimental measurements[111] under an applied strain-rate $\bar{\dot{\gamma}} = 0.7\ \mathrm{s}^{-1}$.

and at $r = R_\mathrm{I}$ is

$$v_o = \frac{R_\mathrm{I}^2}{\mu}\dot{s}_o \int_{R_\mathrm{I}}^{R_\mathrm{I}+w} \frac{dr}{r^2} + \int_{R_\mathrm{I}}^{R_\mathrm{I}+w} \dot{\epsilon}^{\mathrm{pl}}\, dr\ . \tag{3.22}$$

The equation of motion for $\dot{s}$ is reduced to determining an equation for $\dot{s}_o$ since it carries all of the time dependence i.e. $\dot{s} = R_\mathrm{I}^2 \dot{s}_o / r^2$. By integrating Eq. 3.8 across

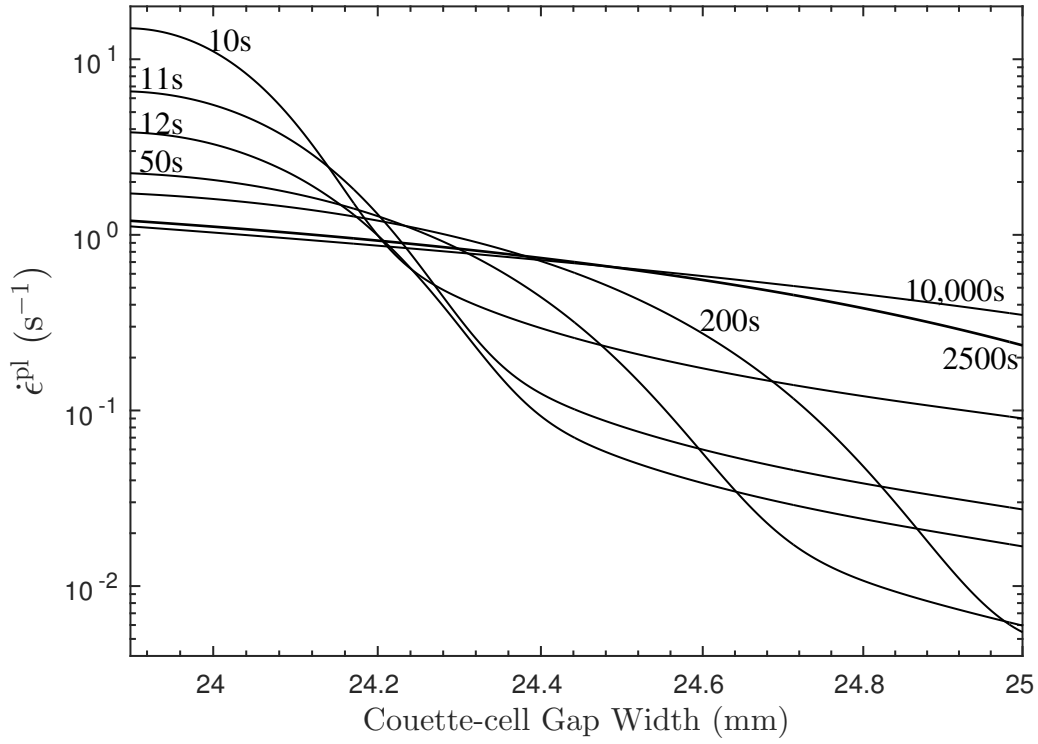

Figure 3.9: Plastic-strain rates at different times across the gap during the finite-gap model simulation.

the entire gap we find

$$\dot{s}_o = \frac{\mu(R_{\rm I}+w)}{R_{\rm I}w}\left(\dot{\gamma}w - \int_{R_{\rm I}}^{R_{\rm I}+w} \dot{\epsilon}^{\rm pl}\, dr\right) . \tag{3.23}$$

3.5.2 Model Simulations

The stress is measured experimentally at the inner cylinder (rotor) and shown in Figs. 3.5 and 3.8. The gap width of $w = 1.1$ mm then implies that the variation in the stress field is at most 8.6%, smallest at the outer cylinder. The initial effective-

PARAMETERS	SYMBOL	UNIT	VALUE
Herschel-Bulkley exponent	n	-	0.65
Herschel-Bulkley yield stress	s_c	Pa	25.5
Herschel-Bulkley coefficient	A	Pa·s^n	4.6
Diffusivity lengthscale	l^2	mm^2	0.01
Elastic shear modulus	μ	Pa	45
Volumetric effective-heat capacity	c_{eff}	Pa	1.0455×10^3
Steady state χ	χ_∞	-	0.11

Table 3.2: The parameters characterizing the finite-gap effective-temperature model. The "-" denotes the parameter is dimensionless.

temperature is a uniform value, $\chi_\infty = 0.055,\ \forall y :\ R_{\text{I}} \leq y \leq R_{\text{I}} + w$ across the gap. The higher stress at the rotor in the finite-gap model replaces the need for a perturbation in χ_o at the rotor, instead the variability of the stress initially drives χ in the vicinity of the rotor to a higher value. This can be seen in Fig. 3.10, where disordering happens very quickly near the rotor but then plateaus at a value less than χ_∞, after which the disordering concentrates on spreading outward across the gap. A perturbation similar to that used in the small-gap model was also tested together with the radially dependent stress and the results differed only negligible from a uniform χ_o.

The strain-localization is also apparent from $\dot{\epsilon}^{\text{pl}}$ in Fig. 3.9, but remains well below the very large strain-localization seen in the small-gap model where χ is immediately driven to χ_∞ at the rotor, a clear signature of a shear band and a completely flowing region. The transition of the gel from the transient shear-banding regime to the homogeneous steady state, which is well captured by the small-gap model, appears

to be absent in the finite-gap dynamics.

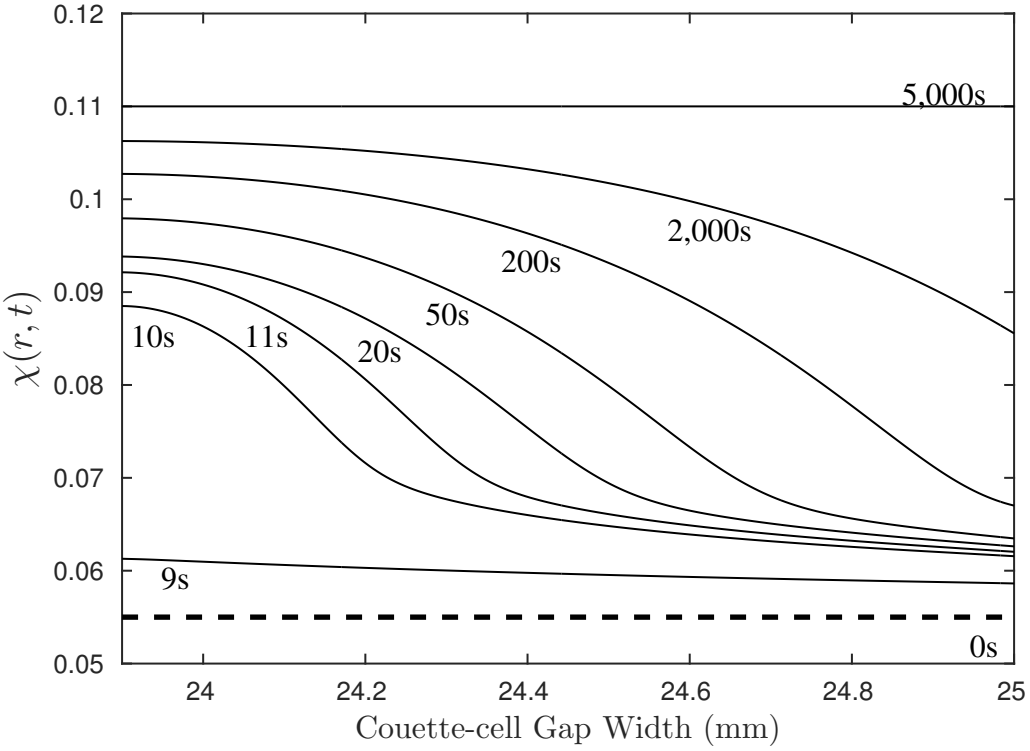

Figure 3.10: The dimensionless effective temperature χ at various times during the shear-induced deformation for the finite-gap model. The initial field $\chi(y,0) = \chi_o$ (heavy black dashed line) is uniform across the gap, while the stress varies radially. A shear band develops early on, plateaus at a value less than χ_∞, and then moves across the gap. The behavior is distinctly different from the small-gap model and the experiments.

Further evidence that the behavior of the evolving structure in the finite-gap model is in stark contrast to that of the small-gap model is reflected in the velocity profiles shown in Fig. 3.11. The two, separate fluidization processes identified by the small-gap model and seen in the experiments are not present here. Instead the velocity of the material outside the moving front does not independently and sluggishly begin to flow; it remains in a jammed state until it encounters the interface of the

shear band. As such there is now no mechanism to cause the sudden arrest of the shear band and spontaneous fluidization of the entire gel. Finally we see the velocity profile approaches a shape that seems significantly influenced by the $1/r^2$ form of the stress field, and not the linear Couette-flow that is expected as the steady state is approached. The parameters for the finite-gap model are shown in Tab. 3.2.

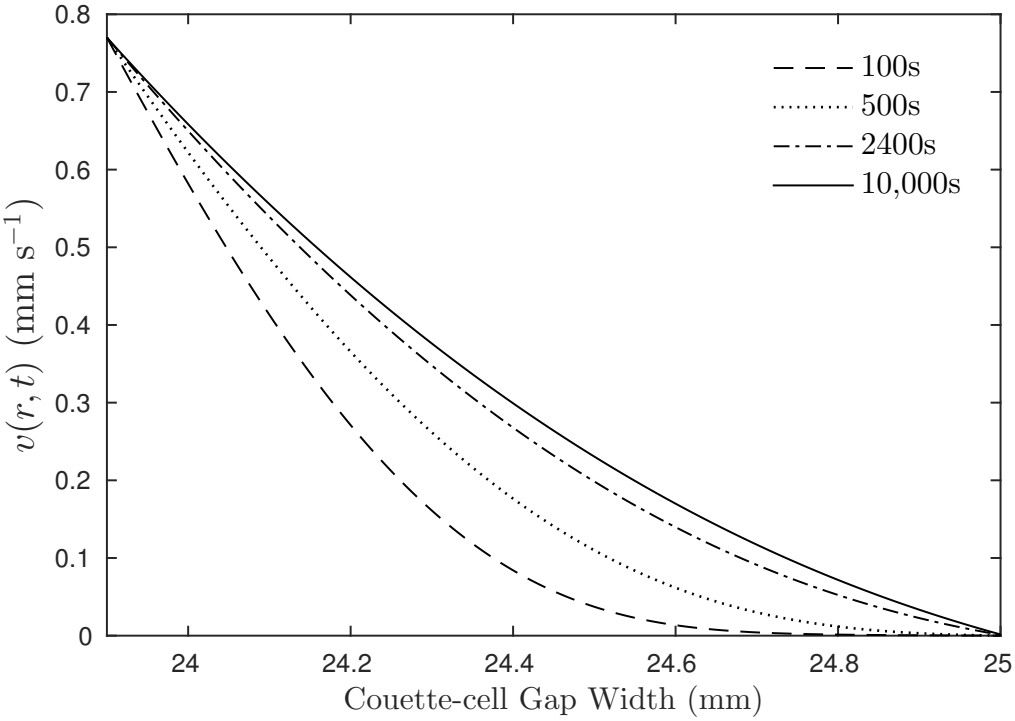

Figure 3.11: Velocity profiles at different times during the finite-gap model simulation. The velocity across the gap does not evolve to a linear Couette-flow profile, and the material outside the flowing region does not simultaneously unjam.

Chapter 4

Bridging from atoms to continua: modeling shear deformation in metallic glass

4.1 Introduction

Metallic glasses are a promising new class of materials possessing many highly desirable mechanical properties, most notably their high strengths which result from high yield stresses that are much closer to the theoretical limit than their crystalline counterparts.[121] They are however not without their drawbacks, in particular metallic glasses fail brittlely, a limitation that curtails their use in structural and technological applications. These materials are alloys of two or more elemental constituents

which can be either metallic metalloid. Depending upon which metal is the dominant component of the alloy, they may be labeled as Zr-based, Al-based, Fe-based, etc. To emphasize the nature of the constituent elements, they can be characterized as metal-metal type or metal-metalloid type. Different alloys have different glass-forming abilities, and good glass formers which can be cast into a fully glassy sample at least 1 mm in its thinnest dimension are conventionally called bulk metallic glasses.[122]

The potential of metallic glasses as engineering materials would be enhanced significantly by an understanding of their behavior at the continuum level with the same degree of predictability that has long been established for more common crystalline materials. A well-formulated continuum theory for metallic glasses would have far fewer degrees-of-freedom (DOF) than detailed atomistic simulations, and would be capable of providing a computationally efficient description of the mechanical response. In particular, it would predict the macroscopic details of plasticity through an integrable set of field equations under the continuum assumption that a representative volume element (RVE) exists. The RVE has been defined as the smallest material volume element of the system for which the usual spatially constant macroscopic constitutive representation is a sufficiently accurate model to represent mean constitutive response.[123] This continuum assumption is equivalent to neglecting the local heterogeneity of the stresses and strains within the RVE, working with averaged quantities, as the effects of the heterogeneities act only indirectly through a certain number of "internal variables".[124] For crystalline materials a great number of meth-

ods have been constructed using the continuum hypothesis to describe elasto-plastic behavior, including nonlocal, energy-based, and multiscale frameworks.[124,125]

Selectively reducing the number of DOF contained in atomistic simulations is essential to a predictive continuum-level description. However, differences in system complexity and purpose of modeling often lead to difficulties in developing a universal method for coarse-graining.[126] Attempts to formulate generalized coarse-graining frameworks which account for a wide range of physical phenomena (e.g. elasticity and electrical conductivity) often result in a complex coarse-graining procedure with large numbers of parameters and a diminished representation compared to frameworks following a phenomena-dependent focus. Several rigorous methods have been developed for equilibrium systems where there is a well-defined partition function.[127,128] In most cases of amorphous solids however, their out-of-equilibrium nature precludes such clear statistical mechanics-based descriptions. Metallic glasses, in particular, deform in an interesting way. Their high strength leaves them without work-hardening capacity, and to the contrary, they exhibit work softening. The unfortunate consequence of this is that deformation is sharply localized into shear bands. Shear banding, as the name implies, is a form of a plastic instability that localizes large shear strains in a relatively thin band when a material is deformed.[121,129] In the study of the mechanical properties of metallic glasses, the most important phenomena-dependent focus of any coarse-graining methodology is the ability to capture the formation of shear bands. A shear band has the ability to broaden and invade the surrounding

material outside the band which remains nearly undeformed.[130–132] Shear bands have been widely observed in metals, polymers, the earth's mantle, granular solids, yield stress fluids, and many other materials, including liquids under shear flow.[129] In metallic glasses shear banding is the primary mode of deformation and failure. At room temperature, metallic glasses yield via the formation of shear bands, and usually fail catastrophically with limited compressive plasticity and little or no tensile ductility.[122]

In the case of metallic glasses and other out-of-equilibrium materials the nature of the RVE has not been well investigated and remains largely unknown. As briefly discussed in Chapter 2 some earlier work has attempted to address the problem of coarse-graining the amorphous microstructure by connecting the original STZ transition-rate equations to finite element calculations[66,133,134] and evolving the system using a kinetic Monte Carlo algorithm. Similar techniques have been applied to three-dimensional systems[135] and connections to the realistic timescales of experiments have been made. Another mesoscale model based on interface pinning-depinning has been proposed which describes plasticity in amorphous solids by allowing local interfaces to slip in a random fashion.[62] Significant limitations exist with these approaches. In nearly all cases the RVE is merely taken to be the size of an individual STZ and the elements of the coarse-grained mesh are assigned *a priori* some allowed number of rearrangements, and so the fundamental question regarding how to correctly average over experimental or atomistic data of the amorphous microstructural has not been

addressed. Moreover these approaches have no connection to fundamental thermodynamic considerations which are known to be essential in describing the shear-induced disordering of the material's structure during plastic deformation. Only rather modest and tangential comparisons to experiments and atomistic simulations using these techniques have been shown so far, usually a demonstration that the model can produce some feature of the deformation qualitatively, such as the presence of a yield stress or a stress-strain history that is typical of a metallic glass. It is the purpose of this Chapter to propose a methodology for coarse-graining the discrete, experimental or atomistic simulation data of an amorphous solid like a metallic glass into a continuum field that is the initial condition to a constitutive law capable of describing the plasticity common to these materials when subjected to shear.

In this study we preform molecular dynamics (MD) simulations of amorphous copper-zirconium (CuZr) under an applied shear rate, and we present a preliminary methodology to coarse-grain the atomistic system with the purpose of identifying and predicting the onset of shear banding. In Sec 4.2 we present the details of the coarse-graining methodology and the observed shear banding in the MD simulations. Then in Sec. 4.3 we define a signal-to-noise ratio and use it to distinguish the shear-band "signal" from a "background" through a criterion that connects the mechanical response to the coarse-grained potential energy. Section 4.4 applies this same coarse-graining procedure to the atomic potential energies of the CuZr glass in the pre-sheared state to extract an initial condition for the effective temperature field. We compare the MD

simulation of the shear along side the results of the effective-temperature evolution and stress-strain history from a two-dimensional quasi-static numerical implementation of the STZ theory. We conclude in Sec. 4.5 with a discussion of how this preliminary work can inform future efforts to develop continuum theories of amorphous materials where coarse-grained representations of atomistic data are used to parametrize and validate the material models.

4.2 Coarse-graining Methodology

MD simulations were preformed using the LAMMPS software[136] with a well-established Embedded-Atom-Method (EAM) interaction potential.[122] The initial pre-sheared glass was formed by taking a 50-50 composition of CuZr with 297,680 total atoms and then quenching the equilibrated liquid at a rate of 10^{11} K/s to a temperature $T = 100$K. The system is $400 \times 400 \times 30$ Å, three-dimensional but thin in the out-of-plane direction (30Å) allowing us to treat the system as effectively two-dimensional. A non-equilibrium molecular dynamics (NEMD) shear simulation shown in Fig. 4.1 was preformed by deforming the simulation box of the quenched glass under simple shear conditions at constant volume and temperature with periodic boundary conditions in all directions enforced by the SLLOD[137] equations of motion. A timestep of 0.005 picoseconds (ps) and an applied shear rate $\dot{\gamma} = 10^{-4}$ ps^{-1} were used. The system was held at 100K for the duration of the shear. The

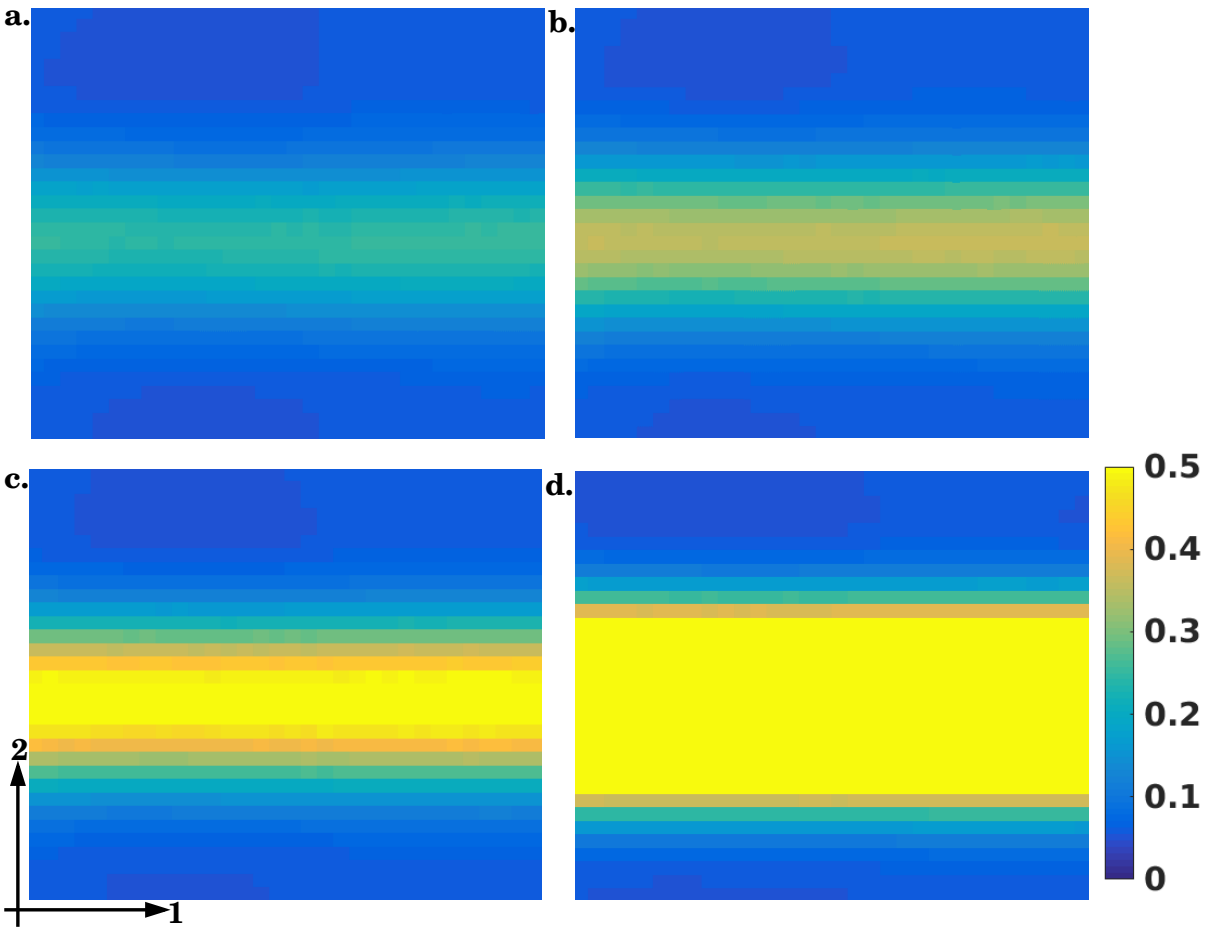

Figure 4.1: The CuZr NEMD simulation containing 297,680 total atoms with dimensions 401 x 401 x 33Å using an EAM potential and periodic boundaries. The thin dimension is perpendicular to the shear direction. Local atomic shear strain $2\epsilon_{12}$ at: a) 11.5%, b) 15%, c) 20%, and d) 50% global strain. The initial system was prepared by quenching the CuZr liquid at a rate of 10^{11}K/s to a temperature of 100K. The glass is then further equilibrated at 100K under constant pressure, and then sheared at a rate $\dot{\gamma} = 10^{-4}\text{ps}^{-1}$ using an NVT thermostat at 100K. The shear band is evident at 11.5% strain.

NEMD shear simulation revealed the formation of a shear band that formed near the center of the simulation box. The shear band was aligned with the direction of shear and continued to broaden as the system was deformed.

The corresponding coarse-grained system is defined by a two-dimensional square grid of equally spaced continuum points. Initial studies showed that the potential energies of the Cu and Zr were essentially uncorrelated with one another in the pre-sheared glass. This motivated us to select a Gaussian function $g_n = g(r_n, c)$ of the form

$$g_n = \frac{2}{\sqrt{2\pi}c} \exp\left(-\frac{r_n^2}{2c^2}\right) \tag{4.1}$$

to weight the contributions of the individual atomic DOF. The function g_n is centered on continuum point α and r_n is the distance from α to atom-n within a coarse-grained region determined by the cut-off radius r_{cut}. The coarse-grained atomic potential energy E_α at continuum point α, for instance, is given by

$$E_\alpha = \frac{\sum\limits_n g_n E_n}{\sum\limits_n g_n} \quad . \tag{4.2}$$

The coarse-graining map is entirely determined by the choice of the parameter c which sets the width of the g_n and hence determines the spatial extent of the MD data influencing the value of the continuum field. The relationship between c and the minimum r_{cut} can be determined from a convergence analysis:

- Select a grid of continuum points $m \times m$, and a fixed c, where $c < r_{cut}$.

- Choose a large cut-off radius r_{max}, in this case $r_{max} = 20c$, and a set S of test values for r_{cut} in terms of c, i.e. $S = \{2c, 3c, 4c, \ldots, 8c\}$. Note $s \in S$ and $s_{max} = r_{max}$.

- Using the fixed c, coarse-grain the MD system with weighting function g_n.

- Calculate the convergence of the L_2 norm of the potential energy

$$||E(s) - E(s_{max})||_2 = \sqrt{\sum_{\alpha=1}^{m^2} \left[E_\alpha(s) - E_\alpha(s_{max})\right]^2} \; . \tag{4.3}$$

  where $E_\alpha(s)$ is the coarse-grained potential energy at point α using a particular r_{cut} from the set S, and $E_\alpha(s_{max})$ is the energy at point α using r_{max}

- Find the r_{cut} for which L_2 is sufficiently converged. This $r_{cut} = r_{conv}$ defines the relationship between any choice of c and the minimum r_{cut} that maintains convergence by

$$q_{conv} = \frac{r_{conv}}{c}$$

  so that $r_{cut} = q_{conv}\ c$. Figure 4.2 shows the degree of convergence of L_2 for the specific choices of c and r_{max}. In the case where the potential energy is the field quantity of interest, L_2 norm convergence to better than 1% is indicated as long as $r_{cut} \geq 3c$.

A similar convergence analysis determined the minimum spacing between continuum points d for a given choice of the coarse-graining width c. Instead of varying r_{cut}

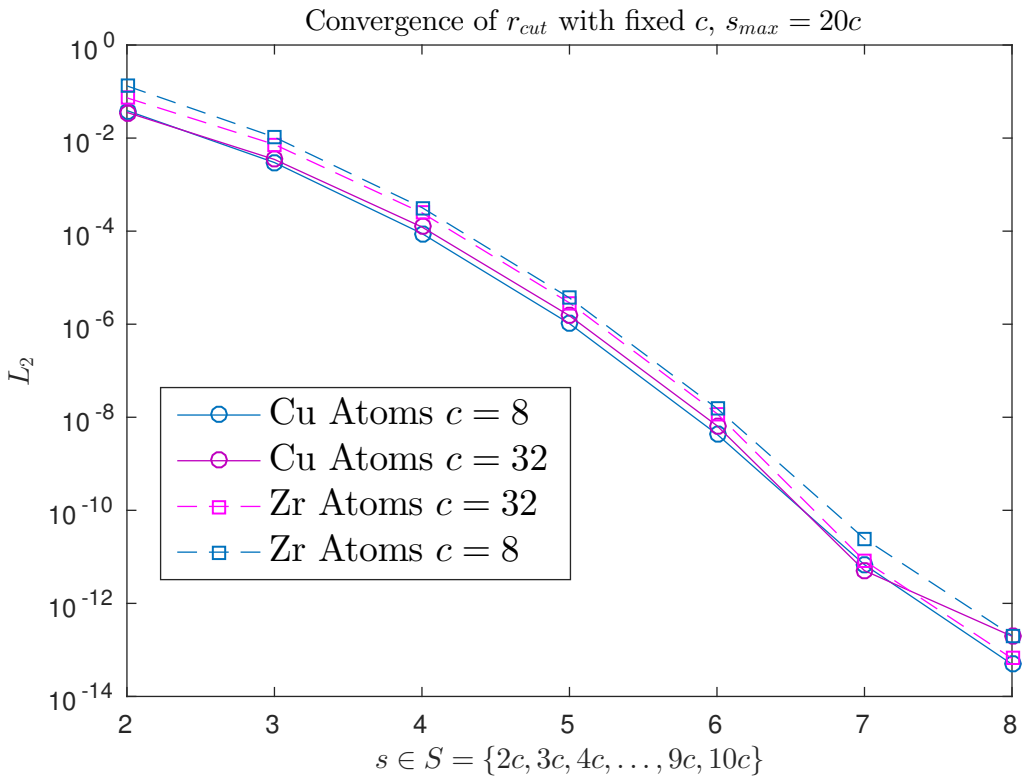

Figure 4.2: Convergence of $||E(s) - E(s_{max})||_2$ indicated that $r_{cut} = 3c$.

as in the previous analysis, we vary d with the goal of finding α establishing the relationship $d = \alpha c$.

- Select a fixed c.
- Select a set S of d spacings (or equivalently a set of grids with a different number of continuum points), for example

$$S = \{25 \times 25, 50 \times 50, 75 \times 75, \}$$

.

- Select a maximum density of grid points to be s_{max} corresponding to minimal spacing d_{min}.

- Define an L_2 norm for the difference in energy E_α between elements of S and s_{max} by

$$||E(s) - E(s_{max})||_2 = \sqrt{\sum_{\alpha=1}^{m^2} \left[E_\alpha(s) - E_\alpha(s_{max})\right]^2} \; .$$

  Here the sum over α again refers to the number and locations of the continuum points in $E_\alpha(s_{max})$ and the corresponding points in $E_\alpha(s)$ must be interpolated from the coarser continuum grid.

- Plot L_2 convergence as done for the convergence analysis of $r_{\rm cut}$, but as function of s. Figure 4.3 shows the L_2 norm as defined above. For a grid of 100×100 points convergence is achieved to better than 0.1%. Two sets of results are presented, one which counts only the Cu atoms in the system and the other counting only the Zr atoms. The results support the same conclusion for achieving the minimal continuum-point convergence.

- Determine α and the relationship $d_{conv} = \alpha\sigma_o$. This procedure should be redone for different values of c to ensure that α remains the same. The α should be a constant if convergence is achieved, and this in turn sets the correct minimum value of d for a given c. In this case for the initial analysis done where $c = 16$

in Fig. 4.3, noting that $d_{conv} = L/100$, we therefore find

$$\alpha = \frac{d_{conv}}{c} = 0.251 \tag{4.4}$$

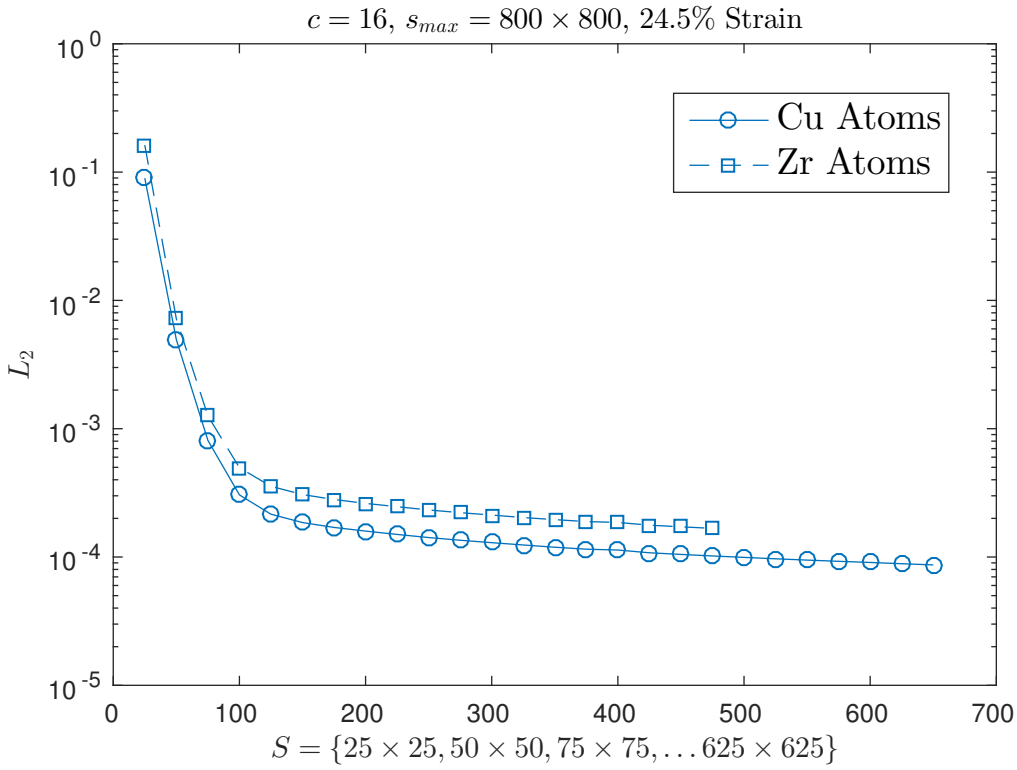

Figure 4.3: Convergence of $||E(s) - E(s_{max})||_2$ for $s_{max} = 800 \times 800$ points indicated that $d_{conv} = 0.251c$.

The application of this coarse-graining procedure to the potential energies of the pre-sheared glass is relatively straightforward, however during the shear simulation it is necessary to compute such coarse-grained field quantities at a given timestep. A proper continuum-level description requires a choice of either Lagrangian or Eulerian coordinates, and we have chosen a Lagrangian approach in what follows, as this is the

typical description for solids. In the Lagrangian description, the material points are defined with respect to a reference configuration and continuum fields are functions of the reference coordinates $\mathbf{X}$ and current time t. In the case of the coarse-grained potential energy $E_\alpha = E_\alpha(\mathbf{X}, t)$. Therefore the MD system is only coarse-grained based on atomic positions in the initial configuration at $t = 0$ before shear and the evolution of these coarse-grained regions is determined by changes in the potential energies of the atoms pre-assigned to them.

The local atomic strain can also be calculated in a way that is consistent with this coarse-graining method through an adaptation of the definition of non-affine displacement originally proposed by Falk and Langer.[59] The measure of non-affinity is determined by minimizing the mean-square difference between the actual displacements of the neighboring atoms relative to the central one and the relative displacements that they would have if they were in a region of homogeneous deformation. The square of the error $D^2_{\min}$ can be written as,

$$D^2_{\min} = \sum_n g_n^2 \sum_i \left(x_n^i - x_o^i - \sum_j F_{ij} \left(X_n^j - X_o^j \right) \right)^2 \tag{4.5}$$

The indices i and j denote spatial coordinates x^i at time t during the shear and X^j in the reference configuration. The index n runs over the atoms within the coarse-graining region α, where $n = 0$ is the reference atom with coordinates x_o^i and X_o^j, chosen to be closest to the centroid of the region. We have found this is a better choice

than an arbitrary atom which can present computational anomalies for regions with a small number of atoms or for large strains. Equation 4.5 differs from the original[59] in that it is a *weighted* least-squares formulation, and because it is generalized for finite deformations. The minimization of $D^2_{\min}$ fits the deformation gradient tensor F_{ij} from which the Green-Lagrange strain can be calculated as

$$\epsilon^{\alpha}_{ij} = \frac{1}{2}\left(\sum_k F^{\alpha}_{ki} F^{\alpha}_{kj} - \delta_{ij}\right) \ . \tag{4.6}$$

Figure 4.1 shows the shear component $2\epsilon_{12}$ at four different global strains[1]. The size of the region α is 50Å. At 11.5% global strain the shear band is apparent and the shear localization begins to increase. The band also broadens perpendicular to the applied shear out to 50% where the shear band subsumes nearly half of the system.

4.3 Signal and Noise in Molecular Dynamics

We have developed the coarse-graining methodology of the previous section with the goals of identifying the mechanical response of the glass in the molecular dynamics simulations. Specifically, we would like to address the following questions:

[1]The global strain γ is the total shear strain due to the imposed velocity at the boundary of the simulation box. It is equivalent to the sum of the shear components of the strain tensor, namely $\gamma = 2\epsilon_{12}$.

1. How do the atomic potential energies of the glass evolve in specific regions of the material undergoing differing degrees of deformation?

2. How does the choice of a coarse-graining lengthscale affect the atomic potential energies in different regions of the material?

3. What is an *optimal* coarse-graining lengthscale for the prediction of shear band development in terms of an applicable constitutive theory?

The focus of this section is to provide a means to address questions 1 and 2, whereby the atomic strain calculation that was described in the previous section is coupled to an identically coarse-grained set of energy states. In particular we would like to use this coupling to distinguish the coarse-grained potential energy states inside the shear band from those outside the band. We also would like to know the effect of different coarse-grained representations on the identification of states inside and outside the band. A full discussion of question 3 is deferred until the next section since this requires a description of the applicable constitutive theory .

A consideration of Fig. 4.1 motivates us to define the shear band as simply the set of coarse-grained atomic strains that have reached or exceeded the net strain, or more precisely the signal of the shear band is the set

$$\mathscr{S} = \{\epsilon_{12}^{\alpha} \mid \epsilon_{12}^{\alpha} \geq \gamma\} \tag{4.7}$$

where γ is the nominally imposed strain at the boundary. Figure 4.4 shows the

continuum states in both the signal and background as the system evolves from the purely elastic ramp-up through the onset of the shear band, and into the flow-stress regime where the coarse-graining lengthscale c is 50Å. Figures 4.5,4.6,and 4.7 show the signal and noise for coarse-grained representations where $c = 32$, 16, and 5Åwhere the coarse-graining takes place over the Cu atoms of the CuZr system.

The signal and noise plots in Figs. 4.4,4.5,4.6,and 4.7 feature an entirely mechanical response, in the sense that the distinction between signal states and background states is a binary choice based solely upon whether a given continuum point α has a local strain that satisfies the criterion of Eq. 4.7. However this criterion for the mechanical response of the system can be directly related to the potential energy. The right side of Figs. 4.4,4.5,4.6,and 4.7 contains histograms of the coarse-grained potential energies at the corresponding continuum points of the signal and background, identifying the signal and background as two distinct energy distributions.

The emergence of the shear band can be readily seen through the relative changes in these distributions. In the purely elastic start-up the system is comprised of a fluctuating mixture of signal and background without any strain localization. The average of $2\epsilon_{12}^{\alpha} = \gamma$ at all times during the deformation to satisfy compatibility. During the elastic regime the distributions of the signal and background comprise essentially the same distribution. At 3.5% strain Tabs. 4.3,4.3,4.3,and 4.3 show the means of the signal and background to be nearly identical, as well as a negligible

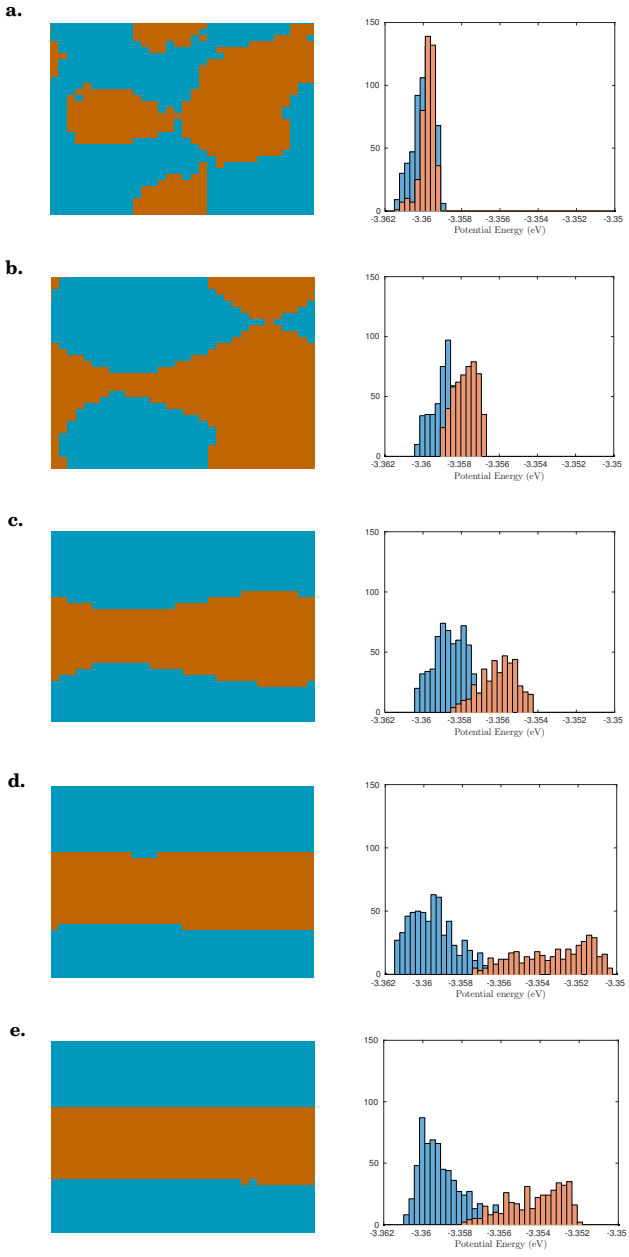

Figure 4.4: Map (left column) of continuum points for a coarse-grained representation of the Cu atoms where $\sigma = 50$Å defining the signal (orange) of the shear band and the background (blue). Histograms (right column) of the corresponding coarse-grained potential energies in the shear band and background. Configurations shown at global shear strain: a) 3.5%, b) 9.5%, c) 10%, d) 10.5%, and e) 27.5% global strain.

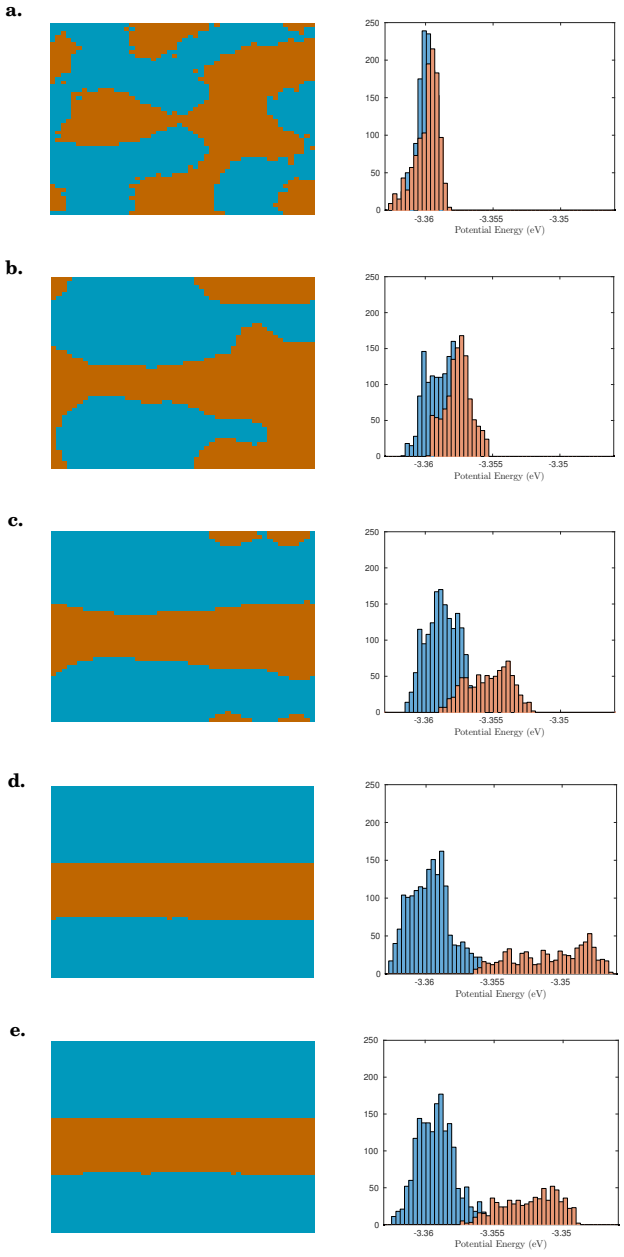

Figure 4.5: Map (left column) of continuum points for a coarse-grained representation of the Cu atoms where $\sigma = 32$Å defining the signal (orange) of the shear band and the background (blue). Histograms (right column) of the corresponding coarse-grained potential energies in the shear band and background. Configurations shown at global shear strain: a) 3.5%, b) 9.5%, c) 10%, d) 10.5%, and e) 27.5% global strain.

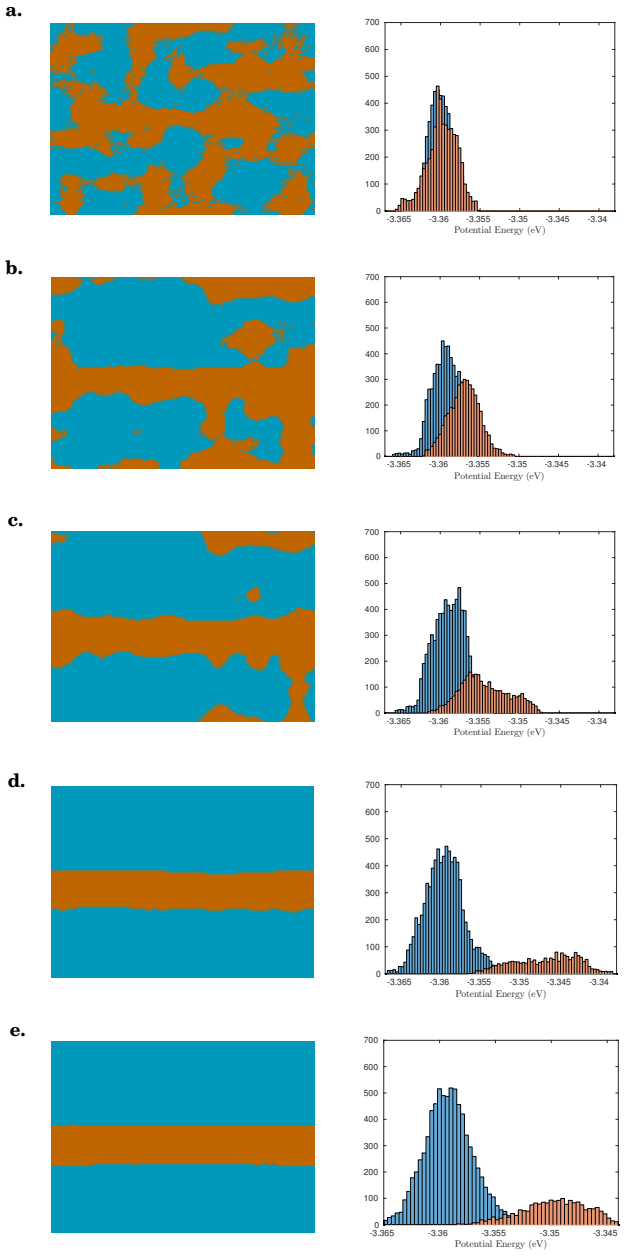

Figure 4.6: Map (left column) of continuum points for a coarse-grained representation of the Cu atoms where $\sigma = 16$Å defining the signal (orange) of the shear band and the background (blue). Histograms (right column) of the corresponding coarse-grained potential energies in the shear band and background. Configurations shown at global shear strain: a) 3.5%, b) 9.5%, c) 10%, d) 10.5%, and e) 27.5% global strain.

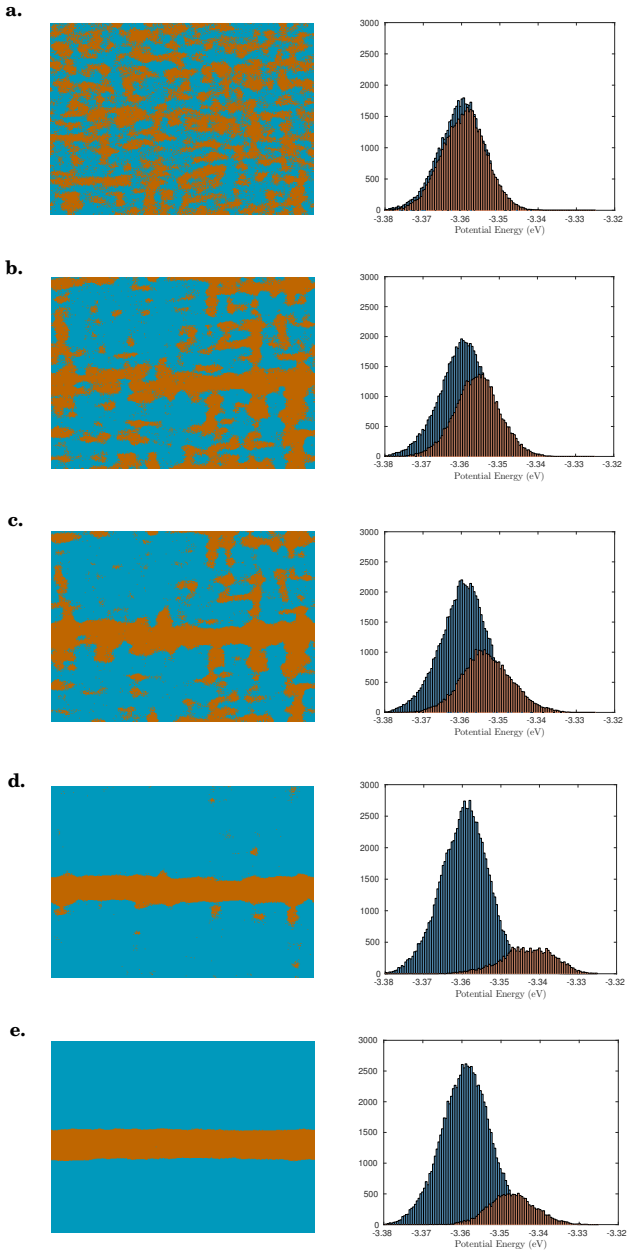

Figure 4.7: Map (left column) of continuum points for a coarse-grained representation of the Cu atoms where $\sigma = 5$Å defining the signal (orange) of the shear band and the background (blue). Histograms (right column) of the corresponding coarse-grained potential energies in the shear band and background. Configurations shown at global shear strain: a) 3.5%, b) 9.5%, c) 10%, d) 10.5%, and e) 27.5% global strain.

signal-to-noise ratio (SN) defined as

$$\mathrm{SN} = \frac{|\mu_s - \mu_b|}{\sigma_b} \tag{4.8}$$

where μ_s and μ_b are the means of the signal and background, respectively, and σ_b is the standard deviation of the background. The SN is also shown in Fig. 4.8 as a function of global strain for different coarse-grained representations. A proto-shear band begins to develop at 9.5% strain and the two distributions begin to show a separation in their mean values. Figure 4.8 shows that while the shear band begins its initial stages of formation as the system is sheared closer to a strain of 9.5%, the signal $\mu_s - \mu_b$ appears to first rise above the noise σ_b (when SN$>$ 1) for $c = 50$ to 16Å. For the values of c presented here, the value of the noise is also lower as the representations become coarser. This would suggest a preference for the coarser representations, with $c > 16$Å, in capturing the presence of the shear band.

The shear band is fully formed across the system at 10.5% strain, as can be seen at each level of coarse-graining shown in Figs. 4.4,4.5,4.6, and 4.7. This also corresponds to the largest SN value, evidenced by both the significant separation in the means of the distributions as well as the occupation of the highest energy states. Once the signal and background distributions have distinctly separated, they remain so throughout the shear simulation. We have observed that once the shear band has formed at approximately 10.5% strain, the SN tends to monotonically increases with

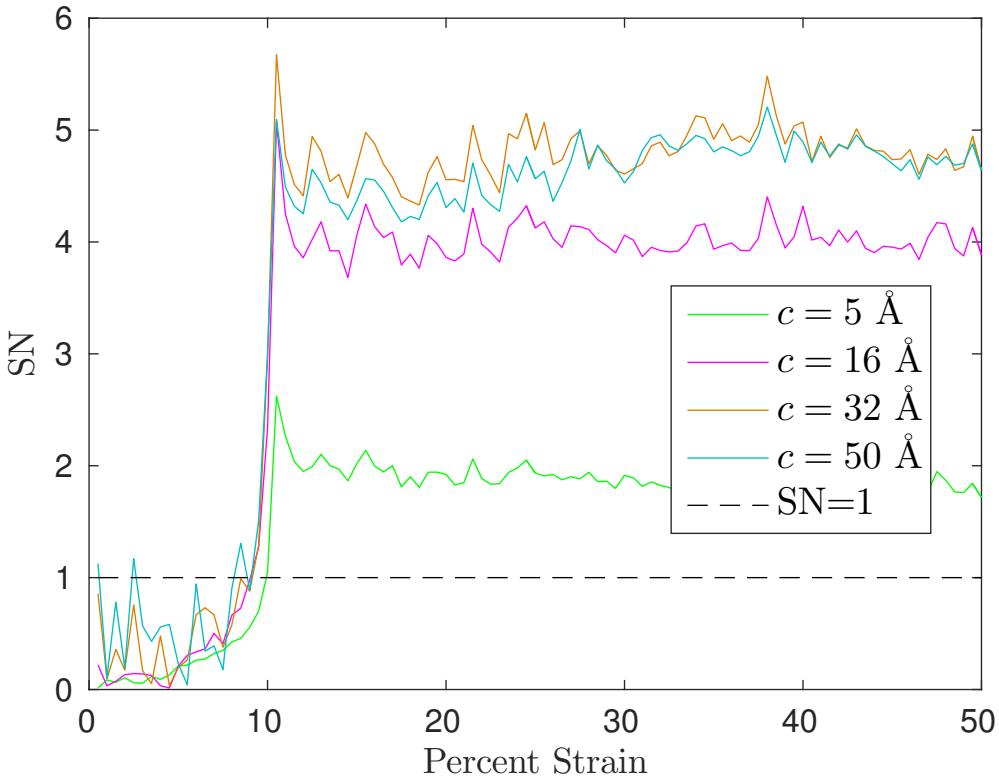

Figure 4.8: The SN as function of global strain for different coarse-grained representations defined by c in g_n. The signal $\mu_s - \mu_b$ exceeds the noise σ_b only when SN > 1 (dashed line).

Strain	μ_s	μ_{bg}	σ_s	σ_{bg}	SN
3.5%	-3.3598	-3.3600	0.0004	0.0005	0.4377
9.5%	-3.3578	-3.3588	0.0006	0.0007	1.4735
10%	-3.3561	-3.3586	0.0009	0.0008	2.9933
10.5%	-3.3533	-3.3595	0.0019	0.0012	5.0282
27.5%	-3.3542	-3.3591	0.0014	0.0011	4.4564

Table 4.1: The statistics of the coarse-grained energy states in the signal and background distributions at different strains for a coarse-grained representation where $c = 50$Å. The mean μ_s and standard deviation σ_s of the signal and the μ_b and σ_b of the background. The signal-to-noise ratio SN $= \frac{|\mu_s - \mu_b|}{\sigma_b}$ defines the strength of the shear band in the energy background.

Strain	μ_s	μ_{bg}	σ_s	σ_{bg}	SN
3.5%	-3.3599	-3.3599	0.0009	0.0007	0.0456
9.5%	-3.3576	-3.3589	0.0010	0.0010	1.2834
10%	-3.3553	-3.3588	0.0016	0.0012	2.9560
10.5%	-3.3508	-3.3596	0.0027	0.0016	5.5121
27.5%	-3.3524	-3.3592	0.0020	0.0014	4.8784

Table 4.2: The statistics of the coarse-grained energy states in the signal and background distributions at different strains for a coarse-grained representation where $c = 32$Å. The mean μ_s and standard deviation σ_s of the signal and the μ_b and σ_b of the background. The signal-to-noise ratio SN $= \frac{|\mu_s - \mu_b|}{\sigma_b}$ defines the strength of the shear band in the energy background.

the width of the coarse-graining as Fig. 4.8 shows. An exception occurs when $c = 32$ is reached if the Cu atoms are used in the analysis, as has been done in the results presented here, although this is not statistically significant. A similar analysis of only the Zr atoms however, reveals a steady monotonic increase in SN after shear band formation up to the imposed $r_{\text{cut}} = L/2$ required by the minimum image convention.

Strain	μ_s	μ_{bg}	σ_s	σ_{bg}	SN
3.5%	-3.3598	-3.3600	0.0019	0.0015	0.1307
9.5%	-3.3569	-3.3593	0.0020	0.0018	1.2811
10%	-3.3544	-3.3590	0.0030	0.0020	2.3322
10.5%	-3.3469	-3.3595	0.0039	0.0025	5.0488
27.5%	-3.3497	-3.3591	0.0029	0.0023	4.0965

Table 4.3: The statistics of the coarse-grained energy states in the signal and background distributions at different strains for a coarse-grained representation where $c = 16$Å. The mean μ_s and standard deviation σ_s of the signal and the μ_b and σ_b of the background. The signal-to-noise ratio SN $= \frac{|\mu_s - \mu_b|}{\sigma_b}$ defines the strength of the shear band in the energy background.

Strain	μ_s	μ_{bg}	σ_s	σ_{bg}	SN
3.5%	-3.3595	-3.3602	0.0058	0.0058	0.1226
9.5%	-3.3558	-3.3599	0.0058	0.0059	0.6920
10%	-3.3534	-3.3596	0.0065	0.0060	1.0346
10.5%	-3.3431	-3.3594	0.0069	0.0063	2.5906
27.5%	-3.3471	-3.3589	0.0058	0.0064	1.8623

Table 4.4: The statistics of the coarse-grained energy states in the signal and background distributions at different strains for a coarse-grained representation where $c = 5$Å. The mean μ_s and standard deviation σ_s of the signal and the μ_b and σ_b of the background. The signal-to-noise ratio SN $= \frac{|\mu_s - \mu_b|}{\sigma_b}$ defines the strength of the shear band in the energy background.

4.4 Effective-Temperature Model

We now return to the last question raised at the beginning of the preceding section, namely, is there an optimal coarse-grained representation of the molecular dynamics potential energy for the purposes of predicting shear band development using the effective temperature theory described in Sec. 2. The coarse-graining methodology presented in Sec. 4.2 provides us with the machinery to extract the initial structural state of the pre-sheared glass via the atomic potential energies as a single, coarse-grained field. Prior studies of purely two-dimensional Lennard-Jones systems have suggested that the potential energy is linearly related to the effective temperature T_{eff} of the glass.[94] The effective temperature of the as-quenched glass can then be used as the initial condition for a continuum model of the evolution of the plastic deformation. Moreover, the methodology we have developed connecting the atomistic quantities to a continuum representation allows us to make direct comparisons between the MD system and the model at any time during the shear deformation.

A flow rule for the plastic component of the rate-of-deformation tensor $\mathbf{D}^{\text{pl}}$ follows from the dynamics of the STZ theory. For a monotonically loaded, athermal system where there are no rate-dependent processes such as aging, which compete with the STZ-transition rates described in Sec. 4.1, and where we assume there to be a low

STZ density, the flow rule can take the form,

$$\mathbf{D}^{\mathrm{pl}} = \frac{\epsilon_{\mathrm{o}}}{\tau_{\mathrm{o}}} \mathrm{e}^{-1/\chi} \left(1 - \frac{1}{||\tilde{\mathbf{S}}||}\right) \mathbf{F}, \tag{4.9}$$

where $\mathbf{F} = \mathbf{F}(\tilde{\mathbf{S}})$ is a monotonic tensor-function of the deviatoric Cauchy stress in terms of the yield stress s_y, $\tilde{\mathbf{S}} = \mathbf{S}/s_y$. When $||\mathbf{S}|| < s_y$ there are no plastic rearrangements and $\mathbf{D}^{\mathrm{pl}} = \mathbf{0}$. A family of symmetric functions of the stress has been identified as having the correct properties for $\mathbf{F}$, such as $\mathbf{F} \to \mathbf{0}$ when $\mathbf{S} \to \mathbf{0}$ and $\mathbf{F} \to \mathbf{F}_\infty$ a finite bound as $\mathbf{S} \to \infty$.[138] Here we have chosen one of the simplest forms

$$\mathbf{F} = -\mathbf{2} + ||\tilde{\mathbf{S}}|| + \exp\left(-||\tilde{\mathbf{S}}||\right)\left(\mathbf{2} + ||\tilde{\mathbf{S}}||\right) \tag{4.10}$$

which has worked well in one-dimensional continuum STZ analyses.[77] The parameter $1/\tau_o$ is the inherent attempt frequency of the material, which is close to the Einstein frequency, and sets a timescale for the "flips" or rearrangments of the STZs. The average STZ is believed to contain approximately 5 to 10 atoms, and this is denoted by the value of ϵ_o.

In the effective-temperature STZ formalism, the dimensionless scalar field χ is defined as

$$\chi = \frac{k_B T_{\mathrm{eff}}}{E_z} \tag{4.11}$$

where k_B is the Boltzmann factor. Although χ is a dimensionless form of T_{eff} we shall

subsequently refer to it as simply "the effective temperature" for readability. Here E_z is a typical energy required to create an STZ. In the athermal limit the dynamical equation for the effective temperature χ takes the form

$$c_o\dot{\chi} = \frac{\mathbf{S} : \mathbf{D}^{\mathrm{pl}}}{s_{\mathrm{y}}} (\chi_\infty - \chi) + \nabla \cdot D_\chi \nabla\chi \ . \tag{4.12}$$

The first term on the RHS in Eq. 4.12 represents a source of plastic work per unit time that does mechanical work on the structural degrees-of-freedom when the $||\mathbf{S}|| > s_y$. The parameter c_o determines the fraction of plastic work that increases the effective temperature. In flowing regions χ converges to a limiting value χ_∞, which represents the steady-state effective temperature where the work done to shear the structure no longer causes an increase in disorder.

The initial value χ_o characterizes the structure of the glass in the pre-sheared state, and ideally would come from an analysis of the atomistic information of the system's constituents. In the absence of this per-atom information, the form of χ_o including the mean value and any seeding of fluctuations about the mean are usually chosen in a way to best match the macroscopic behavior, e.g. the stress-strain curves of the material. The ability of the fluctuations in χ_o to grow and lead to strain localization in the form of a shear band depends on both the size of the fluctuations and the average value of χ_o,[77,116] which underscores the need for χ_o to capture the structural state of the pre-sheared glass with the appropriate level of physical detail.

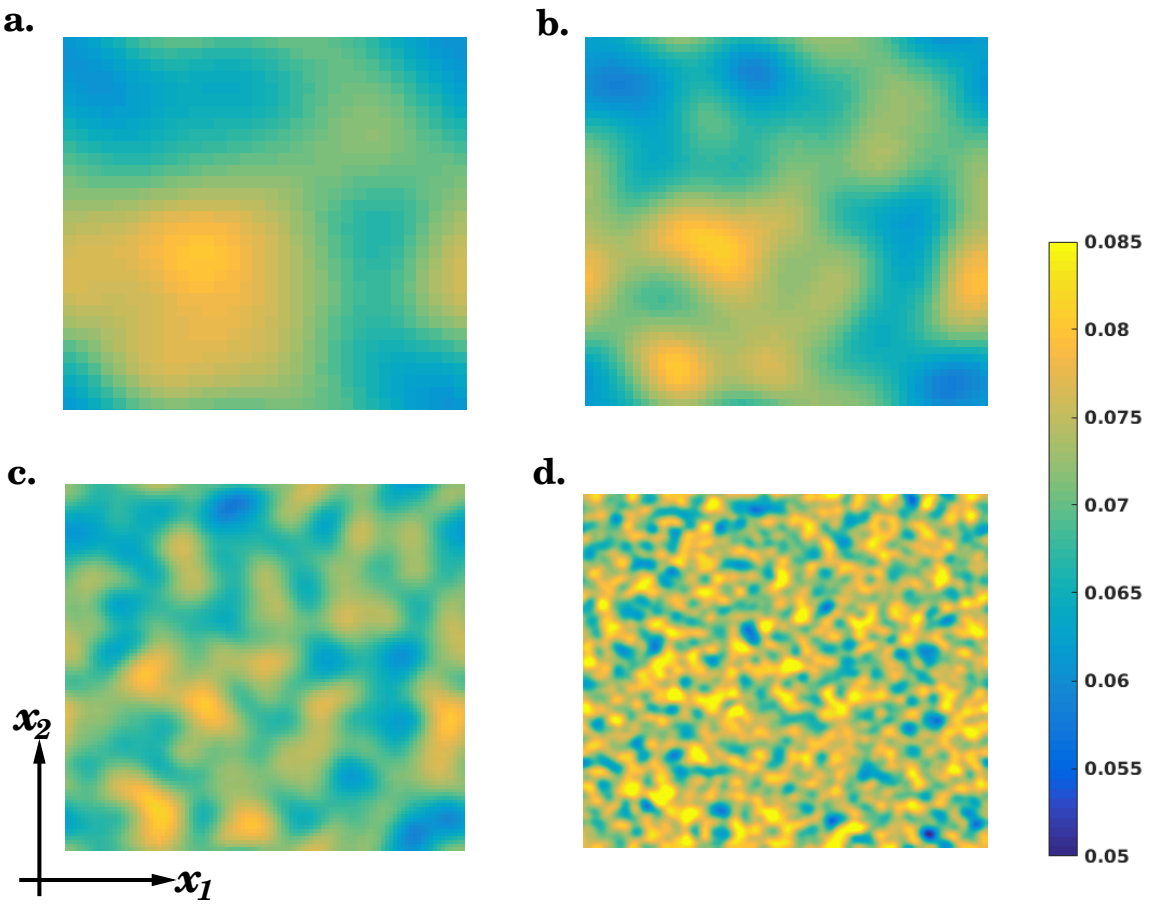

Figure 4.9: The initial condition of the effective temperature in the STZ theory χ_o using different coarse-grained representations: a) $c = 50$Å, b) $c = 32$Å, c) $c = 16$Å, and d) $c = 5$Å.

Previous STZ-theory approaches that have attempted to model the NEMD shear deformation of Lennard-Jones glasses have relied upon postulating a value for χ_o *a priori* without directly extracting it from physical atomistic data, such as the potential energies.[77–79,81] These STZ-effective-temperature simulations were also entirely one-dimensional, but nonetheless have provided important guidance for the development of more sophisticated techniques. Although the range of values of χ_o for a particular system is significantly restricted by the nonlinear form of Eq. 4.12 and its stability.

The final term in Eq. 4.12 describes the diffusion of the effective temperature through a rate-dependent effective thermal diffusivity $D_\chi = l^2\sqrt{\mathbf{D}^{\mathrm{pl}} : \mathbf{D}^{\mathrm{pl}}}$ with dimensions length-squared per unit time, where the lengthscale l is approximately the size of an STZ (on the order of a molecular lengthscale). Because D_χ is a function of the plastic rate-of-deformation, the diffusivity is inhomogeneous and the effective temperature diffuses at different rates in different regions of the material. For example, in regions where the local plastic-strain rate is larger, so too is the value of D_χ.

In this work we have made the specific assumption that the individual atomic potential energies E_n can be linearly related to an effective temperature by

$$\chi_n = \beta \left(E_n - E^o \right) \ . \tag{4.13}$$

This is perhaps the simplest assumption that could be made for χ. Prior investigations

have suggested that this is indeed the correct relationship for a simple Lennard-Jones system,[94] and a generic, though not necessarily linear relationship, also follows from the notion of a specific heat-like quantity relating potential energy to effective temperature. This is to say that as with the familiar thermal temperature T, which can be defined in terms of a specific heat that is nearly uniform over some finite range of T, it is assumed that a similar relationship is valid for the effective temperature in a way that is consistent with the definition in Eq. 2.3, namely

$$\kappa_{\text{eff}} = \frac{\partial U_c}{\partial T_{\text{eff}}} \tag{4.14}$$

where κ_{eff} is the *effective* heat capacity. Direct integration of this definition with Eq. 4.11 results in the mapping given by Eq. 4.13 and that $\beta = k_B/E_z\kappa_{\text{eff}}$. The reference energy E^o corresponds to a state of low disorder in the glass where T_{eff} can be taken to be zero. Ideally this would be the crystalline phase of the quenched liquid. For the 50-50 composition used here, the CuZr system has no stable crystalline phase at $T = 100$K, the value of T during the shear. As such we have treated β and E^o as parameters which we have adjusted to best connect the model's predictions with analysis of the MD.

An atom n with potential energy E_n is mapped to a value of effective temperature χ_n through Eq. 4.2,

$$\chi_n^{\text{MD}} = \beta \left(E_n - E^o - E^{\text{el}} \right) \ . \tag{4.15}$$

Here E^{el} is the per-atom elastic-strain energy determined by a fit to the parabolic realm of the system's total potential energy density U as a function of shear strain ϵ_{12}, since the linear-elastic strain energy is given by $U = \frac{1}{2}C_{ijkl}\epsilon_{ij}\epsilon_{kl}$, where C_{ijkl} is the Hookean-elasticity tensor. The effective temperature however is a measure only of plastic rearrangements and therefore E^{el} has been removed from E_n and hence from contributing to χ_n^{MD}. This is an approximation that becomes an exact correction in the limit where all elastic behavior is perfectly linear. Then relevant coarse-graining over χ_n^{MD} becomes

$$\chi_\alpha^{\mathrm{MD}} = \frac{\sum\limits_n g_n \chi_n^{\mathrm{MD}}}{\sum\limits_n g_n} \ . \tag{4.16}$$

Figure 4.9 shows the result of applying Eq. 4.16 to the as-quenched configuration of the glass, yielding coarse-grained representations of the system before shear $\chi_\alpha^{\mathrm{MD}}(\gamma = 0)$ for different c. The same procedure described in Sec. 4.2 for E_α is applied to determine $\chi_\alpha^{\mathrm{MD}}$ for all subsequent configurations during the shear with the same weighting and averaging in Eq. 4.16 used for the pre-shear system. The left column of Figs. 4.10,4.11,4.12, and 4.13 shows the evolution of $\chi_\alpha^{\mathrm{MD}}$ at various strains during the shear. Here we have considered only one of the species when applying Eq. 4.15, and have arbitrarily chosen the Cu atoms, although we have found that choosing either species gives very similar results for a particular g_n, including the signature of the shear band. This would imply that both species contain similar, relevant structural information. Also while only the Cu-atoms are explicitly treated in this analysis, we note that the Cu-Zr-interactions are still present through the potential energies of the

PARAMETERS		UNIT	Value
Yield stress	s_{y}	GPa	0.85
STZ size	ϵ_o	-	10
Inverse attempt frequency	τ_o	ps	0.1
Elastic shear modulus	μ	GPa	20
Plastic-work fraction	c_{o}	-	0.3
Global shear rate	$\dot{\gamma}$	ps^{-1}	10^{-4}

Table 4.5: The parameters of the STZ effective-temperature model used in all coarse-grained representations. The '-' indicates the parameter is dimensionless.

c	l	χ_∞
50 Å	4.01 Å	0.13
32 Å	8.04 Å	0.13
16 Å	12.06 Å	0.097
5 Å	12.06 Å	0.090

Table 4.6: The values of the diffusivity lengthscale l and the steady-state effective temperatureχ_∞ for different coarse-grained representations defined by c.

Cu-atoms. Ultimately this set of $\chi_\alpha^{\mathrm{MD}}$ in the pre-shear configuration defines a field which is the initial condition χ_o for the continuum STZ model.

Recently a numerical method for simulating the deformation of elasto-plastic materials in the quasi-static limit has been developed[139] by building on a mathematical correspondence with the incompressible NavierStokes equations. It is well-suited for a large class of materials, which typically undergo small elastic deformations and feature large elastic wave speeds, making many plastic deformation problems intrinsically quasi-static. In such situations, this method allows simulating realistic loading rates, which would be prohibitively computationally expensive using explicit methods.[70]

Here we use the methodology of Sec. 4.2 to provide an initial condition for the

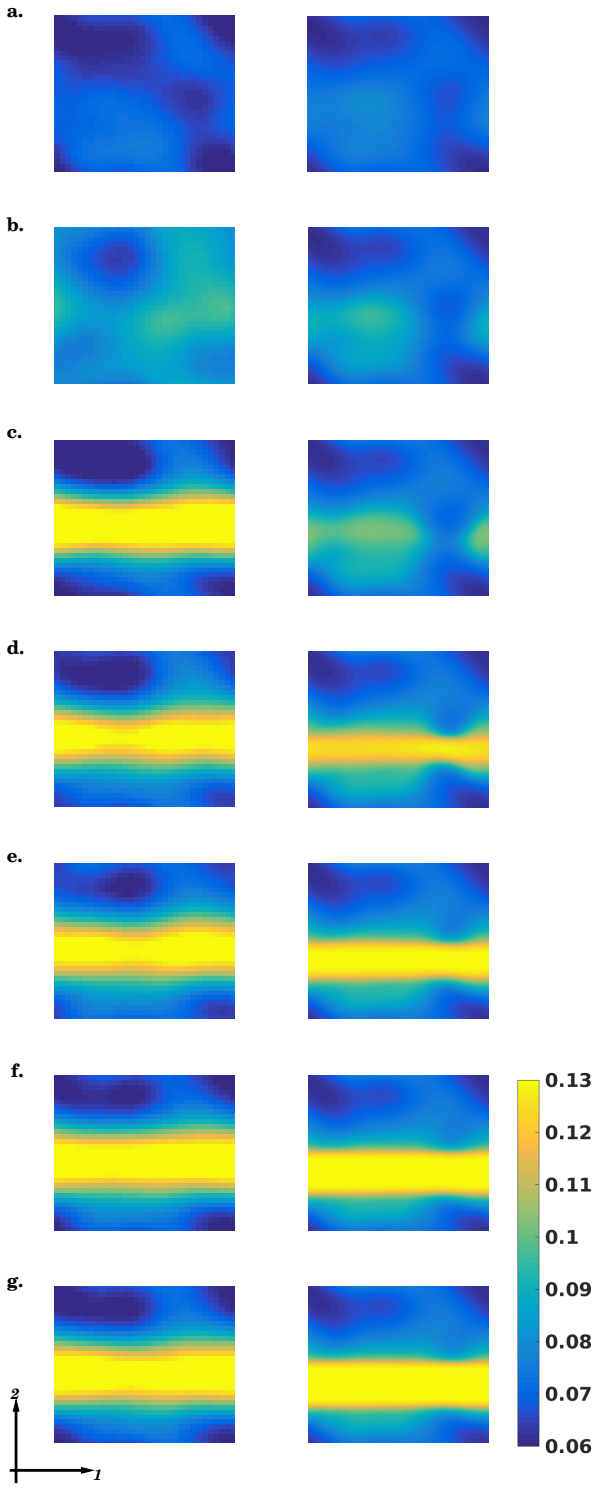

Figure 4.10: The coarse-grained effective temperature of the NEMD shear simulation (left column) $\chi_\alpha^{\mathrm{MD}}$ and the effective temperature of the STZ theory (right column) χ where the system is coarse-grained using $c = 50$Å at: a) 5%, b) 9.5%, c) 10.5%, d) 15.5%, e) 27.5%, f) 42%, and g) 49.5% global strain.

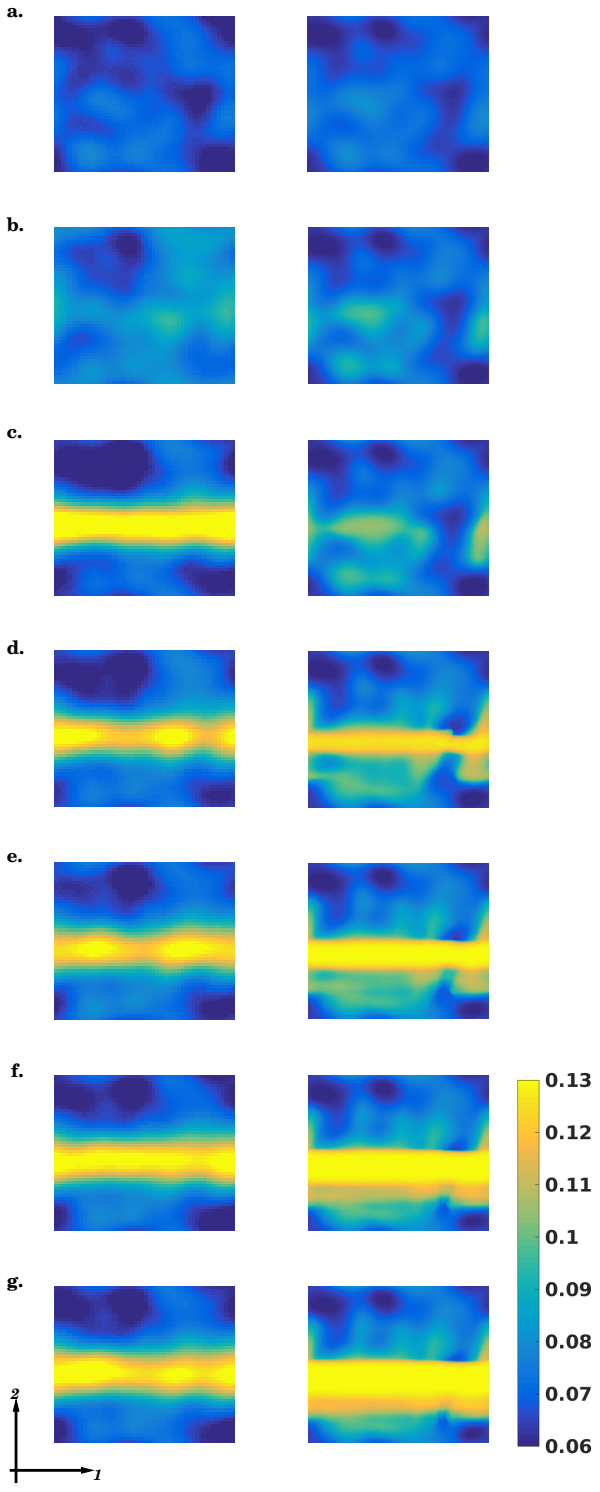

Figure 4.11: The coarse-grained effective temperature of the NEMD shear simulation (left column) $\chi_\alpha^{\mathrm{MD}}$ and the effective temperature of the STZ theory (right column) χ where the system is coarse-grained using $c = 32$Å at: a) 5%, b) 9.5%, c) 10.5%, d) 15.5%, e) 27.5%, f) 42%, and g) 49.5% global strain.

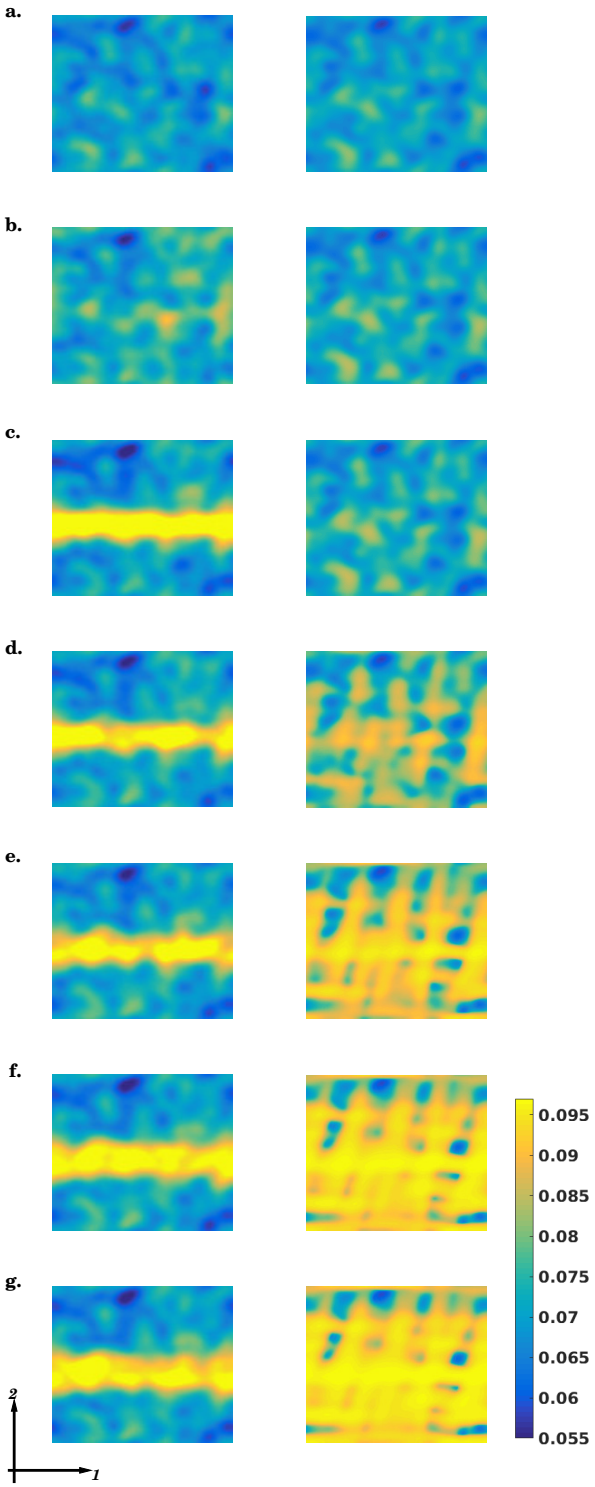

Figure 4.12: The coarse-grained effective temperature of the NEMD shear simulation (left column) $\chi_\alpha^{\mathrm{MD}}$ and the effective temperature of the STZ theory (right column) χ where the system is coarse-grained using $c = 16$Åat: a) 5%, b) 9.5%, c) 10.5%, d) 15.5%, e) 27.5%, f) 42%, and g) 49.5% global strain.

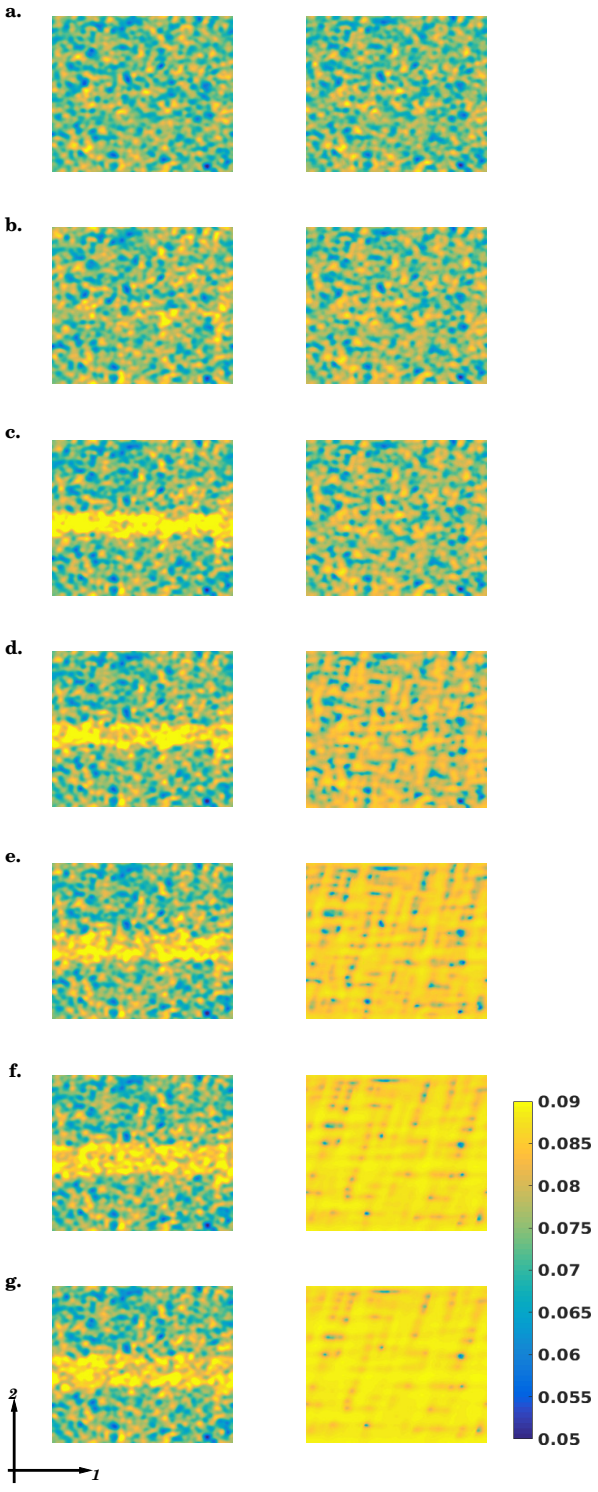

Figure 4.13: The coarse-grained effective temperature of the NEMD shear simulation (left column) $\chi_\alpha^{\mathrm{MD}}$ and the effective temperature of the STZ theory (right column) χ where the system is coarse-grained using $c = 5$Å at: a) 5%, b) 9.5%, c) 10.5%, d) 15.5%, e) 27.5%, f) 42%, and g) 49.5% global strain.

c	β	U_c^o
50 Å	9.5	-3.367 eV
32 Å	6.1	-3.371 eV
16 Å	2.3	-3.39 eV
5 Å	0.92	-3.44 eV

Table 4.7: The values of β and U_c^o in the potential-energy mapping to effective temperature given by Eq. 4.15 for different coarse-grained representations defined by c.

effective-temperature field and then simulate the continuum STZ model using the two-dimensional quasi-static numerical implementation described above. The quasi-static condition requires

$$\nabla \cdot \sigma = 0 \ . \tag{4.17}$$

and is equivalent to the inertial limit where σ is the Cauchy stress tensor. This numerical approach is most suitable for materials that can be well-described by the additive decomposition of the rate-of-deformation tensor into elastic and plastic parts, namely

$$\mathbf{D} = \mathbf{D}^{\mathrm{el}} + \mathbf{D}^{\mathrm{pl}} \ , \tag{4.18}$$

and is the assumption we have made here. The model can be solved by connecting the flow rule for the plastic-strain rate to Newton's laws for deformable bodies by

$$\dot{\sigma} = \mathbf{C} : \mathbf{D}^{\mathrm{el}} = \mathbf{C} : (\mathbf{D} - \mathbf{D}^{\mathrm{pl}}) \tag{4.19}$$

where $\mathbf{C}$ is the Hookean-elasticity tensor.

The values of the parameters of the effective-temperature model are summarized in Tab. 4.5, which are the same across simulations of different coarse-grained initial conditions. The elastic shear modulus was matched to the linear-elastic regime of the atomistic simulation, and the values of ϵ_o and s_y were taken from previous investigations of metallic glasses.[70,139] The fraction of plastic work c_o and the diffusivity lengthscale l were chosen to best match the stress-strain curve shown in Fig. 4.18, in particular matching the stress overshoot and the softening behavior. The values of c_o and l were first determined for the case where $c = 50$, as it seemed to deliver the closed agreement with the observations of the MD system. The values in the mapping described by Eq. 4.15, β and U_c^o, were chosen so that the initial condition $\chi_o = \chi_\alpha^{\mathrm{MD}}(\gamma = 0)$ effected the best agreement between the NEMD simulation and continuum-STZ model and vary slightly as function of c as summarized by Tab. 4.7. The choice of β and U_c was found to have the most dramatic effect on the behavior of the model, and initially these values were chosen to be within the range of previous work[77] and then adjusted to best fit each simulation. The diffusivity and steady-state condition χ_∞ were minimally adjusted for simulations of different c in order to best track the evolution of $\chi_\alpha^{\mathrm{MD}}$ and to maintain numerical stability arising from the value of l. The values l and χ_∞ are shown in Tab. 4.6. The steady-state condition for the effective temperature χ_∞ comes from an estimated average of $\chi_\alpha^{\mathrm{MD}}$ inside the flowing region of the shear band at approximately $\gamma = 50\%$ strain. The average of the flowing region varied slightly for different values of c.

The right column of Figs. 4.10,4.11,4.12, and 4.13 shows the effective temperature of the model evolving as the system is sheared from a coarse-grained initial condition. At 10.5 % strain the shear band which is readily apparent in $\chi_\alpha^{\mathrm{MD}}$ of the NEMD simulation, is somewhat delayed in χ of the continuum model. The increase in χ in the model near the center does indicate the formation of a shear band, but this is not continuous across the system until about 11.5% strain, and takes slightly longer to reach χ_∞ in the center of the band. Figures. 4.14,4.15,4.16, and 4.17 shows the value of $\chi_\alpha^{\mathrm{MD}}$ and χ as a one-dimensional slice at $x_1 = L/2$, and highlights the sharpest contrast among the different coarse-grained representations and their effect on the predictability of χ in the continuum description. Coarser representations, i.e. $c = 50$ and $c = 32$Å certainly appear to better capture the size (width) and location of the shear band, while finer coarse-grained representations lead to a proliferation of noise that in turn leads to numerous individual shear bands and a subsequent system-wide, uniform disordering that is not reflected in the NEMD simulations.

Figure 4.18 shows average of the shear stress S_{12} in the continuum model for different c as well as the NEMD simulation. This comparison of the macroscopic mechanical response lends additional support to notion that the coarser representations provide a more accurate continuum picture, which was also apparent from the earlier comparisons of the structural evolution. The onset of the shear band in all continuum simulations occurs during the softening regime where plastic rearrangements intensify before reaching their steady-state density at the flow stress.

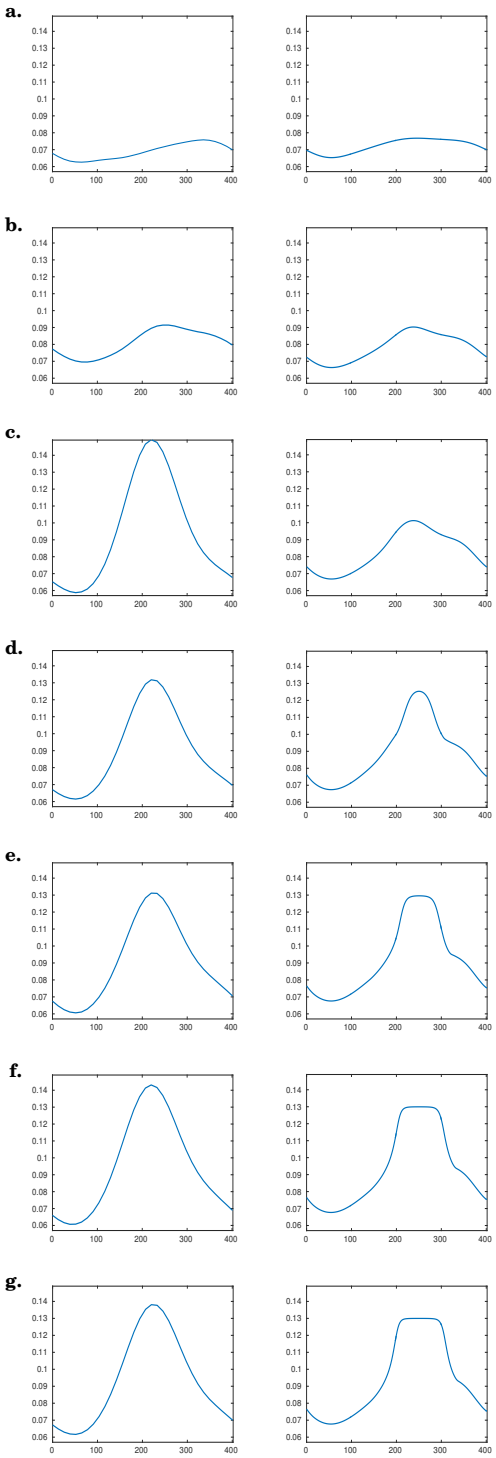

Figure 4.14: The coarse-grained effective temperature of the NEMD shear simulation (left column) $\chi_\alpha^{\mathrm{MD}}$ and the effective temperature of the STZ theory (right column) χ along $x_1 = L/2$ where the system is coarse-grained using $c = 50$Å at: a) 5%, b) 9.5%, c) 10.5%, d) 15.5%, e) 27.5%, f) 42%, and g) 49.5% global strain.

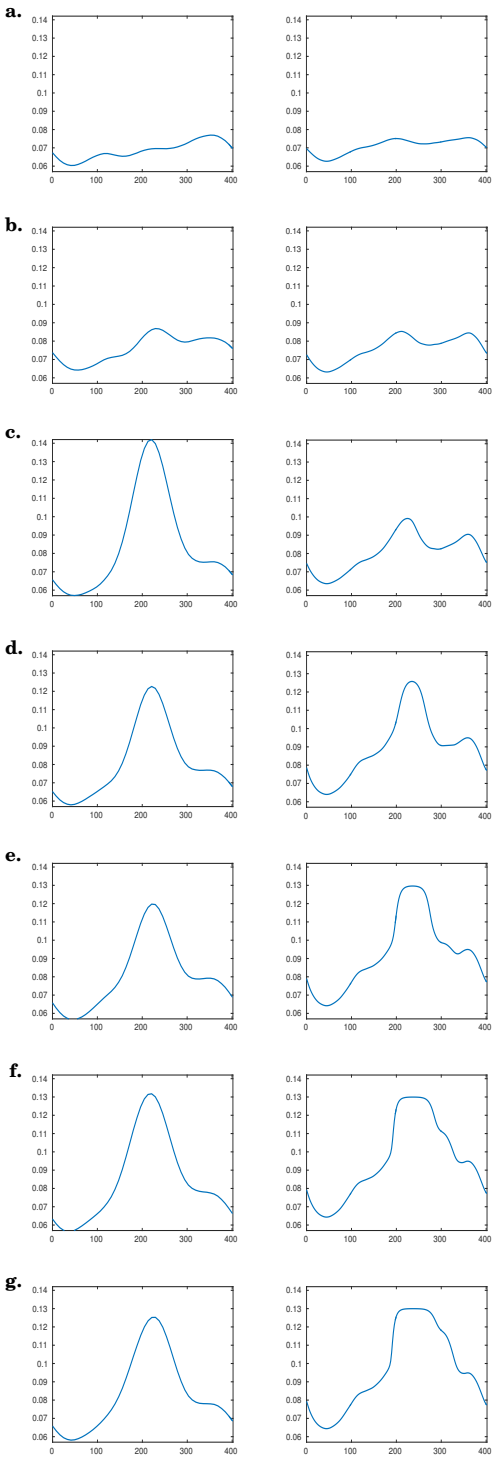

Figure 4.15: The coarse-grained effective temperature of the NEMD shear simulation (left column) $\chi_\alpha^{\mathrm{MD}}$ and the effective temperature of the STZ theory (right column) χ along $x_1 = L/2$ where the system is coarse-grained using $c = 32$Å at: a) 5%, b) 9.5%, c) 10.5%, d) 15.5%, e) 27.5%, f) 42%, and g) 49.5% global strain.

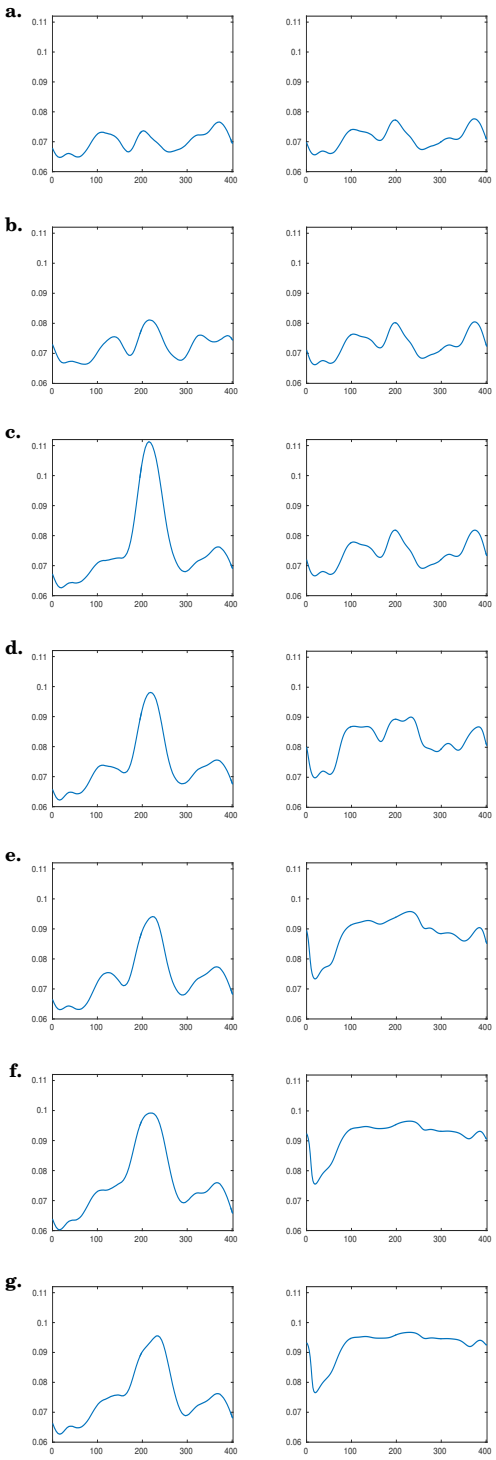

Figure 4.16: The coarse-grained effective temperature of the NEMD shear simulation (left column) $\chi_\alpha^{\mathrm{MD}}$ and the effective temperature of the STZ theory (right column) χ along $x_1 = L/2$ where the system is coarse-grained using $c = 16$Å at: a) 5%, b) 9.5%, c) 10.5%, d) 15.5%, e) 27.5%, f) 42%, and g) 49.5% global strain.

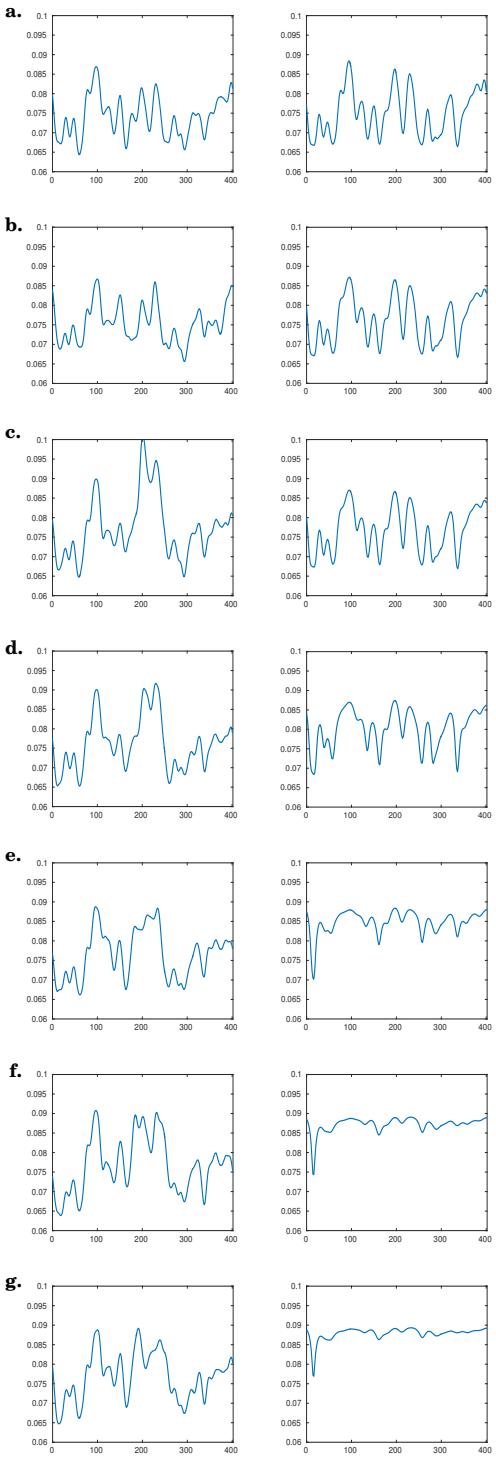

Figure 4.17: The coarse-grained effective temperature of the NEMD shear simulation (left column) $\chi_\alpha^{\mathrm{MD}}$ and the effective temperature of the STZ theory (right column) χ along $x_1 = L/2$ where the system is coarse-grained using $c = 5$Å at: a) 5%, b) 9.5%, c) 10.5%, d) 15.5%, e) 27.5%, f) 42%, and g) 49.5% global strain.

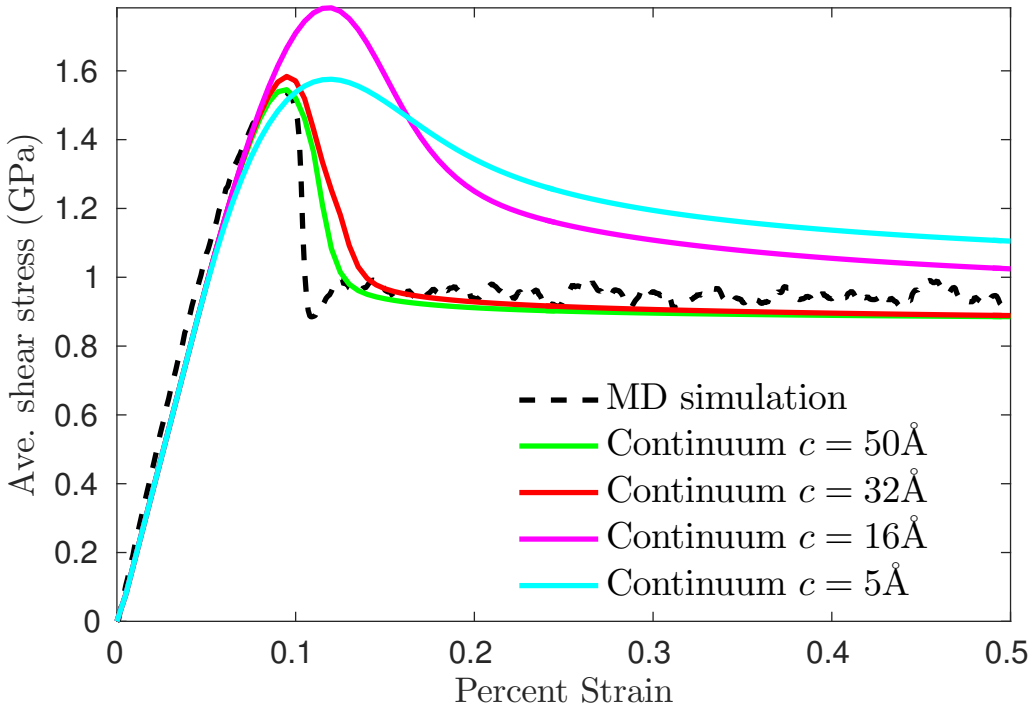

Figure 4.18: The average shear stress S_{12} of the CuZr MD simulation (dashed curve) and continuum effective-temperature theory (solid curves) for different coarse-grained initial conditions χ_o.

4.5 Conclusions

We have presented a study of shear banding using NEMD simulations and a two-dimensional numerical implementation of the continuum STZ effective-temperature theory. The coarse-graining methodology used in this work has been developed with the phenomena-dependent focus of capturing the primary mode of deformation of metallic glasses, shear banding. The methodology is an attempt to identify and directly link the atomistic descriptors of the system, e.g. the local potential energy, to the initial condition for the effective-temperature in the STZ model to develop a well-informed, predictive continuum description of the plasticity.

In the STZ theory the effective temperature is the continuum-based measure of the shear-induced disordering of a material's structure, and as per its definition with respect to the configurational energy and entropy of the system, should evolve mostly closely with the material's potential energy. We have found that to be the case here, but also that the continuum model's accuracy is significantly dependent on the how the atomic information is coarse-grained, which affects the properties of the resulting initial condition and the ability to make one-to-one comparisons between the coarse-grained NEMD and the effective temperature theory. Our analysis indicates that coarser-grained representations between $c = 50 - 32$Å appear to best resolve the variations in the atomic potential energy data so that an instability in χ_o can grow, diffuse, and saturate in a way that corresponds accurately to the NEMD results.. Both the location and width of this flowing region in the effective-temperature model

compare well with the corresponding changes in $\chi_\alpha^{\mathrm{MD}}$ when $c = 50$ and $c = 32$ Å. Moreover, the difference in strain between the onset of a fully formed shear band that is continuous and visible across the MD system and that observed in the effective-temperature model is approximately 5-6% as seen in Fig 4.10c-d. The results of the STZ-effective-temperature modeling in this study are the only we know of in which model validation has been derived directly from atomistic simulation. Both the microstructural evolution and the stress-strain response have been directly compared with the results of the NEMD simulation, which itself employs a well-established EAM potential.

Despite a good deal of measurable agreement using the methodology presented here, this analysis is incomplete and has left us with a number of important questions. The optimal lengthscale for the coarse-graining, i.e. what the value of c in g_n should be, is not completely clear. While the value of SN increases with c after the shear band forms, analysis of SN does not provide clear guidance as to the selection of a unique optimal c, although it does indicate that there is may be a minimal value of c. A study of the range of the parameters β and U_c^o corresponding to initial conditions coming from the coarse-grained atomistic data that lead to shear banding would be beneficial in guiding constitutive theory development, but also, eventually, in guiding alloy development. Criteria for the ability of a single perturbation off a flat, uniform χ_o to grow and localize into a shear band in one-dimension have already been preformed.[77] More generalized criteria still need to be developed to apply to the two

and three-dimensional coarse-grained atomistic data under non-idealized conditions, e.g. where there exist fluctuations from the background with a non-zero mean. An understanding of this sort could connect the level of coarse-graining directly to the initial condition, and allow acceptable levels of coarse-graining which optimize shear banding to be more clearly defined.

Chapter 5

Future Research Directions

This thesis has examined the role of effective temperature as a continuum description of plasticity in two glassy, but yet distinct material systems, a carbopol gel and a metallic glass. In this final chapter a we briefly review the main themes of what has been presented in this thesis and discuss possible avenues of future work.

In Chapter 3 a rheological model using an effective temperature was presented to describe transient shear banding during Couette-cell shear of a carbopol gel. Direct and quantitative comparisons with published experimental measurements were made, as well as an analysis of the two-state fluidization of the gel which followed from the dynamics of the effective temperature. This is the first time that the effective-temperature physics as developed in the context of the STZ theory has been applied to the rheology of complex fluids, and one of the very few instances where it has been used to make direct comparisons with experiments in terms of fundamental

properties of the system, e.g. velocities and shear-band widths. As noted in Chapter 3 a number of assumptions and simplifications were made, which could be replaced with more complete generalizations to provide a more robust and capable model.

Throughout Chapter 3, we have assumed that the diffusivity D_χ and steady-state value χ_∞ of the effective temperature are fixed constants for the system. While we believe this is a good approximation for the specific case of the small-gap system that we have examined in detail, the effective-temperature framework of the STZ theory strongly suggests that these quantities should in general depend on the local shear rate. The more physical picture thus requires that D_χ and χ_∞ be functions of the local, plastic-strain rate. Such a description for the diffusivity $D_\chi = l^2\sqrt{D_{ij}^{\rm pl}D_{ij}^{\rm pl}}$, as was implemented in the two-dimensional analysis of the metallic glass should have a interesting effect on the growth of the width of the transient shear band, since D_χ is the only physics in the model responsible for increasing the spatial extent of the transient shear band through a relaxation of χ. Similarly a rate-dependent steady state $\chi_\infty = \chi_\infty(D_{ij}^{\rm pl})$ could profoundly influence the fluidization time as well as the inter-facial profile. The rate dependence in χ_∞ causes regions with different local $D_{ij}^{\rm pl}$ to evolve to different steady-state effective temperatures. Studying these effects for the parameter regime of the carbopol gel is complicated by a very stiff set of equations of motion which, even in the one-dimensional model of Chapter 3, required the used of MATLAB's stiff integrator with an adaptive timestep.

One important physical phenomena not accounted for in the effective-temperature

model of the carbopol gel experiments are wallslip and aging. Wallslip is by far a more dominate feature that a more sophisticated description might seek to characterize. The experimental reports noted that wallslip occurs in nearly every type of Couette-cell experiment preformed, and is nearly impossible to eliminate even by imposing rough boundary conditions, e.g. sandpaper on the rotor. A boundary layer almost immediately forms at the rotor as the shear is imposed. The experimenters have indicated that this observation suggests a yielding mechanism where the initially solid-like material suddenly fails at the inner wall (rotor) independently of boundary conditions and leaves a strongly sheared lubrication layer at the rotor which then fluidizes the solid-like sample.[111] A model which accounts for this, possibly through a modification of the velocity field, should be able to more accurately compare with experimental data.

In Chapter 4 we presented the results of molecular dynamics simulations of a metallic glass under shear where strain localization appears in the form of a shear band. A methodology to coarse-grain the discrete atomistic data from the simulations was also presented, and a criterion using the local atomic strain was devised to identify which regions of the coarse-grained representation of system are part of the shear band and which are outside the band. From this distinction, distributions of the coarse-grained potential energies within the shear band and in the surrounding material were extracted as the system deforms under a uniform, global strain-rate. The statistics of these distributions were used to extract a signal-to-noise ratio, and it

was observed that just prior to the formation of the shear band, there is a preference for wider (coarser) coarse-graining schemes. Using this methodology a continuum STZ effective-temperature model was initialized from a coarse-grained representation of the atomistic system, and the continuum model was directly compared to the atomistic simulations during the imposed shear. As was suggested by the signal-to-noise results, initial conditions of the effective temperature coming from coarser representations best predict the behavior seen in the atomistic simulations.

As was noted in Chapter 4 however, the coarse-graining methodology for the study of the sheared CuZr system invites a great deal of further study. The most immediate extension of what has been presented in this thesis, is to consider an initial condition for the continuum model coming from the Zr atoms, and assess the consistency of the effect of the various coarse-graining lengthscales. Ideally this should be followed by a consideration of both species in determining the initial effective-temperature field, along with an appropriate understanding of the parameters involved in such a transformation that combines both Cu and Zr species into a unit of effective temperature. Another important pending study is the universality of the optimal range of coarse-graining lengthscales found here. For instance, the effect of the size of the system has not yet been investigated, and it is not clear for the specific system that was studied, what the upper bound for the coarse-graining lengthscale is. Similarly prepared systems should be studied with larger system sizes and the effect of a wider range of coarse-grained representations should be investigated.

CHAPTER 5. FUTURE RESEARCH DIRECTIONS

The ability of a given initial state in the STZ effective-temperature theory to lead to strain localization has been investigated in prior work, as discussed in Chapter 4. However these important earlier investigations are restricted to idealized cases, i.e. where the initial effective temperature has a single perturbation off of a uniform, flat background. In these cases a deformation map was constructed that related the initial condition and the amplitude of the perturbation to the degree of localization. An important new direction of possible future work coming from the results of Chapter 4 is a similar analysis which connects a realistic initial condition where there are many fluctuations of non-zero mean off of this background to the ability to form a shear band. What is the appropriate measure in this case where there are many "perturbations" of varying size? A more detailed study aimed at producing a well-formulated deformation map which addresses this question could also shed light on the appropriate coarse-graining lengthscale, since this choice is critical in preparing the initial condition to generate such a map.

Bibliography

[1] Z. Stachurski, "On structure and properties of amorphous materials," *Materials*, vol. 4, p. 1564, 2011.

[2] M. Falk and J. Langer, "Deformation and failure of amorphous, solidlike materials," *Annu. Rev. Condens. Matter Phys.*, vol. 1, p. 062910, 2011.

[3] J. Reddy, *An Introduction to Continuum Mechanics with Applications*, vol. 1. Cambridge University Press, 2007.

[4] E. Bouchbinder and J. Langer, "Nonequilibrium thermodynamics of driven amorphous materials. i. internal degrees of freedom and volume deformation," *Phys. Rev. E*, vol. 80, p. 031131, 2009.

[5] E. Bouchbinder and J. Langer, "Nonequilibrium thermodynamics of driven amorphous materials. ii. effective-temperature theory," *Phys. Rev. E*, vol. 80, p. 031132, 2009.

[6] E. Bouchbinder and J. Langer, "Nonequilibrium thermodynamics of driven

amorphous materials. iii. shear-transformation-zone plasticity," *Phys. Rev. E*, vol. 80, p. 031133, 2009.

[7] T. Hufnagel, "Finding order in disorder," *Nature Materials*, vol. 3, p. 666, 2004.

[8] J. Schroers, T. Nguyen, S. O'Keeffe, and A. Desai, "Thermoplastic forming of bulk metallic glass—applications for mems and microstructure fabrication," *Mater. Sci. Eng. A*, vol. 449, p. 898, 2007.

[9] D. Lee, M. F. Rubner, and R. Cohen, "All-nanoparticle thin-film coatings," *Nano Lett.*, vol. 6, p. 2305, 2006.

[10] Y. Joshi, "Dynamics of colloidal glasses and gels," *Annu. Rev. Chem. Biomol. Eng.*, vol. 5, p. 181, 2014.

[11] N. Xu and C. O'Hern, "Measurements of the yield stress in frictionless granular systems," *Phys. Rev. E*, vol. 73, p. 061303, 2006.

[12] S. Das, *Statistical Physics of Liquids at Freezing and Beyond*. Cambridge University Press, 2011.

[13] I. M. Kalogeras and H. E. Haag-Lobland, "The nature of the glassy state: structure and glass transitions," *J. Mater. Ed.*, vol. 34, p. 69, 2012.

[14] L. Landau and E. Lifshitz, *Statistical Physics*. Nauka, Moscow, 1964.

[15] K. Trachenko and V. Brazhkin, "Heat capacity at the glass transition," *Phys. Rev. B*, vol. 83, p. 014201, 2011.

BIBLIOGRAPHY

[16] P. G. Debenedetti and F. Stillinger, "Supercooled liquids and the glass transition," *Nature*, vol. 410, p. 259, 2001.

[17] C. Angell, K. Ngai, G. McKenna, P. McMillan, and S. Martin, "Relaxation in glassforming liquids and amorphous solids," *Nature*, vol. 88, p. 3113, 2000.

[18] P. K. Gupta, "Non-crystalline solids: glasses and amorphous solids," *J. Non-Cryst. Solids*, vol. 195, p. 158, 1996.

[19] E. Donovan, F. Spaepen, D. Turnbull, J. Poate, and D. Jacobson, "Calorimetric studies of crystallization and relaxation of amorphous si and ge prepared by ion implantation," *J. Appl. Phys.*, vol. 57, p. 1795, 1985.

[20] B. Bagley and H. Chen, "A calculation of the thermodynamic first order amorphous semiconductor to metallic liquid transition temperature," *AIP Conf. Proc.*, vol. 50, p. 97, 1979.

[21] A. Varshneya, *Fundamentals of Inorganic Glasses*, vol. 2. Society of Glass Technology, Sheffield, UK, 2006.

[22] D. Chrisey and G. Hubler, *Pulsed Laser Deposition of Thin Films*, vol. 1. John Wiley & Sons, New York, 1994.

[23] M. Ojovan and W. Lee, "Self sustaining vitrification for immobilisation of radioactive and toxic waste," *Glass Technology*, vol. 44, p. 218, 2003.

BIBLIOGRAPHY

[24] C. Koch, "Amorphization of single composition powders by mechanical milling," *Scr. Mater.*, vol. 34, p. 21, 1996.

[25] R. Jones, *Fundamental Principles of Sol-Gel Technology*, vol. 1. The Institute of Metals, London, UK, 1989.

[26] N. Andrianov, "Sol-gel method in oxide material technology," *Glass and Ceramics*, vol. 60, p. 320, 2003.

[27] W. Weber, "Models and mechanisms of irradiation-induced amorphization in ceramics," *Nuclear Instruments and Methods in Physics Research B*, vol. 166, p. 98, 2000.

[28] K. Trachenko, "Understanding resistance to amorphization by radiation damage," *Journal of Physics Condensed Matter*, vol. 16, p. R1491, 2004.

[29] D. Saha, Y. Joshi, and R. Bandyopadhyay, "Investigation of the dynamical slowing down process in soft glassy colloidal suspensions: comparisons with supercooled liquids," *Soft Matter*, vol. 10, p. 3292, 2014.

[30] L. Marshall and C. Zukoski, "Experimental studies on the rheology of hard-sphere suspensions near the glass transition," *J. Phys. Chem.*, vol. 94, p. 1164, 1990.

[31] P. Pusey and W. van Megen, "Phase behaviour of concentrated suspensions of nearly hard colloidal spheres," *Nature*, vol. 320, p. 340, 1986.

BIBLIOGRAPHY

[32] A. L. Greer, "New horizons for glass formation and stability," *Nature Materials*, vol. 14, p. 542, 2015.

[33] A. J. Liu and S. R. Nagel, "The jamming transition and the marginally jammed solid," *Annu. Rev. Condens. Matter Phys.*, vol. 1, p. 347, 2010.

[34] J. C. Mauro, R. Loucks, and S. Sen, "Heat capacity, enthalpy fluctuations, and configurational entropy in broken ergodic systems," *J. Chem. Phys.*, vol. 133, p. 164503, 2010.

[35] J. C. Mauro, R. Loucks, and S. Sen, "Response to comment on heat capacity, enthalpy fluctuations, and configurational entropy in broken ergodic systems [j. chem. phys.134, 147101 (2011)]," *J. Chem. Phys.*, vol. 134, p. 147102, 2011.

[36] L. Marshall and C. Zukoski, "Statistical mechanics of glass," *J. of Non-Crystalline Solids*, vol. 396, p. 41, 2014.

[37] M. Reiner, "The deborah number," *Physics Today*, vol. 17, p. 62, 1964.

[38] L. Cipelletti and L. Ramos, "Slow dynamics in glassy soft matter," *J. Phys. Cond. Mat.*, vol. 17, p. 253, 2005.

[39] G. McKenna, T. Narita, and F. Lequeux, "Slow dynamics in glassy soft matter," *J. Rheol.*, vol. 53, p. 489, 2009.

[40] B. Abou, D. Bonn, and J. Meunier, "Nonlinear rheology of laponite suspensions under an external drive," *J. Rheol.*, vol. 47, p. 979, 2003.

BIBLIOGRAPHY

[41] R. D. Leonard, F. Ianni, and G. Ruocco, "Aging under shear: Structural relaxation of a non-newtonian fluid," *J. Rheol.*, vol. 71, p. 011505, 2005.

[42] L. Boué, H. Hentschel, I. Procaccia, I. Regev, and J. Zylberg, "Effective temperature in elastoplasticity of amorphous solids," *Phys. Rev. B*, vol. 81, p. 100201, 2010.

[43] A. Argon and H. Kuo, "Plastic flow in a disordered bubble raft (an analog of a metallic glass)," *Materials Science and Eng.*, vol. 39, p. 101, 1979.

[44] A. Argon, "Plastic deformation in metallic glasses," *Acta Metall.*, vol. 27, p. 47, 1979.

[45] A. Argon and L. Shi, *Simulation of plastic flow and distributed shear relaxations in metallic glasses by means of amorphous bragg bubble raft*, vol. In: V. Vitek (ed), Amorphous Materials: Modeling of Structure and Properties. The Metallurgical Society of AIME, 1982.

[46] D. Turnbull and M. Cohen, "On the freevolume model of the liquidglass transition," *J. Chem. Phys.*, vol. 52, p. 3038, 1970.

[47] D. Turnbull and M. Cohen, "Free-volume model of the amorphous phase: Glass transition," *J. Chem. Phys.*, vol. 34, p. 120, 1961.

[48] F. Spaepen, "A microscopic mechanism for steady state inhomogeneous flow in metallic glasses," *Acta Metall.*, vol. 25, p. 407, 1977.

BIBLIOGRAPHY

[49] A. Hasan, M. Boyce, X. Li, and S. Berko, "An investigation of the yield and postyield behavior and corresponding structure of poly(methyl methacrylate)," *J. Polym. Sci.: Part B*, vol. 31, p. 185, 1993.

[50] A. Hasan and M. Boyce, "A constitutive model for the nonlinear viscoelastic viscoplastic behavior of glassy polymers," *Polym. Eng. Sci*, vol. 35, p. 331, 1995.

[51] H. Eyring, "Viscosity, plasticity, and diffusion as examples of absolute reaction rates," *J. Chem. Phys.*, vol. 4, p. 283, 1936.

[52] D. Srolovitz, T. Egami, and V. Vitek, "Radial distribution function and structural relaxation in amorphous solids," *Phys. Rev. B*, vol. 24, p. 6936, 1981.

[53] D. Srolovitz, K. Maeda, S. Takeuchi, T. Egami, and V. Vitek, "Local structure and topology of a model amorphous metal," *J. Phys. F: Metal Phys.*, vol. 11, p. 2209, 1981.

[54] T. Egami, K. Maeda, and V. Vitek, "Structural defects in amorphous solids a computer simulation study," *Philos. Mag. A*, vol. 41, p. 883, 1980.

[55] D. Srolovitz, V. Vitek, and T. Egami, "An atomistic study of deformation of amorphous metals," *Acta Metallurgica*, vol. 31, p. 335, 1983.

[56] T. Tomida and T. Egami, "Molecular-dynamics study of structural anisotropy and anelasticity in metallic glasses," *Phys. Rev. B*, vol. 48, p. 3048, 1993.

BIBLIOGRAPHY

[57] T. Tomia and T. Egami, "Phys. rev. b," *Molecular-dynamics study of orientational order in liquids and glasses and its relation to the glass transition*, vol. 52, p. 3290, 1995.

[58] S. Y. D. Deng, A. S. Argon, "A molecular dynamics model of melting and glass transition in an idealized two-dimensional material i," *Phil. Trans. R. Soc. Lond. A*, vol. 329, p. 549, 1989.

[59] M. Falk and J. Langer, "Dynamics of viscoplastic deformation in amorphous solids," *Phys. Rev. E*, vol. 57, p. 7192, 1998.

[60] J. Ding, S. Patinet, M. L. Falk, and E. Ma, "Soft spots and their structural signature in a metallic glass," *Proc. Natl. Acad. Sci.*, vol. 329, p. 549, 2014.

[61] C. Maloney and A. Lemaître, "Amorphous systems in athermal, quasistatic shear," *Phys. Rev. E*, vol. 74, p. 016118, 2006.

[62] J. Baret, D. Vandembroucq, and S. Roux, "Extremal model for amorphous media plasticity," *Phys. Rev. Lett.*, vol. 89, p. 195506, 2002.

[63] I. Regev, J. Weber, C. Reichhardt, K. Dahmen, and T. Lookman, "Reversibility and criticality in amorphous solids," *Nat. Commun.*, vol. 6, p. 8805, 2015.

[64] K. M. Salerno, C. Maloney, and M. Robbins, "Avalanches in strained amorphous solids: does inertia destroy critical behavior?," *Phys. Rev. Lett.*, vol. 109, p. 105703, 2012.

BIBLIOGRAPHY

[65] A. Onuki, "Plastic flow in two-dimensional solids," *Phys. Rev. E*, vol. 68, p. 061502, 2003.

[66] V. Bulatov and A. Argon, "Stochastic model for continuum elasto-plastic behavior: Iii. plasticity in ordered versus disordered solids," *Simul. Mater. Sci. Eng.*, vol. 2, p. 203, 1994.

[67] G. Picard, A. Ajdari, F. Lequeux, and L. Bocquet, "Slow flows of yield stress fluids: Complex spatiotemporal behavior within a simple elastoplastic model," *Phys. Rev. E*, vol. 71, p. 010501, 2005.

[68] W. Götze and L. Sjögren, "Relaxation in supercooled liquids," *Rep. Prog. Phys.*, vol. 55, p. 241, 1992.

[69] J. Brader, T. Voigtmann, M. Fuchs, R. Larson, and M. Cates, "Glass rheology: From mode-coupling theory to a dynamical yield criterion," *PNAS*, vol. 106, p. 15186, 2009.

[70] C. Rycroft and F. Gibou, "Simulations of a stretching bar using a plasticity model from the shear transformation zone theory," *J. Comp. Phys.*, vol. 231, p. 2155, 2012.

[71] M. Falk, J. Langer, and L. Pechenik, *Toward a Shear-Transformation-Zone Theory of Amorphous Plasticity*, vol. 1. Springer, The Netherlands, 2005.

BIBLIOGRAPHY

[72] L. Pechenik, "Dynamics of shear-transformation zones in amorphous plasticity: Nonlinear theory at low temperatures," *Phys. Rev. E*, vol. 72, p. 021507, 2005.

[73] L. Pechenik and J. Langer, "Dynamics of shear-transformation zones in amorphous plasticity: Energetic constraints in a minimal theory," *Phys. Rev. E*, vol. 68, p. 061507, 2003.

[74] E. Bouchbinder, "Effective temperature dynamics in an athermal amorphous plasticity theory," *Phys. Rev. E*, vol. 77, p. 051505, 2008.

[75] E. Bouchbinder and J. S. Langer, "Shear-transformation-zone theory of linear glassy dynamics," *Phys. Rev. E*, vol. 83, p. 061503, 2011.

[76] J. Langer, "Dynamics of shear-transformation zones in amorphous plasticity: Formulation in terms of an effective disorder temperature," *Phys. Rev. E*, vol. 70, p. 041502, 2004.

[77] M. Manning, J. Langer, and J. Carlson, "Strain localization in a shear transformation zone model for amorphous solids," *Phys. Rev. E*, vol. 76, p. 056106, 2007.

[78] M. Manning, E. Daub, J. Langer, and J. Carlson, "Rate-dependent shear bands in a shear-transformation-zone model of amorphous solids," *Phys. Rev. E*, vol. 79, p. 016110, 2009.

[79] J. Langer and M. Manning, "Steady-state, effective-temperature dynamics in a glassy material," *Phys. Rev. E*, vol. 76, p. 056107, 2007.

[80] M. Lundberg, K. Krishna, N. Xu, C. O'Hern, and M. Dennin, "Reversible plastic events in amorphous materials," *Phys. Rev. E*, vol. 77, p. 041505, 2008.

[81] E. Daub, D. Klaumünzer, and J. Löffler, "Effective temperature dynamics of shear bands in metallic glasses," *Phys. Rev. E*, vol. 90, p. 062405, 2014.

[82] A. Tool, "Relation between inelastic deformability and thermal expansion of glass in its annealing range," *J. Amer. Ceram. Soc.*, vol. 29, pp. 240–253, 1946.

[83] D. Turnbull and M. Cohen, "Molecular transport in liquids and glasses," *J. Chem. Phys.*, vol. 31, p. 1164, 1959.

[84] T. M. Nieuwenhuizen, "Ehrenfest relations at the glass transition: Solution to an old paradox," *Phys. Rev. Lett.*, vol. 79, p. 1317, 1997.

[85] T. M. Nieuwenhuizen, "Thermodynamics of the glassy state: Effective temperature as an additional system parameter," *Phys. Rev. Lett.*, vol. 80, p. 5580, 1998.

[86] T. M. Nieuwenhuizen, "Thermodynamic picture of the glassy state gained from exactly solvable models," *Phys. Rev. E*, vol. 61, p. 267, 2000.

[87] F. Sciortino, W. Kob, and P. Tartaglia, "Inherent structure entropy of supercooled liquids," *Phys. Rev. Lett.*, vol. 83, p. 3214, 1999.

BIBLIOGRAPHY

[88] F. Sciortino and P. Tartaglia, "Extension of the fluctuation-dissipation theorem to the physical aging of a model glass-forming liquid," *Phys. Rev. Lett.*, vol. 86, p. 107, 2001.

[89] E. L. Nave, F. Sciortino, P. Tartaglia, M. S. Shell, and P. G. Debenedetti, "Test of nonequilibrium thermodynamics in glassy systems: The soft-sphere case," *Phys. Rev. E*, vol. 68, p. 032103, 2003.

[90] S. Edwards and R. Oakeshott, "Theory of powders," *Physica A*, vol. 157, p. 1080, 1989.

[91] A. Lemaître, "Rearrangements and dilatancy for sheared dense materials," *Phys. Rev. Lett.*, vol. 89, p. 195503, 2002.

[92] A. Lemaître, *Jamming, Yielding and Irreversible Deformation in Condensed Matter*. edited by M. C. Miguel and J. M. Rubi (Springer New York), 2004.

[93] E. Dieterich, J. Camunas-Soler, M. Ribezzi-Crivellari, U. Seifert, and F. Ritort, "Single-molecule measurement of the effective temperature in non-equilibrium steady states," *Nature Phys.*, vol. 11, p. 971, 2015.

[94] Y. Shi, M. B. Katz, H. Li, and M. L. Falk, "Evaluation of the disorder temperature and free-volume formalisms via simulations of shear banding in amorphous solids," *Phys. Rev. Lett.*, vol. 98, p. 185505, 2007.

BIBLIOGRAPHY

[95] S. F. Edwards and D. V. Grinev, "Granular materials: towards the statistical mechanics of jammed configurations," *Adv. Phys.*, vol. 51, p. 1669, 2002.

[96] A. Bonn and M. Denn, "Yield stress fluids slowly yield to analysis," *Science*, vol. 324, p. 1401, 2009.

[97] A. Ragouilliaux, G. Ovarlez, N. Shahidzadeh-Bonn, B. Herzhaft, T. Palermo, and P. Coussot, "Transition from a simple yield-stress fluid to a thixotropic material," *Phys. Rev. E*, vol. 76, p. 051408, 2007.

[98] P. Møller, A. Fall, V. Chikkadi, D. Derks, and D. Bonn, "An attempt to categorize yield stress fluid behaviour," *Phil. Trans. R. Soc. A*, vol. 367, p. 5139, 2009.

[99] P. Møller, J. Mewis, and D. Bonn, "Yield stress and thixotropy: on the difficulty of measuring yield stress in practice," *Soft Matter*, vol. 2, p. 274, 2006.

[100] P. Coussot, "Rheophysics of pastes: a review of microscopic modelling approaches," *Soft Matter*, vol. 3, p. 528, 2007.

[101] H. A. Barnes, "Thixotropya review," *J. Non-Newtonian Fluid Mech.*, vol. 70, p. 1, 1997.

[102] G. Ovarlez, S. Rodts, X. Chateau, and P. Coussot, "Phenomenology and physical origin of shear localization and shear banding in complex fluids," *Rheol. Acta*, vol. 48, p. 831, 2009.

BIBLIOGRAPHY

[103] P. Schall and M. van Hecke, "Shear bands in matter with granularity," *Annu. Rev. Fluid Mech.*, vol. 42, p. 67, 2010.

[104] R. Bird, G. Dai, and B. J. Yarusso, "The rheology and flow of viscoplastic materials," *Rev. Chem. Eng.*, vol. 1, p. 1, 1982.

[105] P. Coussot, *Rheometry of pastes, suspensions, and granular materials*. Wiley New York, 2005.

[106] C. Gilbreth, S. Sullivan, and M. Dennin, "Flow transitions in two-dimensional foams," *Phys. Rev. E*, vol. 74, p. 051406, 2006.

[107] G. Ovarlez, K. Krishan, and S. Cohen-Addad, "Investigation of shear banding in three-dimensional foams," *Europhys. Lett.*, vol. 91, p. 68005, 2010.

[108] S. Rodts, J. Baudez, and P. Coussot, "From "discrete" to "continuum" flow in foams," *Europhys. Lett.*, vol. 69, p. 636, 2005.

[109] G. Ovarlez, S. Rodts, A. Ragouilliaux, P. Coussot, J. Goyon, and A. Colin, "Couette flows of dense emulsions: local concentration measurements, and comparison between macroscopic and local constitutive law measurements through magnetic resonance imaging," *Phys. Rev. E*, vol. 78, p. 036307, 2008.

[110] G. Ovarlez, S. Cohen-Addad, K. Krishan, J. Goyon, and P. Coussot, "On the existence of a simple yield stress fluid behavior," *J. Non-Newtonian Fluid Mech.*, vol. 193, p. 68, 2013.

BIBLIOGRAPHY

[111] T. Divoux, D. Tamarii, C. Barentin, and S. Manneville, "Transient shear banding in a simple yield stress fluid," *Phys. Rev. Lett.*, vol. 104, p. 208301, 2010.

[112] T. Divoux, V. Grenard, and S. Manneville, "Rheological hysteresis in soft glassy materials," *Phys. Rev. Lett.*, vol. 110, p. 018304, 2013.

[113] T. Divoux, C. Barentin, and S. Manneville, "From stress-induced fluidization processes to herschel-bulkley behaviour in simple yield stress fluids," *Soft Matter*, vol. 7, p. 8409, 2011.

[114] T. Divoux, D. Tamarii, C. Barentin, S. Teitel, and S. Manneville, "Yielding dynamics of a herschelbulkley fluid: a critical-like fluidization behaviour," *Soft Matter*, vol. 8, p. 4151, 2012.

[115] S. M. Fielding, M. E. Cates, and P. Sollich, "Shear banding, aging and noise dynamics in soft glassy materials," *Soft Matter*, vol. 5, p. 2378, 2009.

[116] R. L. Moorcroft and S. M. Fielding, "Criteria for shear banding in time-dependent flows of complex fluids," *Phys. Rev. Lett.*, vol. 110, p. 086001, 2013.

[117] X. Illa, A. Puisto, A. Lehtinen, M. Mohtaschemi, and M. Alava, "Transient shear banding in time-dependent fluids," *Phys. Rev. E*, vol. 87, p. 022307, 2013.

[118] R. A. Fisher, "The wave of advance of advantageous genes," *Ann. Eugenics*, vol. 7, p. 355, 1937.

BIBLIOGRAPHY

[119] A. Kolmogorov, I. Petrovsky, and N. Piskunov, "Study of the diffusion equation with growth of the quantity of matter and its application to a biology problem (translated)," *Bull. Univ. Moscow, Ser. Intern., Sec. A*, vol. 1, p. 1, 1937.

[120] W. van Saarloos, "Front propagation into unstable states," *Physics Reports*, vol. 386, p. 29, 2003.

[121] A. L. Greer, "Metallic glasses on the threshold," *Materials Today*, vol. 12, p. 1, 2009.

[122] Y. Cheng and E. Ma, "Atomic-level structure and structureproperty relationship in metallic glasses," *Prog. Mater. Sci.*, vol. 56, p. 379, 2011.

[123] W. Drugan and J. Willis, "A micromechanics-based nonlocal constitutive equation and estimates of representative volume element size for elastic composites," *J. Mech. Phys. Solids*, vol. 44, p. 497, 1996.

[124] J. Chaboche, "A review of some plasticity and viscoplasticity constitutive theories," *International Journal of Plasticity*, vol. 24, p. 1642, 2008.

[125] W. Curtin and R. Miller, "Atomistic-continuum coupling in computational materials science," *Modeling Simul. Mater. Sci. Eng*, vol. 11, p. 33, 2003.

[126] P. Derosa, *Multiscale Modeling: From Atoms to Devices*. Taylor and Francis Group Boca Raton, 2011.

BIBLIOGRAPHY

[127] M. Dijkstra, R. van Roij, and R. Evans, "Phase diagram of highly asymmetric binary hard-sphere mixtures," *Phys. Rev. E*, vol. 59, p. 5744, 1999.

[128] P. Bolhuis, A. Louis, and J. Hansen, "Shear-induced volumetric strain in cuzr metallic glass," *Phys. Rev. E*, vol. 64, p. 021801, 2001.

[129] A. L. Greer, "Shear bands in metallic glasses," *Mater. Sci. Eng. R-Rep.*, vol. 74, p. 71, 2013.

[130] H. Guo, J. Wen, N. Xiao, Z. Zhang, and M. Sui, "The more shearing, the thicker shear band and heat-affected zone in bulk metallic glass," *J. Mater. Res.*, vol. 23, p. 2133, 2008.

[131] L. Yao and Y. Luan, "Evolution of shear banding flows in metallic glasses characterized by molecular dynamics," *J. Applied Physics*, vol. 119, p. 234303, 2016.

[132] J. Luo, Y. Shi, and C. Picu, "Shear-induced volumetric strain in cuzr metallic glass," *International Journal of Engineering Science*, vol. 83, p. 99, 2014.

[133] V. Bulatov and A. Argon, "A stochastic model for continuum elasto-plastic behavior: I numerical approach and strain localization," *Simul. Mater. Sci. Eng.*, vol. 2, p. 167, 1994.

[134] E. Homer and C. Schuh, "Mesoscale modeling of amorphous metals by shear transformation zone dynamics," *Acta Mater.*, vol. 57, p. 2823, 2009.

BIBLIOGRAPHY

[135] E. Homer and C. Schuh, "Three-dimensional shear transformation zone dynamics model for amorphous metals," *Modeling Simul. Mater. Sci. Eng*, vol. 18, p. 065009, 2010.

[136] S. Plimpton, "Fast parallel algorithms for short-range molecular dynamics," *J. Comp. Phys.*, vol. 117, p. 1, 1995.

[137] D. Evans and G. Morriss, "Nonlinear-response theory for steady planar couette flow," *Phys. Rev. A*, vol. 30, p. 1528, 1984.

[138] E. Bouchbinder, J. Langer, and I. Procaccia, "Athermal shear-transformation-zone theory of amorphous plastic deformation. ii. analysis of simulated amorphous silicon," *Phys. Rev. E*, vol. 75, p. 036108, 2007.

[139] C. Rycroft, Y. Sui, and E. Bouchbinder, "An eulerian projection method for quasi-static elastoplasticity," *J. Comp. Phys.*, vol. 300, p. 136, 2015.

Vita

The author received his undergraduate degree *summa cum laude* in physics from Marquette University in 2006 and a master's degree in engineering mechanics from Cornell University in 2009. He is currently a postdoctoral researcher at the Karlsruher Institut für Technologie in Karlsruhe, Germany.